ABSTRACT

Modeling of Flexible Fiber Motion and Prediction of Material Properties

Cong Zhang, M.S.M.E.

Committee Chairperson: David A. Jack, Ph.D.

This work employs the rod chain model of Wang *et al.* (2006) to study the motion of discrete flexible fibers. Results are presented for both individual fibers and a stochastic distribution of fibers to study the variations in the transient effects between the rigid and the flexible fiber systems. Results demonstrate that the observed period decreases as the fiber flexure increases, and provide insight into the modifications required for the orientation distribution function of flexible suspensions. To demonstrate the importance in studying the alterations in the transient effects on a processed part, a study of the cured composite stiffness is presented for the flexible fiber system using the micro-mechanical approach of Hsiao and Daniel (1996) along with an adapted version of the rigid fiber micromechanical approach discussed by Jack and Smith (2008).

Modeling Of Flexible Fiber Motion And Prediction Of Material Properties

by

Cong Zhang, B.E.

A Thesis

Approved by the Department of Mechanical Engineering

_____
William Jordan, Ph.D., Chairperson

Submitted to the Graduate Faculty of
Baylor University in Partial Fulfillment of the
Requirements for the Degree
of
Master of Science in Mechanical Engineering

Approved by the Thesis Committee

_____
David A. Jack, Ph.D., Chairperson

_____
William Jordan, Ph.D.

_____
Ronald B. Morgan, Ph.D.

Accepted by the Graduate School
August 2011

_____
J. Larry Lyon, Ph.D., Dean

Page bearing signatures is kept on file in the Graduate School.

TABLE OF CONTENTS

LIST OF FIGURES

ACKNOWLEDGMENTS

Foremost, I would like to express my sincere gratitude to my mentor and advisor Dr. David A. Jack for the continuous support of my masters study and research, for his patience, motivation, enthusiasm, and immense knowledge. His guidance helped me in all the time of research and writing of this thesis.

Besides my advisor, I would like to thank the rest of my thesis committee: Dr. William Jordan and Dr. Ronald B. Morgan for their encouragement, insightful comments, and inspirational questions.

My sincere thanks also go to Dr. Walter Bradley, Dr. Lesley M. Wright and Dr. Carolyn T. Skurla for offering me advice and help during my study at Baylor University.

I thank my fellow friends and colleagues: Nikhil Ashtekar, Babatunde Agboola, Theresa Vo, Haden Duke and William Minnie for the stimulating discussions and for all the fun we have had.

Last but not the least, I would like to thank my family: my parents Jinguo Zhang and Ling Wu, for giving birth to me at the first place and supporting me throughout my life.

To my beloved mother Ling Wu and father Jinguo Zhang

CHAPTER ONE

Introduction

There is a considerable industrial demand for lightweight, durable composites composed of long fibers due to their high strength to weight ratios. Manufacturing fiber reinforced composites with injection molding has become a dominant alternative over other traditional manufacturing processes, such as compression molding and extrusion molding, largely because of its relatively low cost of manufacturing, the ability to process parts with complex shapes, and the potential for increased use in high volume applications. Existing short fiber models for predicting the composites' underlying microstructure are quite proficient at capturing the orientation effects during the processing of the polymer melt and the final product of the cured part for rigid fibers. It would be of an industrial benefit to have similar models available for long fiber systems. Of particular interest is understanding the differences between classical rigid suspension models and the recent flexible suspension models, and present scenarios where the classical models can continue to be applied for systems with long fibers. Recent work in flexible fiber suspension kinematics has focused on a series of models which represent the motion of a single fiber as a series of connected beads or a series of rigid rods connected by force and torque transferring hinges between them.

The orientation and flexure of individual fibers within a processed fiber-reinforced composite plays a significant role in defining the bulk properties: such as elastic modulus [4–6], electrical and thermal conductivity [7], and thermal expansion [8], etc. During processing, the spatially varying fiber orientation alters the observed viscous stress of the polymer melt, which directly affects the processing parameters thus determining the cost and efficiency of processing [9–12]. Jeffery's

equation has been the foundation for rigid fiber orientation research due to three dimensional flow gradients for decades [13]. For example, it predicts that the motion of a single rigid ellipsoid is periodical in a shear flow and follows a very well-established and predictable orbit in three dimensional space. Fiber-fiber interactions in semi-dilute and concentrated suspensions of rigid fibers are assumed to be well represented by the addition of a diffusion term to Jeffery's equation [14–16].

To obtain further advances in the resulting processed part's performance beyond those observed from short fibers, there is a strong industrial desire to incorporate fibers with increased aspect ratios. Long fibers (normally with aspect ratio larger than 20) are desired for manufacturing fiber reinforced composites largely because they offer better mechanical stiffness as well as the thermal and electrical properties when they are aligned than the corresponding short fiber composites. They also offer better material properties for some specific applications, such as impact strength. An apparent draw back is their tendency to flex during processing [17], which both reduces the material improvements anticipated as well as diminishes the accuracy of the existing models for simulating the motion of short rigid fibers. Jeffery's equation is unable to describe the motion of a long flexible fiber, which will experience both bending and twisting during processing [18]. Also, the alignment of long fibers in the flow will cause a great increase in the viscosity of the fluid, thus inducing a higher shear stress on the fibers [11, 19]. A balance of incorporating long fibers into composites with the least possible deformation of the fibers during the manufacturing will offer the optimal material properties.

Several models have employed different mathematical representations for flexible fibers, such as a series of beads [1, 2, 10, 20], rods [21] and spheroids/needles [3, 9, 18, 22–25]. The bead chain model represents a single flexible fiber as a series

of spheres that can stretch, bend and twist relative to each other. The rod chain model optimizes the bead chain model by combining several beads into a rigid rod. Then the rods are connected to represent a single flexible fiber. The spheroid model represents a single flexible fiber with rigid bodies connected by joints. All these three models describe the motion of a flexible fiber under a pure shear flow by solving the motion equations along with satisfying the continuum requirement of the models. The motion of a flexible fiber in a pure shear flow differs from that of a rigid fiber in the same flow in terms of the motion period and orientation space path [18]. Effective models for describing the motion and orientation of flexible fibers must yield results approaching that of Jeffery's equation as fiber rigidity increases.

The rod chain model of Wang *et al.* [21] has been adopted in the present work due to its clarity of the physics and simplicity of the model, which may lend itself to a distribution approach required for industrial simulations. This thesis provides a comparison of the flexible fiber model to the classical Jeffery's equation for rigid fibers. The results show that the motion period of the flexible fiber decreases relative to that of the rigid fiber, and the period is inversely proportional to the stiffness of the fiber. Simulation results of the cured composites for distributions of flexible fibers are also studied to show the areas of overlap and areas of differences between those of a flexible fiber suspension and model results that assume rigid fibers during processing.

A literature review of the modeling of flexible fiber motion and the prediction of material properties for discontinuous fiber reinforced composites is given in Chapter Two. A comparison between models for rigid fiber motion and those for flexible fiber motion is presented in Chapter Two, along with an extensive review of the classical rigid fiber model, Jeffery's equation, multiple flexible fiber models, and especially the rod chain model used in this research. Chapter Two concludes with a discussion of

the existing stiffness approaches for straight fibers, with the extension to flexible fibers left to Chapter Four. Chapter Three compares the orientation results from the Jeffery model for straight fibers to those of the rod chain model. Results are presented for both individual fibers and a stochastic distribution of fibers to study the variations in the transient effects between the rigid and the flexible fiber systems. Scenarios are presented to discuss when the Jeffery model is appropriate for long fibers, as well as a qualitative feel for the anticipated error as the fiber flexure increases. Chapter Four investigates the processed part's stiffness due to variations in the underlying fiber orientation and stiffness. The cured composite stiffness is presented for the flexible fiber system using the micro-mechanical approach of Hsiao and Daniel [4] for individual flexible fibers combined with the spatial homogenization of the stiffness for a distribution of fibers discussed by Jack and Smith [5] previously only for straight fibers. This thesis concludes with a summary of the scientific contributions created by this work along with a listing of anticipated and suggested future research studies.

CHAPTER TWO

Literature Review of Fiber Motion and Orientation Modeling and Stiffness Prediction

This chapter starts with a description of the injection molding process as the background information and then gives a literature review over the models of fiber motion simulation and material property prediction. Three major flexible fiber models are described in details, which are the bead chain model, the needle chain model and the rod chain model. The orientation homogenization method for the prediction of the stiffness of fiber reinforced composites is discussed at the end of this chapter.

2.1 Injection Molding of Fiber Reinforced Composites

Injection molding has become the most commonly used manufacturing process for the fabrication of a range of thermoplastic products with varying sizes, complexity and application [26,27]. Typical product categories include housewares, toys, automotive parts, furniture, rigid packaging items, appliances and medical disposal syringes. Injection molding has the following advantages:

- Accuracy in weight of articles
- Choice of desired surface finish and colors
- Choice of ultimate strength of articles
- Faster production and lower rejection rates
- Faster start-up and shut down procedures
- Minimum wastage
- Stability of processing parameters

- Versatility in processing different raw materials
- Option in article sizes by changing the mold
- Minimum post molding operations

The injection molding process requires the use of an injection molding machine, raw plastic materials, and a mold. An injection molding machine includes a plasticizing/injection unit, a clamping unit, a control system and tempering devices for the mold (Figure 2.1). An injection mold is the central element of the injection molding process. It is made of at least two parts, which are clamped onto the injection molding machine. The mold contains a cavity, into which the thermoplastic material is injected and which forms the final part geometry. The general procedures of injection molding include melting the plastic in the injection molding machine and then injecting the melt into the mold, where it cools and solidifies into final parts.

The complete injection molding cycle takes place in the following steps

1. Plastication: Raw material, normally in the form of pellets or powders, is added into an empty barrel through the feed hopper, as shown in Figure 2.1. The raw material is plasticized to a fluid state with the help external heaters on the barrel in the process of passing through the barrel under the force from the rotation of the screw inside the barrel.
2. Clamping: The mold, as shown in Figure 2.1 closes until the two halves are in close contact.
3. Injection: The screw moves forward axially without rotation and carry the melt into the cavity in the mold. The mold is filled with hot melt. As the molded part in the mold cools down from the melt temperature, further melt is conveyed into the cavity to compensate for volume contraction. Subsequently, the injection unit starts plasticizing and preparing material for the next shot.

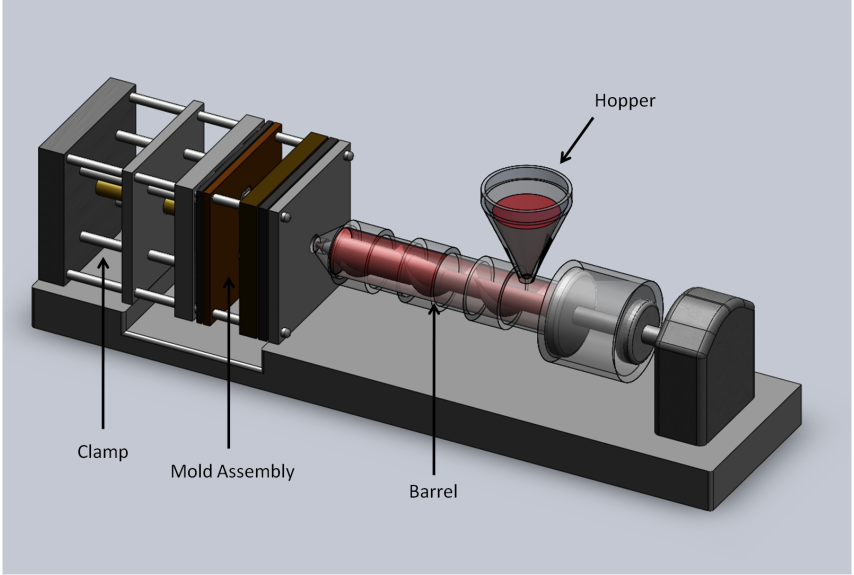

Figure 2.1: A general display of an injection molding machine.

4. Ejection: After the molded part has cooled sufficiently, the mold opens and the finished part is ejected. The mold closes again ready for the next cycle.
5. Repeat stages 2 to 4.

Fiber reinforced thermoplastic composites are widely used in industry, especially in automotive industry, as they can offer low cost, light weight and high durability structural materials. Long fiber reinforced composites offer even much better mechanical performance than the short fiber composites as the higher aspect ratios of the long fibers considerably increase the composite stiffness and strength, and enhance creep and fatigue endurance [28, 29]. The injection molding equipment can be adjusted with some specific tool design in low cost of part production to produce fiber reinforced composites. A number of factors affect the final quality of the injection molded parts. This study focuses on the influence of the long fiber orientation and flexure on the material properties in the final processed part. During the injection stage, the melt flow with the fibers filling the mold goes through three stages identified as three regions: the gate region, the lubrication region and the fountain regain. The

majority of the flow will be contained in the lubrication region. Thus, it is normally assumed the orientation of the fibers are only greatly influenced by this region, which is also the focusing study of this research. The flexure of the long fibers will also come into play to influence (normally decrease) the properties of the final processed composites.

The design or the prediction of the properties of the long fiber reinforced composite materials should take into account many factors, including the fiber orientation and flexure. This study predicts the stiffness of the processed parts by studying the dynamics of the fibers in the flow in the lubrication region of the injection molding process along with compensating the influence of the fiber flexure.

2.2 Short Straight Fiber Motion and Orientation Modeling

The research of fiber motion begins with short rigid fibers. The concepts created and the methods used are the starting point for the research of long flexible fiber motion. This section covers the work on short fiber motion, including the models proposed and the approaches created in order to give enough background information to understand the research on long flexible fiber motion.

2.2.1 Fiber Orientation

The orientation of a short rigid fiber can be described by a unit direction vector $\boldsymbol{p}$, usually expressed in a spherical coordinate system by an angle pair (θ,ϕ) (Figure 2.2) as

$$\boldsymbol{p} = \left\{ \begin{array}{c} \sin\theta\cos\phi \\ \sin\theta\sin\phi \\ \cos\theta \end{array} \right\} \tag{2.1}$$

As the two ends of the fibers are essentially indistinguishable [30], a fiber's orientation can be described by either $\boldsymbol{p}(\theta,\phi)$ or $-\boldsymbol{p}(\theta,\phi)$ without any difference. Then the

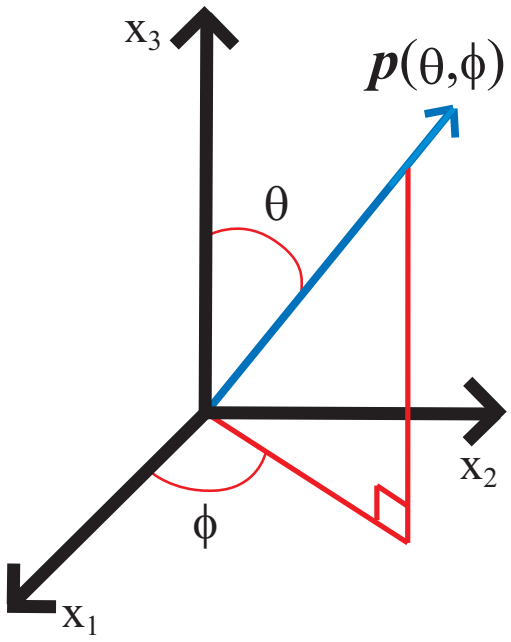

Figure 2.2: Coordinate system defining the unit direction vector $\boldsymbol{p}(\theta, \phi)$ along with angles θ and ϕ.

following relationship is valid when describing fiber orientation

$$(\theta, \phi) \rightarrow (\pi - \theta, \pi + \phi) \tag{2.2}$$

Since modeling individual fibers is industrially impractical, the discrete set of fibers is often assumed to satisfy a given continuous probability distribution function $\psi(\theta, \phi)$. Then the probability of a fiber orienting between the angles θ_i and $\theta_i + d\theta$ and between ϕ_i and $\phi_i + d\phi$ is defined as [31]

$$P(\theta_i \leq \theta \leq \theta_i + d\theta, \phi_i \leq \phi \leq \phi_i + d\phi) = \psi(\theta, \phi) \sin\theta_i d\theta d\phi \tag{2.3}$$

And the probability function $\psi(\theta, \phi)$ has the following property because of Equation (2.2) as

$$\psi(\theta, \phi) = \psi(\pi - \theta, \pi + \phi) \tag{2.4}$$

The orientation of any fiber can be described by some angle pair $(\theta, \phi) \in \mathbb{S}^2$. Thus the distribution function must satisfy the normalization function, which means that

the integral of the distribution function over the unit sphere $\mathbb{S}^2$ equals to one

$$\oint_{\mathbb{S}^2} \psi(\theta, \phi) d\mathbb{S} = \int_0^{2\pi} \int_0^{\pi} \psi \sin\theta d\theta d\phi = 1 \tag{2.5}$$

The fiber distribution function is a complete description if the orientation of a fiber is statistically unrelated with that of any of its neighboring fibers, and is considered to be continuous and varying smoothly with position [30]. However, the calculations with the distribution function are too computationally costly when applied to industrially relevant flows. Besides, the distribution function does not provide a convenient and straight-forward understanding of the physical behaviors of the fibers [5, 6, 30, 32]. Advani and Tucker [6] suggest using tensors to describe the average orientation property over a volume. This volume should be large enough to contain many fibers, but small enough such that the statistics of the orientation are uniform throughout. This assumption is valid when the volume is small compared to the dimension of the part but large compared to the fiber length [33]. For example, for a spherical volume, the diameter of the sphere is at least twice the length of the fibers. The so called orientation tensors are calculated as the moments of the distribution to capture the statistical behavior of the distribution function [6]

$$a_{ij\ldots} = \oint_{\mathbb{S}^2} p_i p_j \ldots \psi(\theta, \phi) d\mathbb{S} \tag{2.6}$$

Notice the odd ordered orientation tensors have components all zero due to the property of the distribution function shown in Equation (2.4). The orientation tensors are symmetric and have the following properties

$$\begin{aligned} a_{ij} &= a_{ji} \\ a_{ijkl} &= a_{klij} = a_{jikl} = a_{ilkj} = \ldots \\ a_{ijklmn} &= a_{jiklmn} = a_{klijmn} = a_{mnklij} = a_{ilkjmn} = a_{inklmj} = \ldots \end{aligned} \tag{2.7}$$

Because of the symmetry of the orientation tensors, there are six independent components of the second order orientation tensor a_{ij}, which are reduced to five as the normalization condition of Equation (2.5) is also considered [34]. Similarly, there are 14 independent components of the fourth order orientation tensor a_{ijkl}, 27 independent components of the sixth order orientation tensor a_{ijklmn}, 44 independent components of the eighth order orientation tensor $a_{ijklmnop}$ and 65 independent components of the tenth order orientation tensor $a_{ijklmnopqr}$ [34]. The orientation tensors are an incomplete representation of the fiber distribution function, but are very useful and widely used in industrial simulations of fiber orientations.

2.2.2 Jeffery's Equation

The investigation into fiber dynamics in various flows has been for decades an active and extensive research topic due to the strong dependence the processed product's material properties have on the underlying fiber orientation [4, 35–38]. Thus predicting the spatially varying fiber orientation is essential for the design of fiber reinforced composites. Models for simulating the motion of short rigid fibers in various flows have been constructed. One of the earliest research on fiber motion and orientation was Jeffery's equation [13], first published in 1923. It describes the motion of an ellipsoidal particle in a newtonian flow by the following equation

$$\dot{\boldsymbol{p}} = \frac{D\boldsymbol{p}}{Dt} = \boldsymbol{\Omega} \cdot \boldsymbol{p} + \lambda[\mathbf{D} \cdot \boldsymbol{p} - \mathbf{D} : \boldsymbol{ppp}] \tag{2.8}$$

where a_r is the fiber aspect ratio and a_e is the effective aspect ratio. For a long cylindrical rod, a_e can be calculated by $a_e = a_r 1.24/\sqrt{\ln(a_r)}$ [39–41]. $\lambda = \frac{a_e^2-1}{a_e^2+1}$ is a shape correction factor for cylindrical rods, $\boldsymbol{\Omega} = (\boldsymbol{\kappa} - \boldsymbol{\kappa}^T)$ is the vorticity tensor, and $\mathbf{D} = (\boldsymbol{\kappa} + \boldsymbol{\kappa}^T)$ is the rate of deformation tensor where $\boldsymbol{\kappa}$ is the gradient of the velocity vector. $\boldsymbol{p}$ is the unit direction vector of the fiber, which is a function of two angle

parameters θ and ϕ as shown in Figure 2.2 and defined in Equation (2.1). In a shear flow the rigid ellipsoid rotates and remains on its initial streamline and periodically repeats the same orbit in the absence of interacting with the environment (other fibers, body forces, etc.) (Figure 2.3). There is an orbit constant C associated with the motion trajectory defined as

$$C = \tan\alpha_0 \sqrt{\cos^2\gamma_0 + \frac{1}{a_e^2}\sin^2\gamma_0} \tag{2.9}$$

where (α_0, γ_0) is the initial orientation and a_e is the equivalent aspect ratio of the ellipsoid. α is the angle between the fiber axis and the vorticity direction (y-axis) of the shear flow and γ is the angle between the orthogonal axis (z-axis) and the $x-z$ projection of the fiber axis. $C \to \infty$ corresponds to a spheroid tumbling in the plane of shear, and $C = 0$ corresponds to a motion where the spheroid spins in the vorticity direction.

Jeffery's equation can be solved numerically to provide the transient solution of the orientation of an individual fiber. It can be shown that Jeffery's equation predicts a periodical behavior for a fiber in a pure shearing flow with an orbital period given by [25]

$$T_{orbit} = \frac{2\pi}{\dot{\gamma}}(a_e + \frac{1}{a_e}) \tag{2.10}$$

where the shear rate $\dot{\gamma} = \sqrt{2\mathrm{tr}(\mathbf{D}^2)}$.

However, Jeffery's equation is only valid for rigid fibers in a dilute suspension, and cannot be used for fibers in a semi-dilute or a concentrated suspension. Folgar and Tucker [37] introduced a diffusion term to the original Jeffery's equation in order to solve this problem, and several authors have proposed improvements on the original model. Neither the Jeffery's equation nor the form with a diffusion term is capable

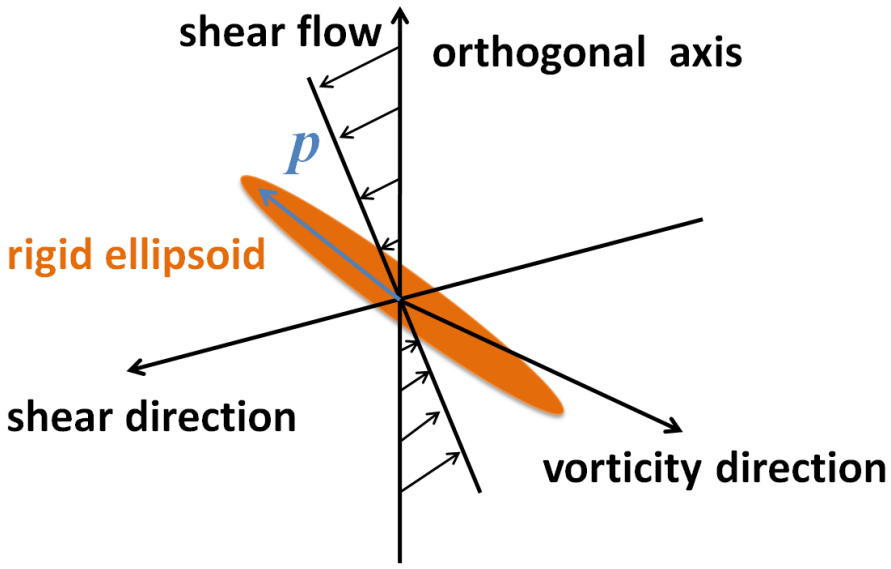

Figure 2.3: A rigid ellipsoid in a shear flow.

of describing the motion of a distribution of long flexible fibers as any fiber bending and twisting is ignored based on the perfect rigidity assumption.

2.2.3 The Folgar-Tucker Model

Jeffery's equation only applies to fiber suspensions with no fiber interactions, requiring a dilute suspension, defined when the inverse of the square of the aspect ratio a_r of the fiber is much greater than the volume fraction V_f of the fibers, i.e. $V_f \leq \frac{1}{a_r^2}$ [30,34]. The semi-dilute suspension is defined such that $\frac{1}{a_r^2} \leq V_f \leq \frac{1}{a_r}$ [30,34]. The concentrated suspension is defined such as $V_f > \frac{1}{a_r}$. For the typical fiber aspect ratios ranging from 10 to 20 [42], the volume fraction of the fiber has to be less than 1% to have a dilute suspension and between 1% and 10% to have a semi-dilute suspension. Typical industrial manufacturing of fiber reinforced composites require the fiber volume fraction to be much greater than 10% thus inducing fiber interactions, which means Jeffery's equation is of little use in industrial applications.

The modeling of fiber interaction is often modeled using a form similar to the theory of rotary Brownian motion [34, 43, 44], where the interacting ellipsoids collide with each other within the flow causing forces and torques on each other. The rotary Brownian motion has been perviously used to model the dynamics of polymer liquids whereby the interactions are models as being caused by directionally dependent diffusion processes [34, 43, 44]. The first model accounting for the fiber interaction by adding a diffusion term is given by Bird [44]:

$$\frac{D\psi}{Dt} = -\nabla \cdot [\dot{\boldsymbol{p}}\psi(\boldsymbol{p}) - \nabla(D_r\psi(\boldsymbol{p}))] = -\nabla \cdot [\dot{\boldsymbol{p}}\psi(\boldsymbol{p})] + \nabla^2[D_r\psi(\boldsymbol{p})] \tag{2.11}$$

where D_r is the rotary diffusivity. When it is assumed that there is no fiber interactions, which results in D_r to be zero, the model of Equation (2.11) is essentially the same as the model of Jeffery's equation. Folgar and Tucker [14] propose a diffusivity function based on the rate of deformation tensor $\mathbf{D}$ along with an empirical derived parameter C_I:

$$D_r = C_I\dot{\gamma} \tag{2.12}$$

where $\dot{\gamma}$ is the scalar magnitude of the rate of deformation tensor $\mathbf{D}$. This model neglects the directional dependence of the collision interaction between the fibers. The Folgar-Tucker model has been the standard for both industrial and academic communities because of its exceptional results.

2.2.4 The Advani-Tucker Model

The orientation tensors are proposed by Advani and Tucker [6] to describe the averaged orientation of a fiber suspension. They also developed the equation of motion for the second order orientation tensor with the diffusivity term as

$$\frac{Da_{ij}}{Dt} = \oint_{\mathbb{S}^2} \dot{\boldsymbol{p}}\psi \cdot \nabla(p_ip_j)d\mathbb{S} - \oint_{\mathbb{S}^2} \nabla(D_r\psi) \cdot \nabla(p_ip_j)d\mathbb{S} \tag{2.13}$$

where the first term on the right-hand side is the rate of change of motion due to hydrodynamic forces, which is essentially the same as given by Jeffery's equation, and the second term is the change due to rotary diffusion. The first term can be rewritten by the chain rule in the following form

$$\begin{aligned}\oint_{\mathbb{S}^2} \dot{\boldsymbol{p}}\psi \cdot \nabla(p_i p_j) d\mathbb{S} &= -\frac{1}{2}\Omega_{ik}a_{kj} + \frac{1}{2}a_{ik}\Omega_{kj} \\ &\quad + \frac{1}{2}\lambda(D_{ik}a_{kj} + a_{ik}D_{kj} - 2D_{kl}a_{ijkl}) \end{aligned} \tag{2.14}$$

where D_{ik}, D_{kj} and D_{kl} are the index forms of the rate of deformation tensor. a_{ijkl} is the index form of the fourth order orientation tensor. Notice that the appearance of the fourth order orientation tensor on the right-hand side of Equation (2.14) induces the classic closure problem. The second term on the right-hand side of Equation (2.13) is also written by the chain rule in the following form

$$\oint_{\mathbb{S}^2} \nabla(D_r\psi) \cdot \nabla(p_i p_j) d\mathbb{S} = \oint_{\mathbb{S}} D_r\psi(2\delta_{ij} - 6p_i p_j) d\mathbb{S}$$

Therefore the motion equation of the second order orientation tensor is written by combining Equation (2.14) and Equation (2.15) in the following form

$$\begin{aligned}\frac{Da_{ij}}{Dt} &= -\frac{1}{2}\Omega_{ik}a_{kj} + \frac{1}{2}a_{ik}\Omega_{kj} + \frac{1}{2}\lambda(D_{ik}a_{kj} + a_{ik}D_{kj} - 2D_{kl}a_{ijkl}) \\ &\quad + \oint_{\mathbb{S}} D_r\psi(2\delta_{ij} - 6p_i p_j) d\mathbb{S} \end{aligned} \tag{2.15}$$

Notice Equation (2.15) also shows the closure problem. By assuming the diffusivity term is of the form given by Folgar and Tucker, the resulting equation of motion of the second order orientation tensor is written as

$$\begin{aligned}\frac{Da_{ij}}{Dt} &= -\frac{1}{2}\Omega_{ik}a_{kj} + \frac{1}{2}a_{ik}\Omega_{kj} + \frac{1}{2}\lambda(D_{ik}a_{kj} + a_{ik}D_{kj} - 2D_{kl}a_{ijkl}) \\ &\quad + C_I\dot{\gamma}(2\delta_{ij} - 6a_{ij}) \end{aligned} \tag{2.16}$$

The computation of the evolution of the second order orientation tensor requires knowledge of at least the fourth order orientation tensor, which induces the classic closure problem.

2.2.5 Orientation Closure

The orientation closure is an approximation method of representing higher order orientation tensors in terms of lower order orientation tensors. A fourth order closure may be expressed as:

$$a_{ijkl} \approx F_{ijkl}(a_{mn}) \tag{2.17}$$

where F_{ijkl} is a function of the second order tensor a_{ij}. A six-order orientation tensor closure may be expressed as

$$a_{ijklmn} \approx G_{ijklmn}(a_{opqr}) \tag{2.18}$$

where G_{ijklmn} is a function of the fourth order orientation tensor a_{oprq}. There have been many methods proposed to address the closure problem. The hybrid closure proposed by Advani and Tucker [6] is the most widely used method in industry because of its algebraic simplicity and numerical robustness. The hybrid closure linearly combines the quadratic closure of Doi [45] and the linear closure of Hand [46] as

$$a_{ijkl} = (1 - f)\hat{a}_{ijkl} + f\bar{a}_{ijkl} \tag{2.19}$$

where the first term on the right-hand side contains the linear closure as

$$\begin{aligned} \hat{a}_{ijkl} = \; & - \; \frac{1}{35}(\delta_{ij}\delta_{kl} + \delta_{ik}\delta_{jl} + \delta_{il}\delta_{jk}) + \frac{1}{7}(a_{ij}\delta kl + a_{ik}\delta_{jl} \\ & + \; a_{il}\delta_{jk} + a_{kl}\delta_{ij} + a_{jl}\delta_{ik} + a_{jk}\delta_{il}) \end{aligned} \tag{2.20}$$

and the second term of Equation (2.19) contains the quadratic closure as

$$\bar{a}_{ijkl} = a_{ij}a_{kl}$$

The hybrid closure is used to investigate the Advani-Tucker model and is frequently used in commercial softwares for simulating injection molding of composites. Although the hybrid closure gives significant improvement over previously existing methods, it tends to over-predict the alignment state [47].

The orthotropic closure is a series of eigenvalue based fourth order fitted closure first proposed by Cintra and Tucker [48] and then modified by Chaubal and Leal [49], VerWeyst *et al.* [12], Chung and Kwon [50], Han and Im [51]. They give better accuracy over the hybrid closure but at the price of more computational efforts. Schache, Jack and Smith [52–54] developed the fourth order neural network based closure (NNET) and demonstrated its effectiveness in simple flows of short fiber suspensions. The NNET balanced the accuracy of the orthotropic closure and the efficiency of the hybrid closure [54]. Montgomery-Smith and Jack [55, 56] developed the fast exact closure (FEC). It is not a closure method in the traditional sense as it does not rely upon an approximation, which is based on selecting fourth order orientation tensors and will give exact solutions for suspensions in the dilute regime. This approach does not involve any curve fitting, instead it relies on solving a series of related ordinary differential equations. With all the existing fourth order orientation tensor closure approximation method, Jack [57, 58] and Jack and Smith [59] demonstrate that further research on fourth order closures is expected to yield only minor improvements in accuracy. Thus it is necessary to carry out investigation into higher order orientation tensor closures in order to gain significant increase in accuracy.

The motion of flexible fiber is more complicated due to its flexibility and thus the deformation under the influence of the flow. It is worthwhile to pursue a similar approach of developing an equation for the evolution of the orientation tensor for

a distribution of flexible fibers. Then a diffusion term can be added to address the intra- and inter-fiber interactions.

2.3 Discrete Element Modeling of Flexible Fiber Motion and Orientation

The modeling of flexible fiber motion takes a different route from that of rigid short fiber, as there has not been an explicit mathematical equation which governs the motion of a distribution of flexible bodies in a flow due to the deformation (bending and twisting) of the flexible bodies under the influence of the flow. The models for individual fibers usually assume that the flexible fiber consists of multiple rigid parts connected with each other. The bending and twisting deformation is reflected by allowing movement of the rigid parts relative to each other. This section first gives a brief overview of the recent flexible fiber models, among which, the bead chain model [1,2], needle chain model [3,22] and rod chain model [21] are the most relevant to this research. A detailed description of these three models are then discussed.

2.3.1 An Overview

Yamamoto and Matsuoka created a bead-chain model in 1992 [1, 2] for simulating the motion of a flexible fiber in a simple shear flow under the conditions of an infinitely dilute system, no hydrodynamic interaction and low Reynolds number. They assumed fibers can be represented by a series of spheres that are lined up and bonded to each other (Figure 2.4). They demonstrated their model by the simulation of the movement of a flexible fiber by solving the developed translational and rotational equations for each individual spheres. The flexibility of a fiber is adjusted by varying the bending constant of the fiber. A large bending constant corresponds to a rigid fiber. In order to verify the model, the motion period was calculated for a rigid fiber, which agreed with that from the prediction by Jeffery's equation. For the

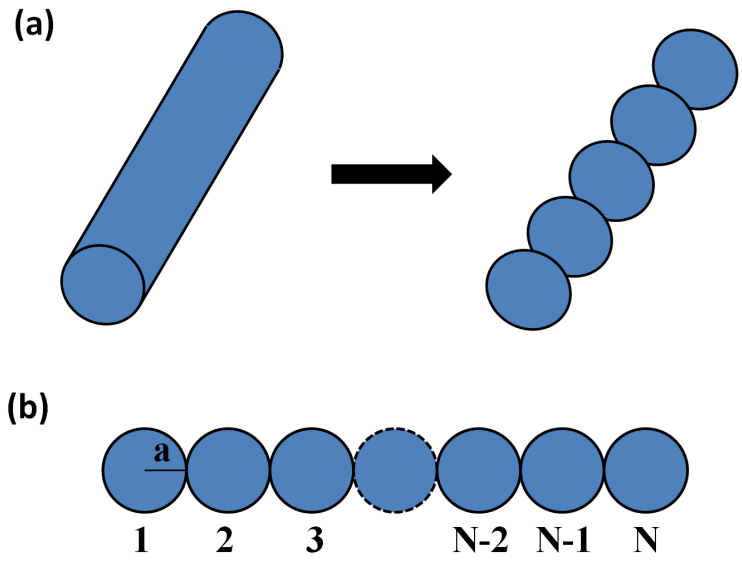

Figure 2.4: (a) Schematic fiber representation of the bead chain model; (b) Schematic fiber model made up of N spheres of radius a [1, 2].

flexible fiber, the motion period decreases dramatically as the bending deformation of the fiber became obvious and the motion orbit deviated from the one Jeffery's equation described, which was similar to the experimental results described by Forgacs and Mason [60]. Simulation results from this model show the movement of every point on the fiber accurately, but require a significant computational effort as the fiber becomes very long, which is the desired case to study for industrial applications. A detail description of the bead chain model for an isolated flexible fiber moving in a simple shear flow is given in Section 2.3.2.

The bead chain model was then modified by Yamamoto and Matsuka [10, 20] to simulate the motion of fibers in a concentrated shear flow. Only the hydrodynamic interaction is considered. They assume the hydrodynamic interaction can be decomposed into two parts, intra- and inter-fiber ones. The intra-fiber interactions are calculated using the N-body mobility matrix for each fiber. The inter-fiber interactions are calculated by the lubrication approximation. This model is used to predict

the influence of several parameters, such as the fiber aspect ratio, fiber flexibility and fiber volume fraction, on the microstructure and the rheological properties of fiber suspensions. The lubrication approximation is also used in a model proposed by Yamane *et al.* [61] to simulate the motion of semi-dilute suspensions of non-Brownian, rod-like particles under simple shear flow. Although this model does not address the motion of flexible fibers, it offers insight into the effectiveness of accounting for short range fiber interactions by the lubrication approximation. Yamane *et al.* found the effect of the hydrodynamic interaction on the viscosity as well as the Folgar-Tucker constant is small, which disagrees with the experimental results. The authors explain this as a result of non-Brownian motion of the rigid rods.

Ross and Klingenberg [3] simulated the dynamics of flexible fiber suspensions by representing a flexible fiber by a series rigid spheroid bodies connected through ball and socket joints (Figure 2.5), which is usually named the needle chain model. The motion of the fiber was determined by solving the translational and rotational equations of motion for each rigid body. This model is used to simulate the motion of both rigid and flexible fibers. The motion period of a single rigid fiber in a shear flow predicted by this model agreed with that from Jeffery's equation and the motion of a flexible fiber was similar to the experimental observations of Forgacs and Mason [60]. The model is similar to that proposed by Yamamoto and Matsuoka, except the joints are modeled as ball and socket, where the resistance can be varied to adapt the model for both flexible and rigid fibers. And this model eludes the need for iterative constraints to maintain fiber connectivity, and can model flexible fibers with large aspect ratios with relatively few spheroids, which will help significantly to reduce the computation time. However, larger needle lengths diminished the accuracy of the model. A detailed description of the needle chain model is given in section 2.3.3. This model

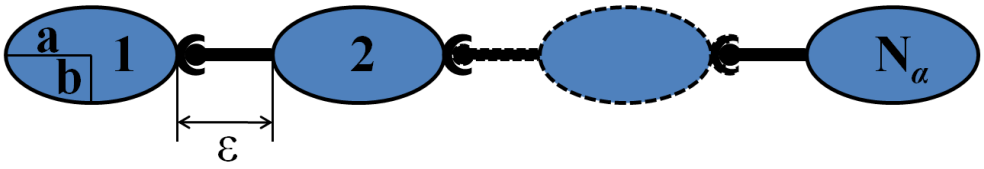

Figure 2.5: A flexible fiber is represented as linked rigid bodies. a and b are the spheroid major and minor axis, respectively. The parameter ε is the separation between spheroids (usually $\varepsilon = 0.01b$) [3].

was also used to simulate the motion of fiber suspensions by only accounting for the repulsive interactions and neglecting the hydrodynamic interactions and particle inertia. The repulsive interactions include both intra- and inter-fiber interactions, such as colloidal forces, short-range repulsion and friction between fibers. The transient behavior of the relative viscosity of the suspension under simple shear flow is investigated. They found the flexibility of fiber increases the hydrodynamic contribution to the viscosity.

Skjetnet, Ross and Klingenberg [22] published a follow-up article to give more insight into the needle chain model. The simulation results for flexible fibers agree with previous experimental observations where the direction and the rate of drift from the Jeffery orbit depend on a few factors, such as fiber stiffness, fiber initial orientation and the flow field. Schmid *et al.* [23] followed the way of the needle chain model and developed a particle-level model to simulate the motion of flexible fibers by treating a flexible fiber as a chain of elongated bodies connected by hinges. This model is used to simulate flocculation in flowing fiber suspensions. The model incorporates fiber flexibility, irregular fiber equilibrium shapes, and frictional fiber interactions. They found flocculation forms due to inter-fiber friction and repulsive interactions in the absence of attractive forces between fibers. The simulations have demonstrated that fiber features (stiffness, fiber shape, etc.) and interaction forces strongly affect

flocculation behavior and floc properties. Switzer and Klingenberg [18, 24] further investigated the relationships between fiber properties and interactions, and the resulting suspension rheological properties for a simple shear flow. Their model is based on the method of Schmid *et al.*, where the flexible suspensions are modeled as chains of neutrally buoyant, linked rigid bodies connected by ball and socket joints immersed in a Newtonian liquid. The fiber interact with other fibers via short-range repulsive forces and friction forces. The simulation results repeat the ones given by Schmid *et al.* and they have shown fiber flexibility results in shear thinning behavior as a result of competition between hydrodynamic forces and fiber elasticity.

The hydrodynamic interactions are taken into account in the model created by Fan *et al.* [62] to simulate the motion of rigid fiber suspensions. The interactions are considered in two folds with a short range interaction via lubrication forces and a long range interaction via slender body approximation. They demonstrated that the method can well simulate the motion of fiber suspensions. Rheological properties, such as the relative viscosity and the Folgar-Tucker's constant, were calculated. They found in the semi-concentrated and concentrated regime, the fibers do not follow the Jeffery's orbits, and instead, they align mostly with the shear direction. Computational time is also an issue with this simulation method. The authors suggested a reduction in the computational time by a master-slave implementation in a distributed computing environment, and it is worth pursuing this in future studies.

Based on the work by Yamane *et al.* and Fan *et al.*, Joung *et al.* [25] created a model to simulate the motion of flexible fiber suspensions. They modified the Yamane and the Fan models to allow a small amount of bending and torsion in the fibers along with a restoring moment acting to straighten the fibers as they interact in the flow. The fibers are modeled as a chain of beads joined with connectors,

which is similar to the bead chain and need chain model but with a different way to determine internal moments and subsequent fiber shapes. The connectors in the fiber chain are allowed to rotate in relation to each other and therefore allow the deformation of the fiber as it interacts with its environment. The fiber interactions include external viscous drag and long ranges hydrodynamic effects and short range lubrication forces between beads. The model was used to obtain the rheological information of the suspensions, such as fiber orientations and suspension viscosity. The model reproduced the Jeffery orbit and motion period for undisturbed rigid fibers. The predicted viscosity for rigid fiber suspensions agreed well with the experimental results. For long flexible fiber suspensions, the prediction for viscosity is markedly improved when fiber flexibility is accounted for. The Joung model warrants future studies and is a candidate for investigations into forming an industrial form using a distribution averaging procedure. This model is also used to investigate the relationship between fiber curvature and viscosity of a fiber suspension [9]. They have shown there is a rapid and large increase in bulk viscosity as fiber curvature is increased. The authors speculated the reason of the curvature-viscosity relationship is due to the propensity of a curved fiber suspension to misalignment and misalignment causes viscosity increasing.

Wang *et al.* [21] performed numerical simulations of the motion of an isolated flexible fiber in a Newtonian flow with a rod chain model. A long flexible fiber is composed by a series of rigid rods, each of which is a rigid straight chain of beads (Figure 2.6). The length of each rod can be adjusted by the number of component beads in order to reflect the flexibility of the fiber. Shorter rods result in a more flexible fiber. The connectivity of the fiber is maintained by internal constraint forces at the joints of the rods. A detailed description of the rod chain model is given in

section 2.3.4. The rod chain model is conceptually similar to the needle chain model but adopts a different way to determine the internal constraint forces. They have found that the fiber exhibit different apparent flexibility depending on the stiffness of the fiber, the strength of the flow field and the initial orientation of the fiber. Results comparing the rod length selection in terms of the computational time and the relative error have been presented and an optimum rod length is suggested to balance the computational time and accuracy. The rod chain model is chosen in this research to carry out flexible fiber orientation modeling and the subsequent material property predictions due to its clarity of the physics and simplicity of the model.

Most of the work on fiber motion is limited to zero Reynolds number flows, where inertia of fluid and particles is neglected, even though the fiber orientation is influenced by the inertia effect at the Reynolds number as small as 10^{-3}. And in many situations, the Reynolds number is large and inertia cannot be neglected. Thus Qi [63] created a modle to simulate the movement of a flexible cylindrical fiber based on the lattice Boltzmann equation to account for the inertia. This methods is equivalent to solving the Navier-Stokes equations where nonlinear inertia effects are intrinsically included. In the model, a long flexible fiber is represented as a chain of rigid cylindrical segments connected with each other by ball and socket joints that allow rotation in three dimensions. Also, there is a constraint force imposed at each joint, which can be solved using joint contacting conditions. It is shown that the flow inertia forces the long flexible fiber perpendicular to the vorticity of the flow and the motion period increases as the Reynolds number increases. These simulation results well correspond with experimental results. This model can be used to study nonlinear inertial interactions between the flexible fibers and the fluid and worth of further pursuing.

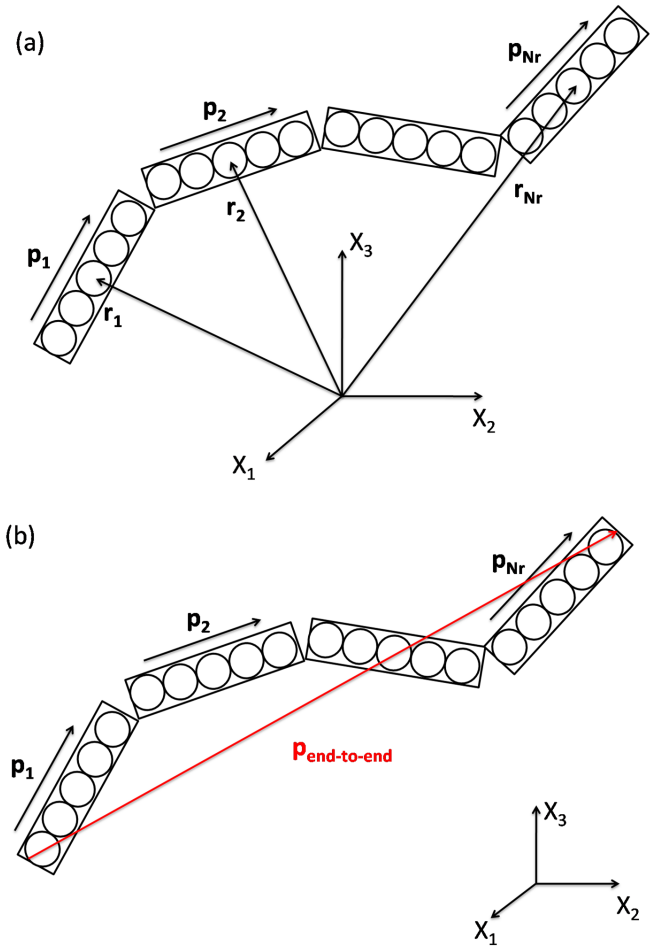

Figure 2.6: (a) The schematics of the rod chain model, (b) end-to-end vector showing the orientation of the flexible fiber.

Lindstrom and Uesaka [64, 65] extended the work of Schmid *et al.* [23] but with significant modifications by allowing the model to simulate the motion of semi-dilute/semi-concentrated fiber suspensions taking into account fiber hydrodynamic interactions and fiber-flow coupling. A fiber is modeled as a chain of segments, interacting with the fluid through viscous and dynamic drag forces. The two-way coupling between the solid and the fluid phase is taken into account by enforcing momentum conservation. The model includes long-range and short-range hydrodynamic fiber-fiber interactions, as well as mechanical interactions. Simulation results are consistent with the experimental results for both the semi-dilute and the concentrated

regimes. From their results, they show the viscosity depends primarily on volume concentration, and that fiber aspect ratio has only a weak influence.

2.3.2 The Bead Chain Model

This section gives the detailed construction of the bead chain model for an isolated flexible fiber of Yamamoto and Matsuoka [1,2]. Modification can be made to address fiber interactions, the details of which can be found in these two publications [10, 20]. In the bead chain model [1, 2], the fiber is represented as a cylindrical rod made up of N spheres each of radius a, connected with each other (Figure 2.4). The cylindrical rod/fiber is of length $2aN$, diameter $2a$ and an aspect ratio of N. Each pair of neighboring spheres can stretch, bend, and twist by changing their bond distance, bond angle, and torsion angle respectively.

For a pair of adjacent spheres i and j, there will be a force F^s exerted on each sphere to recover the equilibrium. This force is proportional to the change in the equilibrium distance r_0 between the two spheres, where the actual distance is r (Figure 2.7(a)). The force is expressed as a simple spring restoring force as [1, 2]

$$F^s = -k_s(r - r_0) \tag{2.21}$$

where k_s is the stretching force constant, expressed as $k_s = \frac{\pi a}{2}E$ with E being the elastic modulus of the fiber. The direction of the force is pointing from the center of the sphere i to the center of the sphere j, which is along a unit direction vector n_{ij} defined as [1, 2]

$$\mathbf{n}_{ij} = \frac{\mathbf{r}_j - \mathbf{r}_i}{\|\mathbf{r}_j - \mathbf{r}_i\|} \tag{2.22}$$

where $\mathbf{r}_i$ and $\mathbf{r}_j$ are the position vector of the centers of sphere i and sphere j.

The bending torque between spheres is a function of the bond angle θ_b between the spheres (Figure 2.7(b)). There will be a bending torque T^b exerting on each sphere

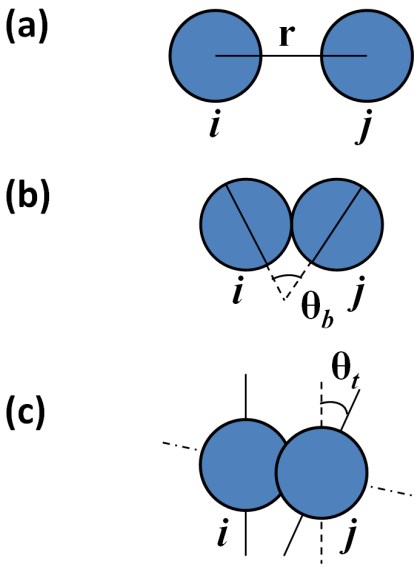

Figure 2.7: The deformation of a bead-represented fiber: (a) stretching; (b) bending; (c) twisting [1, 2].

to back the equilibrium bond angle if the bond angle is changed from its equilibrium angle θ_{b0}. The bending torque is expressed as [1, 2]

$$T^b = -k_b(\theta_b - \theta_{b0}) \tag{2.23}$$

where k_b is the bending torque constant, expressed as $k_b = \frac{\pi a^3}{8}E$. The direction of the torque is around the vector that is perpendicular to $\mathbf{n}_{ij}$.

The torsional torque is a function of the torsion angles θ_t (Figure 2.7(c)). There will be a torsion torque T^t exerting on each sphere to recover the equilibrium torsion angle if the torsion angle is changed from its equilibrium angle θ_{t0}. The torque is expressed as the following equation [1, 2]

$$T^t = -k_t(\theta_t - \theta_{t0}) \tag{2.24}$$

where k_t is the twisting torque constant, expressed as $k_t = \frac{\pi a^3}{4}G$ with G being the shear modulus of the fiber.

The bead chain model is considered to be immersed in a Newtonian fluid of viscosity η_0, and subjected to a macroscopic flow whose velocity field $\mathbf{v}(\mathbf{r})$ is given by [1,2]

$$\mathbf{v}(\mathbf{r}) = \boldsymbol{\kappa} \cdot \mathbf{r} \tag{2.25}$$

where $\boldsymbol{\kappa}$ is the velocity gradient tensor, and $\mathbf{r}$ is the global coordinate system.

The translational friction force and angular friction torque between the sphere and the fluid are assumed to be proportional to the relative translational velocity and the relative angular velocity of the sphere with respect to the microscopic flow respectively (Figure 2.8). Let $\mathbf{r}_i$ be the position vector of the center of the sphere i and θ_i be the angle position. Then the translational friction force is [1,2]

$$\mathbf{F}_i^h = -6\pi\eta_0 a(\mathbf{v}_i - \mathbf{v}(\mathbf{r}_i)) \tag{2.26}$$

where $6\pi\eta_0 a$ is the Stokes' friction constant, $\mathbf{v}_i$ is the translational velocity of the sphere i and $\mathbf{v}(\mathbf{r}_i)$ is the microscopic translational velocity of the fluid. Similarly, the angular friction torque is [1,2]

$$\mathbf{T}_i^h = -8\pi\eta_0 a^3(\boldsymbol{\omega}_i - \boldsymbol{\omega}(\mathbf{r}_i)) \tag{2.27}$$

where $8\pi\eta_0 a^3$ is the rotational friction constant, $\boldsymbol{\omega}_i$ is the angular velocity of the sphere i and $\boldsymbol{\omega}(\mathbf{r}_i)$ is the macroscopic angular velocity of the fluid, expressed as $\boldsymbol{\omega}(\mathbf{r}_i) = \frac{1}{2}\mathrm{rot}\mathbf{v}(\mathbf{r}_i)$, where rot represents the curl operator.

The translational and rotational motions are written as [1,2]

$$m\frac{d\mathbf{v}_i}{dt} = \sum \mathbf{F}_i^s + \sum \mathbf{f}_{ij} + \mathbf{F}_i^h \tag{2.28}$$

$$\frac{2}{5}ma^2\frac{d\boldsymbol{\omega}_i}{dt} = \sum \mathbf{T}_i^b + \sum \mathbf{T}_i^t + \sum \mathbf{f}_{ij} \times a\mathbf{n}_{ij} + \mathbf{T}_i^h \tag{2.29}$$

where m is the mass of the sphere. $\mathbf{f}_{ij}$ is the tangential friction force, which is perpendicular to $\mathbf{n}_{ij}$, exerting on the sphere i by the sphere j at the contact point. The

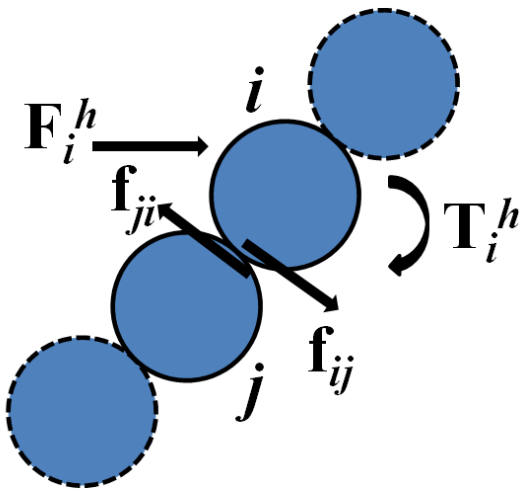

Figure 2.8: The forces and torques applied on the fiber by the flow [1, 2].

summation terms in Equations (2.28) and (2.29) mean to consider the effects of the neighboring spheres on both sides of the sphere i. Imposing the non-slip condition, the translational velocities of each sphere are the same at their contact point, which yields the following equation [1, 2]

$$\mathbf{v}_i + a\boldsymbol{\omega}_i \times \mathbf{n}_{ij} = \mathbf{v}_j + a\boldsymbol{\omega}_j \times \mathbf{n}_{ji} \tag{2.30}$$

In the actual simulation, the differentiation of Equation (2.30) is used and it is of the form as [1, 2]

$$\begin{aligned} \frac{d\mathbf{v}_i}{dt} &+ a\frac{d\boldsymbol{\omega}_i}{dt} + a\boldsymbol{\omega}_i \times (\boldsymbol{\omega}_i \times \mathbf{n}_{ji}) \\ &= \frac{d\mathbf{v}_j}{dt} + a\frac{d\boldsymbol{\omega}_j}{dt} \times \mathbf{n}_{ji} + a\boldsymbol{\omega}_j \times (\boldsymbol{\omega}_j \times \mathbf{n}_{ji}) \end{aligned} \tag{2.31}$$

Thus, in the bead chain model, the simulation is carried out in the following procedure.

1. An initial configuration is given to each sphere and the properties and parameters of the flow is set.

2. Based on the initial conditions, the stretching force, bending torque, and twisting torque are calculated by Equations (2.21), (2.23) and (2.24).
3. The translational friction force and the angular friction torque are calculated by Equation (2.26) and (2.27).
4. The tangential friction forces are solved by Equations (2.28), (2.29) and (2.31).
5. The translational velocity and the angular velocity at the next time step $t + \Delta t$ are updated by Equations (2.28) and (2.29) with a finite difference technique.
6. The position at the next time step $t + \Delta t$ is updated in the following manners

$$\mathbf{r}_i(t + \Delta t) = \mathbf{r}_i(t) + \Delta t \mathbf{v}_i(t) + \frac{1}{2}(\Delta t)^2 \frac{d\mathbf{v}_i}{dt} \quad (2.32)$$

$$\theta_i(t + \Delta t) = \theta_i(t) + \Delta t \omega_i(t) + \frac{1}{2}(\Delta t)^2 \frac{d\omega_i}{dt} \quad (2.33)$$

7. The motion of all the spheres and thus that of the fiber can be described by repeating steps 2 to 6.

2.3.3 The Needle Chain Model

In the needle chain model [3,22], connectivity matrices are employed to describe how the spheroid bodies are connected by the ball and socket joints. The fiber is composed of N_α rigid bodies. Matrices are constructed by numbering the bodies and joints. Body number starts with 0, but is only reserved for the fixed reference frame and joint 1 is between body 0 and 1. The end body of the fiber is body 1. The numbering of other bodies and joints are shown in Figure 2.9. The authors convert the index information into a system graph, which consists of points, called vertices, and lines connecting the vertices, called arcs. The vertices $(s_1, ..., s_{N_\alpha})$ represent the bodies and the arcs $(u_1, ..., u_{N_\alpha})$ represent the joints. Two integer functions, $i^{(+)\alpha}(a)$ and $i^{(-)\alpha}(a)$ are defined to relate vertex indices and arc indices. For arc number $a = 1, ..., N_\alpha$, $i^{(+)\alpha}(a)$ is the index of the vertex from which arc u_α emanates, and $i^{(-)\alpha}(a)$

is the index of the vertex toward which arc u_α is pointing. Then the connectivity matrices $\mathbf{S}^\alpha$ and $\mathbf{T}^\alpha$ are defined in terms of the integer functions and the system graph [3, 22] as

$$S_{ia}^{\alpha} = \begin{cases} +1 & \text{if } i = i^{(+)\alpha}(a) \\ -1 & \text{if } i = i^{(-)\alpha}(a) \quad i, a = 1, ..., N_\alpha \\ 0 & \text{otherwise} \end{cases} \tag{2.34}$$

and

$$T_{ia}^{\alpha} = \begin{cases} +1 & \text{if } u_a \text{ belongs to the path between } s_0 \text{ and } s_i \\ & \text{and is directed toward } s_0 \\ -1 & \text{if } u_a \text{ belongs to the path between } s_0 \text{ and } s_i \\ & \text{and is directed away } s_0 \\ 0 & \text{if } u_a \text{ does not belong to the path between} \\ & s_0 \text{ and } s_i \\ & i, a = 1, ..., N_\alpha \end{cases} \tag{2.35}$$

For the numbering method used in Figure 2.9, the above matrices are given by [3, 22]

$$\mathbf{S}^\alpha = \begin{bmatrix} -1 & 1 & 0 & \cdots & 0 \\ 0 & -1 & 1 & \ddots & \vdots \\ & & \ddots & \ddots & 0 \\ \vdots & & \ddots & -1 & 1 \\ 0 & & \cdots & 0 & -1 \end{bmatrix} \tag{2.36}$$

$$\mathbf{T}^\alpha = \begin{bmatrix} -1 & -1 & -1 & \cdots & -1 \\ 0 & -1 & -1 & \cdots & -1 \\ & & -1 & \cdots & -1 \\ \vdots & & \ddots & \ddots & \vdots \\ 0 & & \cdots & 0 & -1 \end{bmatrix} \tag{2.37}$$

The above matrices have the following property [3, 22]

$$\mathbf{T}^\alpha \mathbf{S}^\alpha = \mathbf{S}^\alpha \mathbf{T}^\alpha = \mathbf{I}^\alpha \tag{2.38}$$

where $\mathbf{I}^\alpha$ is an $N_\alpha \times N_\alpha$ identity matrix.

In order to establish the relationship between the spheroid positions, a set of body-fixed connectivity vectors, $\mathbf{c}_{ia}^{\alpha}(i, a = 1, 2, ..., N_\alpha)$, are introduced by the authors. The directions of the vectors are from the center of mass of spheroid i to joint a, as

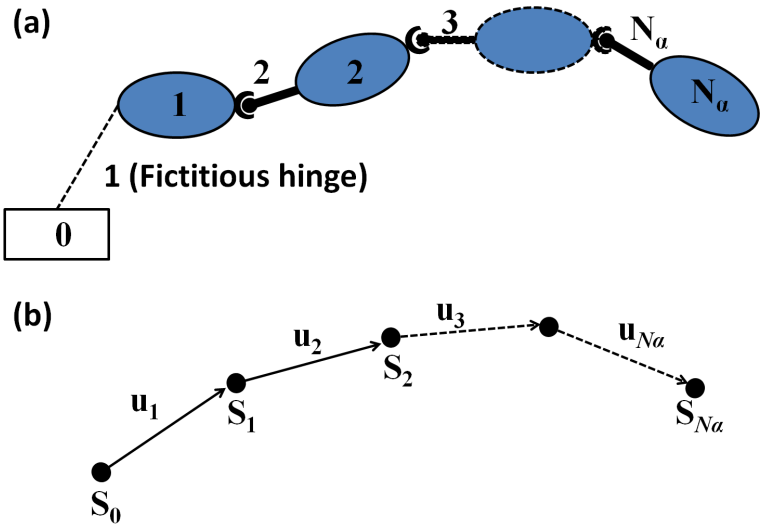

Figure 2.9: (a)Illustration of body and hinge index numbering used in constructing the connectivity matrices, (b)system graph for (a) [3].

shown in Figure 2.10. For a joint a not connected to with spheroid i, this vector is defined as the zero vector. The spheroid positions are related by these vectors in the following way [3, 22]

$$\begin{aligned} (\mathbf{r}_{i^{(-)\alpha}(a)} + \mathbf{c}_{i^{(-)\alpha}(a)a}) &- (\mathbf{r}_{i^{(+)\alpha}(a)} + \mathbf{c}_{i^{(+)\alpha}(a)a}) = 0 \\ a &= 1, 2, ..., N_\alpha \end{aligned} \tag{2.39}$$

The above N_α equations can be written in the matrix form as [3, 22]

$$(\mathbf{S}^\alpha)^T \mathbf{r}^\alpha + (\mathbf{C}^\alpha)^T \mathbf{1}_{N_\alpha} = 0 \tag{2.40}$$

where $\mathbf{S}^\alpha$ is the connectivity matrix defined in Equation (2.35) with the superscript ^{T} denoting transpose, $\mathbf{r}^\alpha = [\mathbf{r}_1^\alpha, \mathbf{r}_2^\alpha, ..., \mathbf{r}_{N_\alpha}^\alpha]^T$, $\mathbf{1}_{N_\alpha}$ is an $N_\alpha \times 1$ matrix of ones, and $\mathbf{C}^\alpha$ is an $N_\alpha \times N_\alpha$ matrix with components $\mathbf{C}_{ia}^\alpha = S_{ia}^\alpha \mathbf{c}_{ia}^\alpha$. Multiplying Equation (2.40) by $\mathbf{T}^\alpha$ and using the property given by Equation (2.38), the spheroid positions can be expressed in terms of the connectivity vectors as [3, 22]

$$\mathbf{r}^\alpha = -(\mathbf{C}^\alpha \mathbf{T}^\alpha)^T \mathbf{1}_{N_\alpha} \tag{2.41}$$

or in index form [3, 22]

$$\mathbf{r}_i^\alpha = \sum_{j=1}^{N_\alpha} \mathbf{d}_{ji}^\alpha \tag{2.42}$$

where $\mathbf{d}_{ji}^\alpha = -(\mathbf{C}^\alpha \mathbf{T}^\alpha)_{ji}$ and the center of mass $\mathbf{R}_i^\alpha$ of spheroid i relative to the fiber center mass $\mathbf{r}_C^\alpha$ can be expressed as [3, 22]

$$\mathbf{R}_i^\alpha = \mathbf{r}_i^\alpha - \mathbf{r}_C^\alpha \tag{2.43}$$

Substituting Equation (2.42) into Equation (2.43) gives the following form ([3, 22])

$$\mathbf{R}^\alpha = -(\mathbf{C}^\alpha \mathbf{T}^\alpha \nu^\alpha)^T \mathbf{1}_{N_\alpha} \tag{2.44}$$

where $\nu_{ij} = \delta_{ij} - 1/N_\alpha$, or in index form [3, 22]

$$\mathbf{R}_i^\alpha = \sum_{j=1}^{N_\alpha} \mathbf{b}_{ji}^\alpha \tag{2.45}$$

where $\mathbf{b}_{ji}^\alpha = -(\mathbf{C}^\alpha \mathbf{T}^\alpha \nu^\alpha)_{ji}$. Substituting Equation (2.45) into Equation (2.43) [3,22],

$$\mathbf{r}_i^\alpha = \sum_{j=1}^{N_\alpha} \mathbf{b}_{ji}^\alpha + \mathbf{r}_C^\alpha \tag{2.46}$$

Differentiating Equation (2.46) gives the translational velocity of spheroid i as [3, 22]

$$\dot{\mathbf{r}}_i^\alpha = \sum_{j=1}^{N_\alpha} \boldsymbol{\omega}_j^\alpha \times \mathbf{b}_{ji}^\alpha + \dot{\mathbf{r}}_C^\alpha \tag{2.47}$$

where $\boldsymbol{\omega}_j^\alpha$ is the angular velocity of the spheroid j, which is related to the relative angular velocities of spheroid $j-1$ through the connectivity matrix $\mathbf{T}^\alpha$ [3, 22],

$$\boldsymbol{\omega}_j^\alpha = -\sum_{a=1}^{N_\alpha} T_{aj}^\alpha \boldsymbol{\Omega}_a^\alpha \tag{2.48}$$

where $\boldsymbol{\Omega}_a^\alpha$ is the angular velocity of spheroid $i^{(-)\alpha}(a)$ relative to that of spheroid $i^{(+)\alpha}(a)$.

The motion of a spheroid body is described by Newton's second law and the law of moment of momentum. The free-body diagram is given for spheroid body i is given

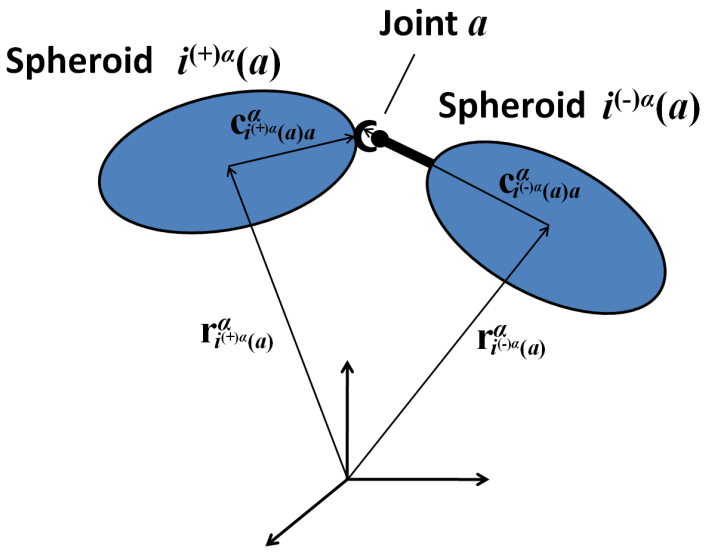

Figure 2.10: Illustration of the connectivity vectors in the model kinetics [3].

in Figure 2.11, where $\mathbf{F}_i^\alpha$ is the resultant external force acting through the center of mass, $\mathbf{M}_i^\alpha$ is the resultant external torque, $\mathbf{X}_b^{(c)\alpha}$ and $\mathbf{X}_c^{(c)\alpha}$ are the internal constraint forces in joints b and c respectively and $\mathbf{Y}_b^\alpha$ and $\mathbf{Y}_c^\alpha$ are the resultant internal torques in joints b and c respectively. Newton's second law takes the following form [3, 22]

$$m_i^\alpha \ddot{\mathbf{r}}_i^\alpha = \mathbf{F}_i^\alpha + \sum_{a=1}^{N_\alpha} S_{ia}^\alpha \mathbf{X}_a^{(c)\alpha} \tag{2.49}$$

and the law of momentum yields [3, 22]

$$\dot{\mathbf{H}}_i^\alpha = \mathbf{M}_i^\alpha + \sum_{a=1}^{N_\alpha} S_{ia}^\alpha (\mathbf{c}_{ia}^\alpha \times \mathbf{X}_a^{(c)\alpha} + \mathbf{Y}_a^\alpha) \tag{2.50}$$

where m_i^α is the mass, $\ddot{\mathbf{r}}_i^\alpha$ is the translational acceleration, and $\dot{\mathbf{H}}_i^\alpha$ is the time rate of change of the angular momentum of spheroid i. The resultant external force $\mathbf{F}_i^\alpha$ is the combination of hydrodynamic forces $\mathbf{F}_i^{(h)\alpha}$, inter-particle forces $\mathbf{F}_i^{(p)\alpha}$ and body forces $\mathbf{F}_i^{(g)\alpha}$. The resultant external toque $\mathbf{M}_i^\alpha$ is the combination of hydrodynamic torques, and torques produced by external moments or inter-particle forces $\mathbf{M}_i^{(p)\alpha}$.

Neglecting the hydrodynamic interactions and fluid inertia, the hydrodynamic forces and torques are given in terms of the rate of strain tensor $\mathbf{E}^{(\infty)}$ and the vorticity

$\mathbf{\Omega}^{(\infty)}$ as [3, 22]

$$\mathbf{F}_i^{(h)\alpha} = \mathbf{A}_i^{(h)\alpha} \cdot (\mathbf{U}_i^{(\infty)\alpha} - \dot{\mathbf{r}}_i^{\alpha}) \tag{2.51}$$

and

$$\mathbf{M}_i^{(h)\alpha} = \mathbf{C}_i^{(h)\alpha} \cdot (\mathbf{\Omega}^{(\infty)\alpha} - \boldsymbol{\omega}_i^{\alpha}) + \widetilde{\mathbf{H}}_i^{(h)\alpha} : \mathbf{E}^{(\infty)} \tag{2.52}$$

where $\mathbf{U}_i^{(\infty)\alpha}$ is the ambient fluid translational velocity evaluated at the center of mass of spheroid i. $\mathbf{A}_i^{(h)\alpha}$, $\mathbf{C}_i^{(h)\alpha}$ and $\widetilde{\mathbf{H}}_i^{(h)\alpha}$ are the resistance tensors, which depend only on the instantaneous orientation of spheroid i.

The inter-particle force $\mathbf{F}_i^{(p)\alpha}$ depends only on the instantaneous spheroid positions and orientations, which include any inter- or intra-fiber interactions. $\mathbf{M}_i^{(p)\alpha}$ accounts for any externally applied moments or inter-particles forces that do not act through the spheroid center of mass. The body force is due to gravity, given by $\mathbf{F}_i^{(g)\alpha} = \frac{4}{3}\pi ab^2 \Delta\rho \mathbf{g}$, where $\mathbf{g}$ is the acceleration of gravity and $\Delta\rho$ is the density difference between fiber and the flow.

The resultant internal torques $\mathbf{Y}_a^{(B)\alpha}$ at the joints comprise of the bending torque $\mathbf{Y}_a^{(B)\alpha}$ and twisting torque $\mathbf{Y}_a^{(T)\alpha}$. The bending torque is assumed to be proportional to the difference between the bending angle θ_a^{α} and its equilibrium value $\theta_a^{(0)\alpha}$ [3, 22],

$$\mathbf{Y}_a^{(B)\alpha} = -k_B^{\alpha}(\theta_a^{\alpha} - \theta_a^{(0)\alpha})\mathbf{n}_{pb} \tag{2.53}$$

where $\mathbf{n}_{pb}$ is the unit vector normal to plane of bending [3, 22] defined as

$$\mathbf{n}_{pb} = \frac{\mathbf{c}^{\alpha}_{i^{(-)\alpha}(a)a} \times \mathbf{c}^{\alpha}_{i^{(+)\alpha}(a)a}}{\|\mathbf{c}^{\alpha}_{i^{(-)\alpha}(a)a} \times \mathbf{c}^{\alpha}_{i^{(+)\alpha}(a)a}\|} \tag{2.54}$$

and θ_a^{α} is given by [3, 22]

$$\cos\theta_a^{\alpha} = \frac{\mathbf{c}^{\alpha}_{i^{(-)\alpha}(a)a} \cdot \mathbf{c}^{\alpha}_{i^{(+)\alpha}(a)a}}{\|\mathbf{c}^{\alpha}_{i^{(-)\alpha}(a)a}\|\|\mathbf{c}^{\alpha}_{i^{(+)\alpha(a)}a}\|} \tag{2.55}$$

The bending constant is given in terms of young's modulus E and moment of inertia I as

$$k_B^\alpha = \frac{EI}{a} \tag{2.56}$$

Similarly, the twisting torque $\mathbf{Y}_a^{(T)\alpha}$ is assume to be proportional to the difference between the twisting angle ϕ_a^α and its equilibrium value $\phi_a^{(0)\alpha}$ [3, 22],

$$\mathbf{Y}_a^{(T)\alpha} = -k_T^\alpha(\phi_a^\alpha - \phi_a^{(0)\alpha})\frac{\mathbf{c}^\alpha_{i^{(-)\alpha}(a)a}}{\|\mathbf{c}^\alpha_{i^{(-)\alpha}(a)a}\|} \tag{2.57}$$

The twisting angle is given in terms of body-fixed vector $\mathbf{u}_i^\alpha$, which extend from the center of mass and are oriented perpendicular to the $\mathbf{c}_{ia}^\alpha$ vectors. The twisting angle is given by [3, 22]

$$\cos\phi_a^\alpha = \frac{\mathbf{u}^\alpha_{i^{(-)\alpha}(a)} \cdot \mathbf{u}'_a}{\|\mathbf{u}'_a\|} \tag{2.58}$$

where $\mathbf{u}'_a = \mathbf{u}^\alpha_{i^{(+)\alpha}(a)} - \mathbf{u}^\alpha_{i^{(+)\alpha}(a)} \cdot \mathbf{c}^\alpha_{i^{(-)\alpha}(a)a}$. The twisting constant is given in terms of shear modulus E and moment of inertia I as

$$k_T^\alpha = \frac{GI}{a} \tag{2.59}$$

With all the forces and torques defined along with neglecting particle inertia, Equation (2.49) and (2.50) reduce to [3, 22]

$$\mathbf{F}_i^{(h)\alpha} + \mathbf{F}_i^{(p)\alpha} + \mathbf{F}_i^{(g)\alpha} + \sum_{a=1}^{N_\alpha} S_{i\alpha}^\alpha \mathbf{X}_a^{(c)\alpha} = 0 \tag{2.60}$$

and

$$\mathbf{M}_i^{(h)\alpha} + \mathbf{M}_i^{(p)\alpha} + \sum_{a=1}^{N_\alpha} S_{i\alpha}^\alpha(\mathbf{c}_{ia}^\alpha \times \mathbf{X}_a^{(c)\alpha} + \mathbf{Y}_a^\alpha) = 0 \tag{2.61}$$

Putting Equation (2.47) into Equation (2.51) and substituting the terms on Equation

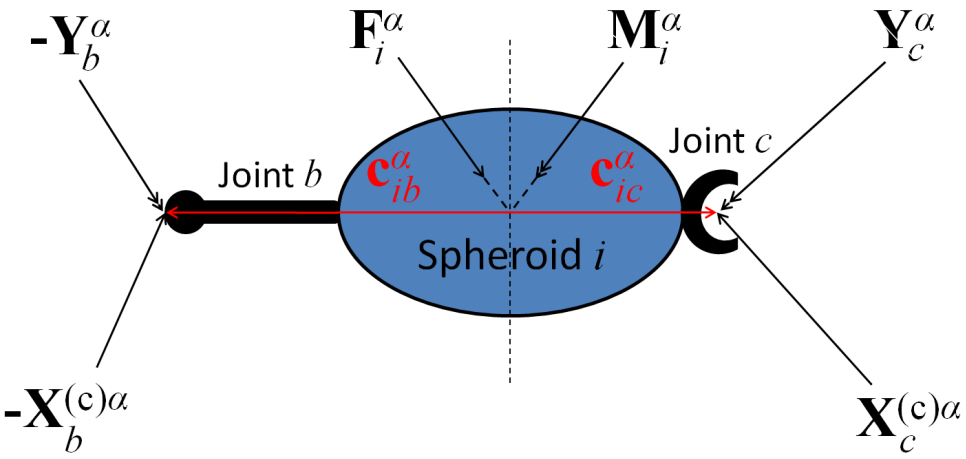

Figure 2.11: Free-body diagram for spheroid i in fiber α [3].

(2.60), the motion of the fiber center of mass is obtained as [3, 22]

$$\dot{\mathbf{r}}_C^\alpha = -(\mathbf{A}^\alpha)^{-1} \cdot [\sum_{j=1}^{N_\alpha} \sum_{k=1}^{N_\alpha} \mathbf{A}_j^{(h)\alpha} \cdot (\boldsymbol{\omega}_k^\alpha \times \mathbf{b}_{kj}^\alpha) - \sum_{j=1}^{N_\alpha} (\mathbf{A}_j^{(h)\alpha} \cdot \mathbf{U}_j^{(\infty)\alpha} + \mathbf{F}_j^{(p)\alpha} + \mathbf{F}_j^{(g)\alpha})] \tag{2.62}$$

where $\mathbf{A}^\alpha = \sum_{i=1}^{N_\alpha} \mathbf{A}_i^{(h)\alpha}$. Then the translational equation of motion for spheroid i is given by combining Equation (2.47) and Equation (2.62) as [3, 22]

$$\dot{\mathbf{r}}_C^\alpha = \sum_{j=1}^{N_\alpha} \boldsymbol{\omega}_j^\alpha \times \mathbf{b}_{ji}^\alpha - (\mathbf{A}^\alpha)^{-1} \cdot [\sum_{j=1}^{N_\alpha} \sum_{k=1}^{N_\alpha} \mathbf{A}_j^{(h)\alpha} \cdot (\boldsymbol{\omega}_k^\alpha \times \mathbf{b}_{kj}^\alpha) - \sum_{j=1}^{N_\alpha} (\mathbf{A}_j^{(h)\alpha} \cdot \mathbf{U}_j^{(\infty)\alpha} + \mathbf{F}_j^{(p)\alpha} + \mathbf{F}_j^{(g)\alpha})] \tag{2.63}$$

The rotational equations of motion are evaluated by first solving Equation (2.60) to obtain the constraint forces. Then Equation (2.52) and the obtained internal constraint forces along with Equation (2.51) in the form of Equation (2.47), are substituted into Equation (2.61). After solving the final equation, the rotational equation of motion for spheroid i is [3, 22]

$$\sum_{j=1}^{N_\alpha} \mathbf{Q}_{il}^\alpha \cdot \boldsymbol{\omega}_l^\alpha = \mathbf{D}_i^\alpha \tag{2.64}$$

where

$$\mathbf{Q}_{il}^{\alpha} = \delta_{il}\mathbf{C}_{i}^{(h)\alpha} - \sum_{j=1}^{N_\alpha} \widetilde{\mathbf{d}}_{ij}^{\alpha} \cdot \mathbf{A}_{j}^{(h)\alpha} \cdot \widetilde{\mathbf{b}}_{lj}^{\alpha}$$
$$+ \sum_{j=1}^{N_\alpha}\sum_{k=1}^{N_\alpha} \widetilde{\mathbf{d}}_{ij}^{\alpha} \cdot \mathbf{A}_{j}^{(h)\alpha} \cdot (\mathbf{A}^{\alpha})^{-1} \cdot \mathbf{A}_{k}^{(h)\alpha} \cdot \widetilde{\mathbf{b}}_{lk}^{\alpha}, \tag{2.65}$$

$$\mathbf{D}_{i}^{\alpha} = \mathbf{M}_{i}^{(p)\alpha} - \sum_{j=1}^{N_\alpha} \mathbf{d}_{ij}^{\alpha} \times [\mathbf{A}_{j}^{(h)\alpha} \cdot \mathbf{U}_{j}^{(\infty)\alpha} + \mathbf{F}_{j}^{(p)\alpha} + \mathbf{F}_{j}^{(g)\alpha}$$
$$-\mathbf{A}_{j}^{(h)\alpha} \cdot (\mathbf{A}^{\alpha})^{-1} \cdot \sum_{k=1}^{N_\alpha} (\mathbf{A}_{k}^{(h)\alpha} \cdot \mathbf{U}_{k}^{(\infty)\alpha} + \mathbf{F}_{k}^{(p)\alpha} + \mathbf{F}_{k}^{(g)\alpha})]$$
$$+\mathbf{C}_{i}^{(h)\alpha} \cdot \mathbf{\Omega}^{(\infty)} + \widetilde{\mathbf{H}}_{i}^{(h)\alpha} : \mathbf{E}^{(\infty)} + \sum_{j=1}^{N_\alpha} S_{ij}^{\alpha}\mathbf{Y}_{j}^{\alpha}, \tag{2.66}$$

$$\widetilde{\mathbf{d}}_{ij}^{\alpha} = \begin{bmatrix} 0 & -d_{z_{ij}}^{\alpha} & d_{y_{ij}}^{\alpha} \\ d_{z_{ij}}^{\alpha} & 0 & -d_{x_{ij}}^{\alpha} \\ -d_{y_{ij}}^{\alpha} & d_{x_{ij}}^{\alpha} & 0 \end{bmatrix}, \tag{2.67}$$

$$\widetilde{\mathbf{b}}_{ij}^{\alpha} = \begin{bmatrix} 0 & -b_{z_{ij}}^{\alpha} & b_{y_{ij}}^{\alpha} \\ b_{z_{ij}}^{\alpha} & 0 & -b_{x_{ij}}^{\alpha} \\ -b_{y_{ij}}^{\alpha} & b_{x_{ij}}^{\alpha} & 0 \end{bmatrix} \tag{2.68}$$

The angular velocities ω_{l}^{α} are solved from Equation (2.64) by combining the components of the tensor $\mathbf{Q}_{il}^{\alpha}$ into a $3N_\alpha \times 3N_\alpha$ matrix and inverting it. From Equation (2.63) and (2.64), the dynamical behavior of the flexible fiber can be fully described.

2.3.4 The Rod Chain Model

The rod chain model is an effective approach for predicting the motion of flexible fibers, and is chosen in the present context due to its ease of implementation as well as its computational efficiency [21]. There are four assumptions associated with the Rod chain model: (1) the suspension is Newtonian; (2) Brownian motion is neglected; (3) decoupling of flow and fiber orientation is valid; and (4) there is no interactions between rods and fibers and (5) fibers are inextensible. The fiber is represented as

a chain of N_r rigid rods with each rod composed of N beads. Each rod has a unit direction vector to indication the orientation of the rod, where as the orientation of the fiber is determined by a unit end-to-end vector $\boldsymbol{p}_{end-to-end}$ as shown in Figure 2.6.

To simplify the following equations, quantities are made dimensionless through the shear rate $\dot{\gamma}$, fiber radius a, and the fluid viscosity η as [21]

$$\hat{t} = t\dot{\gamma} \tag{2.69}$$

$$\hat{l} = l/a \tag{2.70}$$

$$\hat{\mathbf{F}} = \frac{\mathbf{F}}{\pi\eta a^2\dot{\gamma}} \tag{2.71}$$

$$\hat{\mathbf{T}} = \frac{\mathbf{T}}{\pi\eta a^3\dot{\gamma}} \tag{2.72}$$

where in Equations (2.69) - (2.72) the hat symbol $\hat{}$ is used for the dimensionless parameter.

The changing motion of the fluid surrounding the fiber depicted in Figure 2.12 causes hydrodynamic forces and torques to be exerted on the fiber. The resulting deformation causes resisting forces and torque within the fiber. Assuming the hydrodynamic friction force exerted on each bead is proportional to the velocity difference between the bead and the flow, the hydrodynamic friction force on rod i is the sum of the forces on each bead within a rod [21], given by

$$\hat{\mathbf{F}}_i^h = 6N(\hat{\boldsymbol{\kappa}} \cdot \hat{\mathbf{r}}_i - \hat{\mathbf{v}}_i), \qquad i = 1 \sim N_r \tag{2.73}$$

where N is the number of beads in the rod, N_r is the number of rods in a fiber, $\hat{\mathbf{r}}_i$ is the center position vector of rod i, $\hat{\mathbf{v}}_i$ is the velocity of the center of rod i.

The hydrodynamic angular friction torque on rod i is given by [21]

$$\hat{\mathbf{T}}_i^h = -2N^3(\hat{\boldsymbol{\omega}}_i - \hat{\boldsymbol{\omega}}_\infty), \qquad i = 1 \sim N_r \tag{2.74}$$

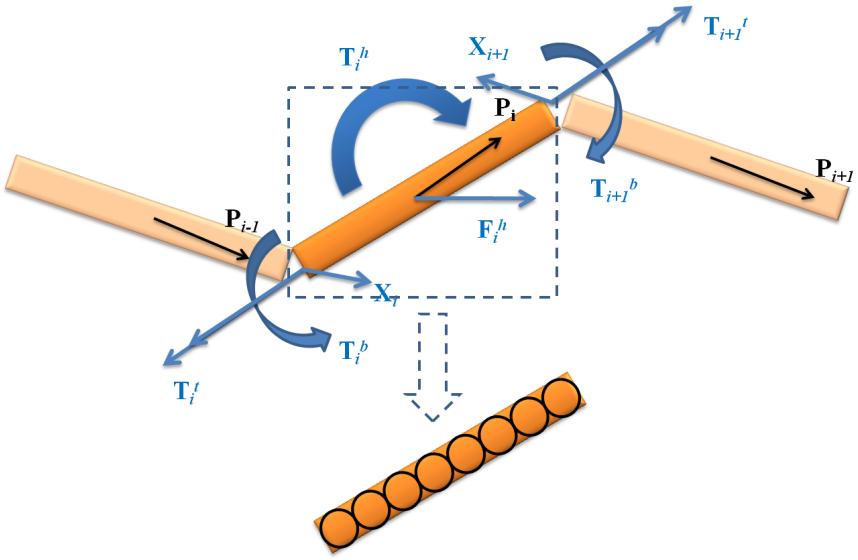

Figure 2.12: The external and internal forces and torques on rod i.

where $\hat{\boldsymbol{\omega}}_i$ is the angular velocity vector of the center of rod i and $\hat{\boldsymbol{\omega}}_\infty$ is the angular velocity vector of the flow at the position of the center of rod i.

The bending torque between two neighboring rods is proportional to the difference between the bending angle and the equilibrium angle [21], given by

$$\hat{\mathbf{T}}_i^b = -\hat{k}^b(\theta_i^b - \theta_{eq}^b)\mathbf{n}_i^b, \qquad i = 2 \sim N_r \tag{2.75}$$

and the bending torques at the ends of the fiber are

$$\hat{\mathbf{T}}_1^b = \hat{\mathbf{T}}_{N_r+1}^b = 0$$

where $\mathbf{n}_i^b = \frac{\mathbf{p}_{i-1}\times\mathbf{p}_i}{\|\mathbf{p}_{i-1}\times\mathbf{p}_i\|}$ is the unit vector normal to the plane of bending of rod i, the bending angle is $\theta^b = \cos^{-1}\left(\frac{\mathbf{p}_{i-1}\cdot\mathbf{p}_i}{\|\mathbf{p}_{i-1}\cdot\mathbf{p}_i\|}\right)$. In the present study we assume all fibers are straight when there are no applied loads, thus $\theta_{eq}^b = 0$ throughout the remainder of the text. $\hat{k}^b = \frac{k^b}{\pi\eta a^3\dot{\gamma}}$ and the bending constant k^b is related to the bending stiffness of the fiber via $k^b = \frac{EI^b}{2Na}$, where $I^b = \frac{\pi a^4}{4}$.

The twisting torque between two neighboring rods is [21]

$$\hat{\mathbf{T}}_i^t = -\hat{k}^t(\theta_i^t - \theta_{eq}^t)\mathbf{p}_i, \qquad i = 2 \sim N_r \tag{2.76}$$

and the twisting torques at the ends of the fiber are

$$\hat{\mathbf{T}}_1^t = \hat{\mathbf{T}}_{N_r+1}^t = 0$$

where a body-fixed unit vector $\mathbf{u_i}$ perpendicular to rod i is defined in order to determine the twisting angle $\theta_i^t = \cos^{-1}\left(\frac{\mathbf{u}_{i-1}\cdot\mathbf{u}_i'}{\|\mathbf{u}_{i-1}\cdot\mathbf{u}_i'\|}\right)$, where $\mathbf{u_i'} = \mathbf{u_{i-1}} - (\mathbf{u_{i-1}}\cdot\mathbf{p_i})\mathbf{p}_i$. $\hat{k}^t = \frac{k^t}{\pi\eta a^3\dot{\gamma}}$ and the torsion constant k^t is related to the torsion stiffness of the fiber via $k^t = \frac{GI^t}{2a}$, where $I^t = \frac{\pi a^4}{2}$. In the present study we assume fibers are initially straight. Thus the equilibrium twist angle is $\theta_{eq}^t = 0$.

The motion equation for each rod is [21]

$$\frac{d\hat{\mathbf{v}}_i}{d\hat{t}} = \frac{1}{2NRe}\left(\hat{\mathbf{F}}_i^h + \hat{\mathbf{X}}_i - \hat{\mathbf{X}}_{i+1}\right), \qquad i = 1 \sim N_r \tag{2.77}$$

where $\hat{\mathbf{X}}_i$ is the internal constraint force between rod i and $i+1$, $Re = \frac{\pi a^2\rho\dot{\gamma}}{\eta}$ is the particle Reynolds number, and ρ is the density of the fiber.

The angular momentum balance equation for each rod is [21]

$$\begin{aligned}\frac{d\hat{\boldsymbol{\omega}}_i}{d\hat{t}} = \frac{1}{2N^3Re}[&\hat{\mathbf{T}}_i^h + \hat{\mathbf{T}}_i^b - \hat{\mathbf{T}}_{i+1}^b + \hat{\mathbf{T}}_i^t \\ &-\hat{\mathbf{T}}_{i+1}^t - N\mathbf{p}_i \times (\hat{\mathbf{X}}_i + \hat{\mathbf{X}}_{i+1})], \qquad i = 1 \sim N_r\end{aligned} \tag{2.78}$$

For continuity purposes, the velocities at the joint of two neighboring rods are the same. Thus we have the following continuity equation for each joint [21]

$$\begin{aligned}&\frac{d\hat{\mathbf{v}}_i}{d\hat{t}} + \frac{d\hat{\boldsymbol{\omega}}_i}{d\hat{t}} \times N\mathbf{p}_i + \hat{\boldsymbol{\omega}}_i \times N\left(\hat{\boldsymbol{\omega}}_i \times \mathbf{p}_i\right) = \frac{d\hat{\mathbf{v}}_{i+1}}{d\hat{t}} \\ &-\frac{d\hat{\boldsymbol{\omega}}_{i+1}}{d\hat{t}} \times N\mathbf{p}_{i+1} - \hat{\boldsymbol{\omega}}_{i+1} \times N\left(\hat{\boldsymbol{\omega}}_{i+1} \times \mathbf{p}_{i+1}\right), \qquad i = 1 \sim N_r - 1\end{aligned} \tag{2.79}$$

Substituting Equation (2.77) and (2.78) into Equation (2.79), an Equation is obtained for solving the internal constraint forces shown as [21]

$$\begin{aligned}(\hat{\mathbf{X}}_i - 2\hat{\mathbf{X}}_{i+1} + \hat{\mathbf{X}}_{i+2}) - 3[\mathbf{p}_i \times (\hat{\mathbf{X}}_i + \hat{\mathbf{X}}_{i+1}) \\ \times \mathbf{p}_i + \mathbf{p}_{i+1} \times (\hat{\mathbf{X}}_{i+1} + \hat{\mathbf{X}}_{i+2}) \times \mathbf{p}_{i+1}] \\ = (\hat{\mathbf{F}}^h_{i+1} - \hat{\mathbf{F}}^h_i) - \frac{1}{N}[(\hat{\mathbf{T}}^h_i + \hat{\mathbf{T}}^b_i - \hat{\mathbf{T}}^b_{i+1} \\ + \hat{\mathbf{T}}^t_i - \hat{\mathbf{T}}^t_{i+1}) \times \mathbf{p}_i + (\hat{\mathbf{T}}^h_{i+1} + \hat{\mathbf{T}}^b_{i+1} \\ - \hat{\mathbf{T}}^b_{i+2} + \hat{\mathbf{T}}^t_{i+1} - \hat{\mathbf{T}}^t_{i+2}) \times \mathbf{p}_{i+1}] \\ - 2ReN^2[\hat{\boldsymbol{\omega}}_i \times (\hat{\boldsymbol{\omega}}_i \times \mathbf{p}_i) \\ + \hat{\boldsymbol{\omega}}_{i+1} \times N(\hat{\boldsymbol{\omega}}_{i+1} \times \mathbf{p}_{i+1})], \qquad i = 2 \sim N_r - 1 \end{aligned} \tag{2.80}$$

Note, because there are no constraint forces at the ends of the fiber, thus $\hat{\mathbf{X}}_1 = \hat{\mathbf{X}}_{N_r+1} = 0$ and thus there are $3 \times (N_r - 1)$ internal constraints.

The position vector of the center of the fiber is updated by the following equation [21]

$$\hat{\mathbf{r}}^{new}_m = \hat{\mathbf{r}}^{old}_m + \Delta\hat{t} \sum \hat{\mathbf{v}}^{old}_i / N_r, \qquad i = 1 \sim N_r \tag{2.81}$$

and the unit direction vector of each rod can be updated by the following equation [21]

$$\mathbf{p}^{new}_i = \frac{\mathbf{p}^{old}_i + \hat{\boldsymbol{\omega}}^{new}_i \times \mathbf{p}^{old}_i \Delta\hat{t}}{\|\mathbf{p}^{old}_i + \hat{\boldsymbol{\omega}}^{new}_i \times \mathbf{p}^{old}_i \Delta\hat{t}\|}, \qquad i = 1 \sim N_r \tag{2.82}$$

When there are an odd number of rods, then the center position of each rod is updated as [21]

$$\begin{aligned} \hat{\mathbf{r}}_{(N_r+1)/2} &= \hat{\mathbf{r}}_m \\ \hat{\mathbf{r}}_i &= \hat{\mathbf{r}}_m + N \sum_{n=\frac{N_r+1}{2}+1}^{i} (\mathbf{p}_{n-1} + \mathbf{p}_n), \qquad i = \frac{N_r+1}{2} + 1 \sim N_r \\ \hat{\mathbf{r}}_i &= \hat{\mathbf{r}}_m - N \sum_{n=\frac{N_r+1}{2}-1}^{i} (\mathbf{p}_{n-1} + \mathbf{p}_n), \qquad i = \frac{N_r+1}{2} - 1 \sim N_r \end{aligned} \tag{2.83}$$

When there are an even number of rods, then the center position of each rod is updated as [21]

$$\begin{aligned}
\hat{\mathbf{r}}_{N_r/2+1} &= \hat{\mathbf{r}}_m + N\mathbf{p}_{N_r/2+1} \\
\hat{\mathbf{r}}_{N_r/2+1} + N \sum_{n=\frac{Nr}{2}+2}^{i} (\mathbf{p}_{n-1} + \mathbf{p}_n), &\qquad i = \frac{N_r}{2} + 2 \sim N_r \\
\hat{\mathbf{r}}_{N_r/2} &= \hat{\mathbf{r}}_m - N\mathbf{p}_{N_r/2} \\
\hat{\mathbf{r}}_{N_r/2} - N \sum_{n=\frac{Nr}{2}-1}^{i} (\mathbf{p}_n + \mathbf{p}_{n+1}), &\qquad i = \frac{N_r}{2} - 1 \sim 1
\end{aligned} \tag{2.84}$$

The translational velocity for each rod is updated by the following equation [21]

$$\hat{\mathbf{v}}_i^{new} = \frac{\hat{\mathbf{r}}_i^{new} - \hat{\mathbf{r}}_i^{old}}{\Delta\hat{t}} \tag{2.85}$$

The implementation of the rod chain model is discussed in Chapter Three as well as a comparison with Jeffery's equation.

2.4 Prediction of Elastic Properties of Fiber Reinforced Composites

The elastic properties of short fiber reinforced composites is determined by the orientation state of the fibers within the underlying matrix. All the models used to predict the elastic properties are based on the same basic assumptions [66]: (1) The fibers and the matrix are linearly elastic, the matrix is isotropic, and the fibers are either isotropic or transversely isotropic; (2) the fibers are axisymmetric, identical in shape and size, and can be characterized by an aspect ratio; (3) the fibers and matrix are well bonded at their interface, and remain that way during deformation. Thus, no interfacial slip is considered, nor fiber/matrix debonding or matrix micro-cracking.

2.4.1 Unidirectional Stiffness Prediction

This section discusses the models for predicting the stiffness of a piece of unidirectional short fiber composites, especially the Tandon-Weng model, which is adopted in the material property prediction in this research.

2.4.1.1 Bounding Models. This approach assumes an approximate field for either the stress or the strain in the composite and then by minimizing or maximizing some functional of the stress and strain the unknown filed is found through a variational principle. The predicted stiffness is not an exact value, instead it is either larger or smaller than the actual value, depending on the variational method. The robust bounding property is the advantage of this approach. The first model to give robust upper and lower bounds are attributed to Voigt and Reuss [67] respectively. The Voigt model (Equation (2.86)) can be derived by minimizing the potential energy based on the assumption that the fiber and matrix have the same uniform strain. Similarly, the Reuss model (Equation (2.87)) can be derived by maximizing the complementary energy based on the assumption that the fiber and matrix have the same uniform stress.

$$\mathbf{C}^{Voigt} = \mathbf{C}^m + V_f(\mathbf{C}^f - \mathbf{C}^m) = V_f\mathbf{C}^f + V_f\mathbf{C}^m \tag{2.86}$$

$$\mathbf{S}^{Reuss} = \mathbf{S}^m + V_f(\mathbf{S}^f - \mathbf{S}^m) = V_f\mathbf{S}^f + V_f\mathbf{S}^m \tag{2.87}$$

The models of Voigt and Reuss give bounds for isotropic composites, which is hardly the real case. Besides, they give very broad gaps between the lower and higher bounds when fiber and matrix have very different materials, which provides litter information for the actual composite stiffness. Thus, Hashin and Shtrikman [68, 69] developed an alternative model by adopting a different variational principle for heterogeneous materials. There is a reference material in their method, based on which

the subsequent development is carried out. A single variation principle is used to give both the upper and the lower bounds by making appropriate reference materials. Choosing the stiffer component (usually fiber) as the reference material will give the upper bound while choosing the less stiffer component (usually matrix) will give the lower bound. When the reference material is with zero or infinite stiffness, the Hashin-Shtrikman model becomes the Voigt-Reuss model. Walpole [70,71] re-derived the Hashin-Shtrikman bounds using classical energy principles and extended them to anisotropic materials, which are called the Hashin-Shtrikman-Walpole bounds. These bounds were further extended to short fiber composites [72] and explicit formula for aligned ellipsoids were developed by Weng [73] and by Eduljee *et al.* [74, 75]. Weng gives the general bounding formula in terms of the stiffness $\mathbf{C}$ shown as

$$\mathbf{C} = [V_f \mathbf{C}^f \mathbf{Q}^f + V_m \mathbf{C}^m \mathbf{Q}^m][V_f \mathbf{Q}^f + V_m \mathbf{Q}^m]^{-1} \tag{2.88}$$

where the tensors $\mathbf{Q}^f$ and $\mathbf{Q}^m$ are defined as below:

$$\begin{aligned} \mathbf{Q}^f &= [\mathbf{I} + \mathbf{E}^0 \mathbf{S}^0 (\mathbf{C}^f - \mathbf{C}^0)]^{-1} \\ \mathbf{Q}^m &= [\mathbf{I} + \mathbf{E}^0 \mathbf{S}^0 (\mathbf{C}^m - \mathbf{C}^0)]^{-1} \end{aligned} \tag{2.89}$$

Note that $\mathbf{E}^0$ is the Eshelby's tensor [76] associated with the properties of the reference material with stiffness $\mathbf{C}^0$ and compliance $\mathbf{S}^0$.

The strain concentration tensor associated with the lower bound is given by Equation (2.88) when choosing matrix as the reference material.

$$\hat{\mathbf{A}}^{lower} = [\mathbf{I} + \mathbf{E}^m \mathbf{S}^m (\mathbf{C}^f - \mathbf{C}^m)]^{-1} \tag{2.90}$$

Eduljee and McCullough [74, 75] argue that the lower bound should be a model as it provides the most accuracy. Notice that the lower bound is identical to the Mori-Tanaka model, as shown by Equation (2.105).

Correspondingly, the strain concentration tensor is given from Equation (2.88) by choosing fiber as the reference material.

$$\hat{\mathbf{A}}^{upper} = [\mathbf{I} + \mathbf{E}^f \mathbf{S}^f (\mathbf{C}^m - \mathbf{C}^f)]^{-1} \tag{2.91}$$

where $\mathbf{E}^f$ is the Eshelby tensor computed for inclusions of matrix material surrounded by the fiber material.

Leilens *et al.* [77] suggest that at very high fiber volume fractions the composite stiffness should be much closer to the upper bound, or equivalently to the Mori-Tanaka prediction using fiber as the continuous phase. They interpolated the lower and upper bounds to give the predictive equation for the strain concentration factor, given by

$$\hat{\mathbf{A}}^{Lielens} = \{(1-f)[\hat{\mathbf{A}}^{lower}]^{-1} + f[\hat{\mathbf{A}}^{upper}]^{-1}\}^{-1} \tag{2.92}$$

where f is the interpolation factor depending on the fiber volume fraction, given by

$$f = \frac{V_f + V_f^2}{2} \tag{2.93}$$

2.4.1.2 Eshelby's Equivalent Inclusion. A fundamental model is Eshelby's equivalent inclusion [76]. This model solves for the elastic stress field in an around and ellipsoidal particle in an infinite matrix and can be used to model the stress and strain fields around a cylindrical fiber. Because this model only considers a single particle surrounded by an infinite matrix and the stiffness predicted by this model increases linearly with fiber volume fraction. One of the most important results from Eshelby is that the strain ε^C is uniform within an ellipsoidal inclusion and is related to the transformation strain by the following equation

$$\varepsilon^C = \mathbf{E}\varepsilon^T \tag{2.94}$$

where ε^T is also called the eigenstrain, which is the uniform strain acquired if it were a separate body from the matrix, and $\mathbf{E}$ is called the Eshelby's tensor which only depends on the inclusion aspect ratio and the matrix elastic constants.

For a dilute concentration short fiber reinforced composite, the average composite stiffness $\mathbf{C}$ in terms of strain-concentration tensor $\mathbf{A}$ and the matrix properties can be expressed by [66]

$$\mathbf{C} = \mathbf{C}^m + V_f(\mathbf{C}^f - \mathbf{C}^m)\mathbf{A} \tag{2.95}$$

where $\mathbf{C}^f$ and $\mathbf{C}^m$ are the stiffness tensors of the fiber and the matrix respectively. And the equation for the compliance in terms of the stress-concentration tensor $\mathbf{B}$ is:

$$\mathbf{S} = \mathbf{S}^m + V_f(\mathbf{S}^f - \mathbf{S}^m)\mathbf{B} \tag{2.96}$$

where $\mathbf{S}^f$ and $\mathbf{S}^m$ are the compliance tensors of the fiber and the matrix respectively and V_f is the fiber volume fraction. $\mathbf{A}$ and $\mathbf{B}$ are essentially ratios between the average fiber strain/stress ($\bar{\varepsilon}^f$,$\bar{\sigma}^f$) and the corresponding average of the composite ($\bar{\varepsilon}$,$\bar{\sigma}$), given by

$$\bar{\varepsilon}^f = \mathbf{A}\bar{\varepsilon} \tag{2.97}$$

$$\bar{\sigma}^f = \mathbf{B}\bar{\sigma} \tag{2.98}$$

The dilute Eshelby model replaces $\mathbf{A}$ in Equation (2.95) with $\mathbf{A}^{Eshelby}$ shown in the following equation

$$\mathbf{A}^{Eshelby} = [\mathbf{I} + \mathbf{E}\mathbf{S}^m(\mathbf{C}^f - \mathbf{C}^m)]^{-1} \tag{2.99}$$

The elastic modulus of short fiber composites can be predicted by the use of $\mathbf{A}^{Eshelby}$ in Equation (2.95)

2.4.1.3 Self-Constraint Method. Another approach to account for finite fiber volume fraction is the self-consistent method, which is generally credited to Hill [78] and Budiansky [79]. The application to short-fiber composites was developed by Laws and McLaughlin [80] and by Chou, Nomura and Taya [81]. This approach gives the strain concentration tensor in the following form

$$\mathbf{A}^{SC} = [\mathbf{I} + \mathbf{ES}(\mathbf{C}^f - \mathbf{C})]^{-1} \tag{2.100}$$

Without knowing the initial values of $\mathbf{C}$ and $\mathbf{S}$, an initial guess is made first to obtain the values of $\mathbf{E}$ and $\mathbf{A}^{SC}$ from Equation (2.100). And then these values are plugged into Equation (2.95) to update the values of the stiffness until it converges.

2.4.1.4 Halpin-Tsai Equations. The Halpin-Tsai equations [82] have been extensively used for predicting the properties of short-fiber composites. Halpin and Tsai found that three of Hermans' equations for stiffness could be expressed in the following form

$$\begin{aligned} \frac{P}{P_m} &= \frac{1 + \zeta\eta V_f}{1 - \eta V_f} \\ \eta &= \frac{(P_f/P_m) - 1}{(P_f/P_m + 1)} \end{aligned} \tag{2.101}$$

where P represents any one of the composite moduli, and P_f and P_m are the corresponding moduli of the fibers and matrix, while ζ is a parameter that depends on the matrix Poisson ratio and on the particular elastic property being considered. P in Equation (2.101) is a generic term, which can be the plane strain bulk modulus K_{23} for aligned fibers, the transverse shear modulus G_{23} for aligned fibers, the longitudinal shear modulus G_{12} for align fibers, bulk modulus K for particulate and shear modulus G for particulate respectively. The value of the parameter ζ is between 0 and ∞. Halpin and Tsai found that ζ varies as a function of the aspect ratio $\frac{l}{d}$. By

comparing the predicted results with those given by the 2-D finite element results, they also found that $\zeta = 2\frac{l}{d}$ gave good predictions for E_{11} of short fiber composites. Hewitt and de Malherbe [83] suggested making ζ as a function of fiber volume fraction V_f to predict the stiffness at high fiber volume fraction, and they gave a proposed equation $\zeta = 1 + 40V_f^{10}$ based on curve-fitting, which gave the value of G_{12} in good agreement with that given by 2-D finite element results.

Nielsen and Lewis [84, 85] modified the Halpin-Tsai equation by adding an additional term, which leads to the following form

$$\frac{P}{P_m} = \frac{1 + \zeta\eta V_f}{1 - \psi(V_f)\eta V_f} \tag{2.102}$$

where η has been defined in Equation (2.101) and $\psi(V_f)$ is a function of the maximum fiber volume fraction $V_{f_{max}}$ to give the appropriate behavior at the lower and upper volume fraction limits, the equation for both cases given by

$$\psi(V_f) = 1 + \left(\frac{1 - V_{f_{max}}}{V_{f_{max}}^2}\right) V_f \tag{2.103}$$

$$\psi(V_f) = \frac{1}{V_f}\left[1 - \exp\left(\frac{-V_f}{1 - (V_f/V_{f_{max}})}\right)\right] \tag{2.104}$$

The Nielson and Lewis model improves the predictions for shear modulus G of particle-reinforced composites and G_{12} of continuous-fiber reinforced composites.

2.4.1.5 Mori-Tanaka Predictions. Several models were created for non-dilute composite materials based on Mori and Tanaka's work [86]. The Mori-Tanaka strain concentration tensor $\mathbf{A}^{MT}$ assumes a different form from that of the Eshelby model's, which is given by [86]

$$\mathbf{A}^{MT} = \mathbf{A}^{Eshelby}[(1 - v_f)\mathbf{I} + v_f\mathbf{A}^{Eshelby}]^{-1} \tag{2.105}$$

This is the basic equation of the Mori-Tanaka model, based on which Taya and

Mura [87] and Taya and Chou [88] first developed the Mori-Tanaka predictions for the longitudinal modulus of a short-fiber reinforced composites.

Tandon and Weng [89] developed equations for the complete set of elastic constants of a short-fiber composites based on Mori and Tanaka's work, including the longitudinal modulus E_{11}, transverse modulus E_{22}, shear modulus G_{12} along the x_1 direction in the $x_1 - x_3$ plane, shear modulus G_{23} along the x_2 direction in the $x_1 - x_2$ plane, Poisson's ratio ν_{12} between the x_2 and the x_1 directions, and Poisson's ratio ν_{23} between the x_3 and the x_2 directions. This model is used in this research as this approach is one of the most accurate ones [66]. The equations for elastic moduli are given by [66, 89, 90]

$$E_{11} = \frac{E_m}{1 + V_f(A_1 + 2\nu_m A_2)} \tag{2.106}$$

$$E_{22} = \frac{E_m}{1 + V_f[-2\nu_m A_3 + (1 - \nu_m)A_4 + (1 - \nu_m)A_5 A]/2A} \tag{2.107}$$

Similarly, the shear modulus can be calculated as

$$G_{12} = G_m \left(1 + \frac{V_f}{\frac{G_m}{G_f - G_m} + 2(1 - V_f)S_{1212}}\right) \tag{2.108}$$

$$G_{23} = G_m \left(1 + \frac{V_f}{\frac{G_m}{G_f - G_m} + 2(1 - V_f)S_{2233}}\right) \tag{2.109}$$

And Poisson's ratios are calculated in the following way

$$\nu_{12} = \frac{\nu_m A - \nu_f(A_3 - \nu_m A_4)}{A + \nu(A_1 + 2\nu_m A_2)} \tag{2.110}$$

$$\nu_{23} = -1 + \frac{E_{22}}{2G_{23}} \tag{2.111}$$

where A and $A_i, i \in 1,2,3,4,5$ are parameters given by

$$\begin{aligned} A_1 &= D_1(B_4 + B_5) - 2B_2 \\ A_2 &= (1 + D_1)B_2 - (B_4 + B_5) \\ A_3 &= B_1 - D_1 B_3 \\ A_4 &= (1 + D_1)B_1 - 2B_3 \\ A_5 &= \frac{1 - D_1}{B_4 - B_5} \\ A &= 2B_2 B_3 - B_1(B_4 + B_5) \end{aligned} \tag{2.112}$$

where the values of parameters $B_i, i \in 1,2,3,4,5$ are given by

$$\begin{aligned} B_1 &= V_f D_1 + D_2 + (1 + V_f)(D_1 S_{1111} + 2S_{2211}) \\ B_2 &= V_f + D_3 + (1 - V_f)(D_1 S_{1122} + S_{2222} + S_{2233}) \\ B_3 &= V_f + D_3 + (1 - V_f)(S_{1111} + (1 + D_1)S_{2211}) \\ B_4 &= V_f D_1 + D_2 + (1 - V_f)(S_{1122} + D_1 S_{2222} + S_{2233}) \\ B_5 &= V_f + D_3 + (1 - V_f)(S_{1122} + S_{2222} + D_1 S_{2233}) \end{aligned} \tag{2.113}$$

and the values of parameters $D_i, i \in 1,2,3$ are given by

$$\begin{aligned} D_1 &= 1 + \frac{2(\nu_f - \mu_m)}{\lambda_f - \lambda_m} \\ D_2 &= \frac{\lambda_m + 2\mu_m}{\lambda_f - \lambda_m} \\ D_3 &= \frac{\lambda_m}{\lambda_f - \lambda_m} \end{aligned} \tag{2.114}$$

where λ_f, μ_f and λ_m, μ_m are Lame's constants for the fiber and the matrix respectively

and can be calculated by the following equations

$$\begin{aligned}
\lambda_m &= \frac{E_m \nu_m}{(1+\nu_m)(1-2\nu_m)} \\
\lambda_f &= \frac{E_f \nu_f}{(1+\nu_f)(1-2\nu_f)} \\
\mu_m &= \frac{E_m}{2(1+\nu_m)} \\
\mu_f &= \frac{E_f}{2(1+\nu_f)}
\end{aligned} \tag{2.115}$$

The $S_{ijkl}, i, j, k, l \in 1, 2, 3$ terms in Equation (2.113) are the components of the Eshelby's tensor for a fiber-like spheroid inclusion, which can be calculated by the following equations

$$S_{1111} = \frac{1}{2(1-\nu_m)} \left(1 - 2\nu_m + \frac{3a_r^2 - 1}{a_r^2 - 1} - \left[1 - 2\nu_m + \frac{3a_r^2 - 1}{a_r^2 - 1} \right] g \right)$$

$$S_{1122} = S_{1133} = \frac{1}{2(1-\nu_m)} \left[1 - 2\nu_m - \frac{1}{a_r^2 - 1} \right] + \frac{1}{2(1-\nu_m)} \left[1 - 2\nu_m - \frac{3}{2(a_r^2 - 1)} \right] g$$

$$S_{1212} = S_{1313} = \frac{1}{4(1-\nu_m)} \left(1 - 2\nu_m + \frac{a_r^2 + 1}{a_r^2 - 1} - \frac{1}{2} \left[1 - 2\nu_m + \frac{3(a_r^2 + 1)}{a_r^2 - 1} \right] g \right)$$

$$S_{2211} = S_{3322} = -\frac{1}{2(1-\nu_m)} \frac{a_r^2}{a_r^2 - 1} + \frac{1}{4(1-\nu_m)} \left(\frac{3a_r^2 - 1}{a_r^2 - 1} - (1 - 2\nu_m) \right) g$$

$$S_{2222} = S_{3333} = \frac{3}{8(1-\nu_m)} \frac{a_r^2}{a_r^2 - 1} + \frac{1}{4(1-\nu_m)} \left[1 - 2\nu_m - \frac{9}{4(a_r^2 - 1)} \right] g$$

$$S_{2233} = S_{3322} = \frac{1}{4(1-\nu_m)} \left(\frac{a_r^2}{2(a_r^2 - 1)} - \left[1 - 2\nu_m + 4\frac{3}{4(a_r^2 - 1)} \right] g \right)$$

$$S_{2323} = S_{3232} = \frac{1}{4(1-\nu_m)} \left(\frac{a_r^2}{2(a_r^2 - 1)} - \left[1 - 2\nu_m - 4\frac{3}{4(a_r^2 - 1)} \right] g \right) \tag{2.116}$$

where a_r is the aspect ratio of fiber and the value of g is given by the following equation:

$$g = \frac{a_r}{(a_r - 1)^{3/2}} [a_r (a_r^2 - 1)^{1/2} - \cosh^{-1} a_r] \tag{2.117}$$

2.4.2 Orientation Homogenization Method

Homogenization method is one of the most commonly used methods to predict material properties of non-aligned fiber reinforced composites. This method is based on unit cell analysis, assuming that the composite is formed by a periodic repetition of a unit cell, and the material properties are themselves periodic functions of some characteristic variables of the unit cell. This assumption lead to the conclusion that when the cell size shrinks to 0, the predicted material properties converge to the equivalent homogeneous properties of the material. Advani and Tucker [6, 31] popularized orientation averaging approach to predict the elastic properties of non-aligned short fiber composites. Their approach averages the elastic constants of unidirectional fibers to estimate the elastic properties of a short fiber composite with any given fiber orientation distribution. It has been demonstrated by Gusev *et al.* [91] that the orientation averaging method gives reliable predictions for engineering design application.

The equation (Equation (2.118)) for predicting the stiffness of an injection molded short fiber reinforced composite is given by Advani and Tucker without detailed proof. The development of this approach is based on a continuum model where the properties of the two phases are averaged with a homogeneous continuum, the properties of which are predicted by the previously discussed unidirectional stiffness prediction models. The properties of the composite material are then obtained as the average of these unidirectional properties over all directions weighted by the probability distribution function.

$$\begin{aligned} \langle C_{ijkl} \rangle &= b_1(a_{ijkl}) + b_2(a_{ij}\delta_{kl} + a_{kl}\delta_{ij}) + b_3(a_{ik}\delta_{jl} + a_{il}\delta_{jk} \\ &+ a_{jl}\delta_{ik} + a_{jk}\delta_{il}) + b_4(\delta_{ij}\delta_{kl}) + b_5(\delta_{ik}\delta_{jl} + \delta_{il}\delta_{jk}) \end{aligned} \tag{2.118}$$

In Equation (2.118), the scalars $b_i, i \in 1,2,,3,4,5$ are related to the components of the underlying unidirectional stiffness tensor in the contracted form, given by

$$\begin{aligned} b_1 &= C_{11} + C_{22} - 2C_{12} - 4C_{66} \\ b_2 &= C_{12} + C_{22} \\ b_3 &= C_{66} + \frac{1}{2(C_{23} - C_{22})} \\ b_4 &= C_{23} \\ b_5 &= \frac{1}{2(C_{22} - C_{23})} \end{aligned} \tag{2.119}$$

The fourth order tensor a_{ijkl} and the second order tensor a_{ij} in Equation (2.118) were defined in Equation 2.6. Fiber orientation tensors were proposed by Advani and Tucker [6] to describe an average orientation property of the composite. The composite under consideration must be over a sufficietnly large enough volume to contain many fibers, but small enough such that the statistics of the orientation is uniform all though. This assumption can be realized when the volume is compared to the dimension of the composite but large with respect to the fiber length. The proof of the orientation averaging approach proposed by Advani and Tucker was later given by Jack and Smith [5]. They employed the Laplace series of complex spherical harmonics to expand the fiber orientation distribution function assuming only that the distribution is symmetric about a single axis, given by

$$\psi(\theta, \phi) = \sum_{l=0}^{\infty} \alpha_l(\theta, \phi) \tag{2.120}$$

where each $\alpha_l(\theta, \phi)$ is a function of the complete spherical harmonics which are a 2D analogy of a series expansion on a sphere similar in concept to the 1D Fourier series. They developed an analytical form based on the fiber orientation tensor to calculate both the expectation and variance of the material stiffness tensor. In this research,

the orientation averaging method is used following the approach discussed in Jack and Smith [5], which will be discussed in detail in Chapter Four.

CHAPTER THREE

Comparison of Rigid Fiber Motion and Flexible Fiber Motion

This chapter compares the rod chain model with model based on Jeffery's equation. A concept of critical buckle aspect ratio is employed to define the rigidity or flexibility of a fiber, above which a fiber is flexible enough to be bent and twisted. When a fiber has an aspect ratio under the critical buckle aspect ratio, fiber motion predicted by the rod chain model overlaps perfectly with that of Jeffery's equation. The trajectories of a single rigid fiber with different initial orientations are shown by the rod chain model, which are in line with what Jeffery's equation predicts. The configuration of a single flexible fiber at different times shows the flexure of the fiber.

3.1 Rod Chain Model Implementation

The motion and orientation evolution of a single flexible fiber composed of a series of rods is determined by the following procedures implemented by an in-house code developed in Matlab, as shown in Appendix A.

1. At $t = 0$, an initial configuration of a flexible fiber and a flow field is given by the scripts in Appendix A on page 103. The fiber is generally stationary at this time.
2. Obtain the hydrodynamic friction forces $\mathbf{F}_i^h$ and the angular friction torques $\mathbf{T}_i^h$ on each of the rod and the bending torques $\mathbf{T}_i^b$ and the twisting torques $\mathbf{T}_i^t$ between each pair of the rods by solving Equations (2.73) $\sim$ (2.76) at time t, which is implemented by the scripts in Appendix A on page 101.
3. Obtain the internal constraint forces $\mathbf{X}_i$ by solving Equations (2.80) at time t, which is implemented by the scripts in Appendix A on page 104.

4. Update the angular velocities $\boldsymbol{\omega}_i$ at $t + \Delta t$ for each of the rod from Equation (2.78) by using the $\mathbf{X}_i$ solved from the last step by the Euler method, which is implemented by the scripts on page 100.
5. Update the position vector of the center of the fiber $\mathbf{r}_m$ at $t + \Delta t$ from Equation (2.81), which is implemented by the scripts on page 100.
6. Update the unit direction vectors of each of the rod $\boldsymbol{p}_i$ at $t + \Delta t$ from Equation (2.82), which is implemented by the scripts on page 100.
7. Update the position vectors of the centers of each of the rods $\mathbf{r}_i$ at $t + \Delta t$ by Equations (2.84) and (2.83), which is implemented by the scripts on page 106.
8. Update the translational velocities of each of the rod $\mathbf{v}_i$ from Equation (2.85), which is implemented by the scripts on page 101.
9. Repeat steps $1 \sim 7$.

After the above procedures, the motion of each of the component rods can be described. And then the evolution of the motion of the fiber can be simulated. In this work, simulation for one single flexible fiber takes about one hour to finish for time step size $\Delta t = 0.001$ on a PC with a Windows 7 64-bit operating system, a Intel(R) Core(TM)2 Quad CPU and 4.00 GB RAM. $\Delta t = 0.001$ was chosen because it was the largest time step that could generate stable numerical solutions for the differential equations for up to 1000 seconds of flow time. For simulation of a large number of fibers, the scripts were run on the supercomputer clusters Kodiack at Baylor University with 100 threads simultaneously running and 10 fibers on each thread.

3.2 Comparison of the Rod Chain Model and Jeffery's Equation

Jeffery's equation does not apply to long flexible fibers, as the equation can only describe the motion of perfectly rigid ellipsoids. As shown in the detailed description of the rod chain model, it allows the fiber to bend and twist, which is a way to take into

account the flexibility and thus the deformation of the fiber. This section compares the results from Jeffery's equation and the rod chain model for fibers with the same aspect ratio. From the comparison, the necessity of incorporating the deformation of fibers is shown.

The flexibility of a fiber depends on its aspect ratio, stiffness and the strength of the flow. Forgacs *et al.* [60,92] demonstrated there is a critical buckle aspect ratio r_c of a fiber above which the axial force along the fiber will be large enough to bend the fiber. This critical buckle aspect ratio depends on the relative strength of the fiber reflected by a ratio included in the following equation

$$\frac{\eta\dot{\gamma}}{E} = \frac{\ln(2r_c) - 1.75}{2r_c^4} \tag{3.1}$$

Throughout the following examples in this chapter, the fibers are placed within a pure shear flow with the velocity vector components expressed as $v_1 = \dot{\gamma}x_3$ and $v_2 = v_3 = 0$ where the scalar $\dot{\gamma}$ is the shear rate. This particular flow field will tend to rotate a fiber about the x_2 axis, where it will spend most of its time near the x_1 axis. This particular flow is selected to study for two reasons. The first is the periodic nature of the solution will highlight flaws in solution approaches due to the nature of the coupled ODEs, and the second is its prevalence in industrial applications where most industrial molded products experience a significant degree of shear during processing. In order to maintain the most accuracy, all the simulation work has been finished with only one bead in each rod.

When the aspect ratio of a fiber is smaller than its critical buckle aspect ratio, which also means the fiber is effectively rigid, fiber motion should exhibit the same trajectory as that predicted by Jeffery's equation. For a flow with $E/\eta\dot{\gamma} = 2 \times 10^5$ the critical buckle aspect ratio from Equation (3.1) is 21.13, and thus a fiber with aspect ratio of 10 will be effectively rigid. The motion orbit of a fiber with an aspect

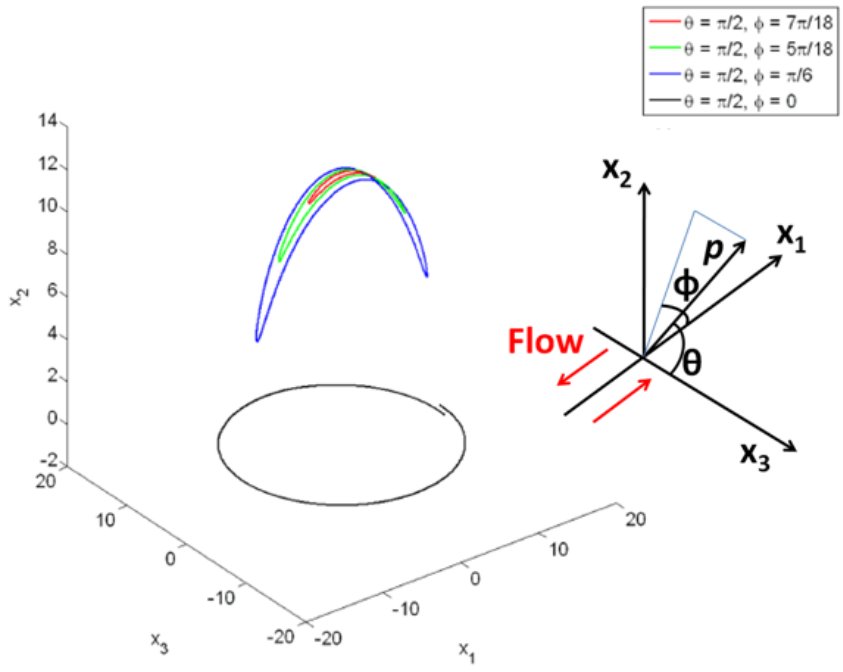

Figure 3.1: The orbits of a rigid fiber with different initial angles with the vortex axis x_3 ($N = 1, N_r = 10, a_r = 10, E/\eta\dot{\gamma} = 2 \times 10^5, r_c = 21.13$).

ratio of 10 is shown in Figure 3.1. The motion orbit indicates the motion trajectory of either one of the ends of the rigid fiber. A straightforward way to look at the the motion orbit is to imagine that there is a light dot on one of the ends of the rigid fiber, and the orbit is seen as the trajectory of the light dot as the fiber moves. The fiber motion orbit observed in Figure 3.1 for the rigid fiber motion solved using the rod chain model kinematics is a stable orbit, which is also the case predicted from Jeffery's equation for a rigid fiber. Figure 3.2 plots the first and third components of the end-to-end unit vector from Figure 2.6 for the fiber orientation obtained using the rigid-fiber kinetics of Jeffery's equation and fiber orientation obtained using the rod chain model. Figure 3.2 (a) is of a fiber of aspect ratio $a_r = 10$ and with flow and fiber stiffness parameters of $E/\eta\dot{\gamma} = 2 \times 10^5$, thus the critical buckle aspect ratio is $r_c = 21.13$. For this scenario, the Jeffery model and the rod chain model predict the same fiber orientation results. This observation is essential to aid in the validation of

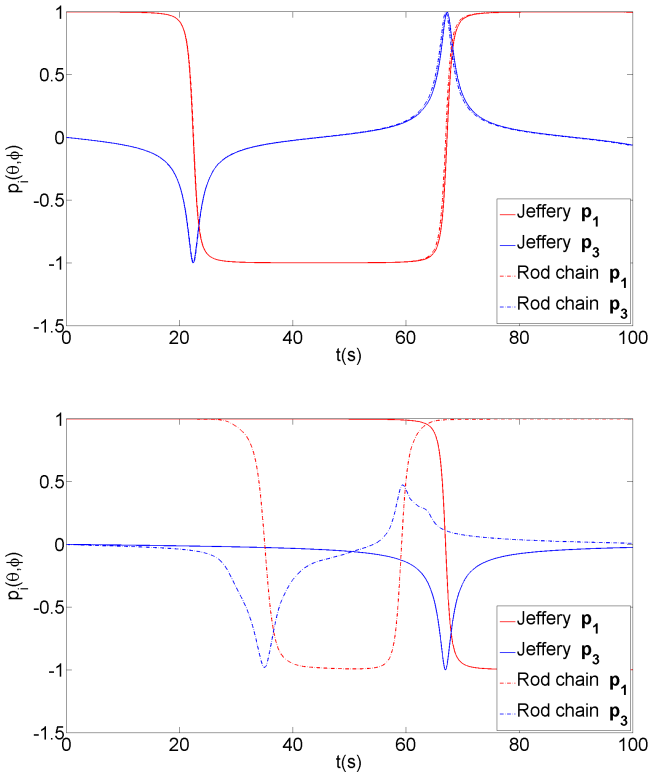

Figure 3.2: Motion period(a) ($N = 1, N_r = 10, a_r = 10, E/\eta\dot{\gamma} = 2 \times 10^5, r_c = 21.13$), initial unit direction vector $\boldsymbol{p} = [1, 0, 0]^T$, (b) ($N = 1, N_r = 30, a_r = 30, E/\eta\dot{\gamma} = 2 \times 10^3, r_c = 4.75$), initial unit direction vector $\boldsymbol{p} = [1, 0, 0]^T$).

the rod chain model since in the limiting case of a rigid fiber the flexible fiber model must approach the same orientation configuration as that predicted by the Jeffery model.

As the fiber increases in length or as the shear rate becomes stronger, the fiber will be bent and twisted significantly in the flow, as depicted in Figure 3.3. The deformation of the fiber in the flow suggests that the fiber in this example is relatively flexible and deformable due to the large fiber aspect ratio. Due to the bending of the fiber, different rods in the fiber will have different unit direction vectors. In order to examine the overall change of the fiber orientation for a flexible fiber, the end-to-end unit vector introduced in Figure 2.6 is plotted in Figure 3.2 (b) for a flexible fiber. For comparison purposes, the flexible fiber orientation is compared to that

of the rigid fiber as predicted by Jeffery's equation. Notice that the flexible fiber's orientation still is periodic, but the period of the orbit is considerably decreased as compared to that of the Jeffery fiber. This alteration in the orientation period and state will drastically alter both the final processed part's orientation state as well as the processing parameters of industrial parts as the fiber orientation is directly coupled with that of the effective shear stresses.

One deficiency of the rod chain model is that the bead number N does not appear to alter the motion period when the rod number $N_r = 1$, as observed in Figure 3.4. This can be explained from Equations (2.74), (2.78) and (2.82). When $N_r = 1$, the whole fiber is only a single rigid rod. So there is no bending torque $\mathbf{T}^b$, twisting toque $\mathbf{T}^t$, or internal constraint forces $\mathbf{X}$. Then $\frac{d\boldsymbol{\omega}}{dt}$ is only dependent on the value of hydrodynamic angular friction toque $\mathbf{T}^h$, which is proportional to N^3 as suggested by Equation (2.74). Then the N^3 in Equation (2.78) in the denominator will be canceled out, which makes $\frac{d\boldsymbol{\omega}}{dt}$ independent of N. When the unit direction vector $\boldsymbol{p}$ is updated by Equation (2.82), it will also be irrelevant to N. So the evolution of $\boldsymbol{p}$ does not depend on N when $N_r = 1$. This will bring a contradiction when the product of N and N_r actually represents the aspect ratio of the fiber, which influences the motion period of the fiber as suggested by Equation (2.10).

It is often more appropriate to characterize the bulk average of orientation, particularly when considering the final processed material stiffness. As discussed in Chapter Two, orientation tensors are generally used to described the bulk orientation of all the fibers in the flow, which can be calculated by Equation (2.6). Then for a second order orientation tensor, it is calculated by

$$a_{ij} = \oint_{\mathbb{S}^2} p_i p_j \psi(\theta, \phi) d\mathbb{S} \tag{3.2}$$

If a uniform distribution of fiber orientations is assume, then from Equation (2.5)

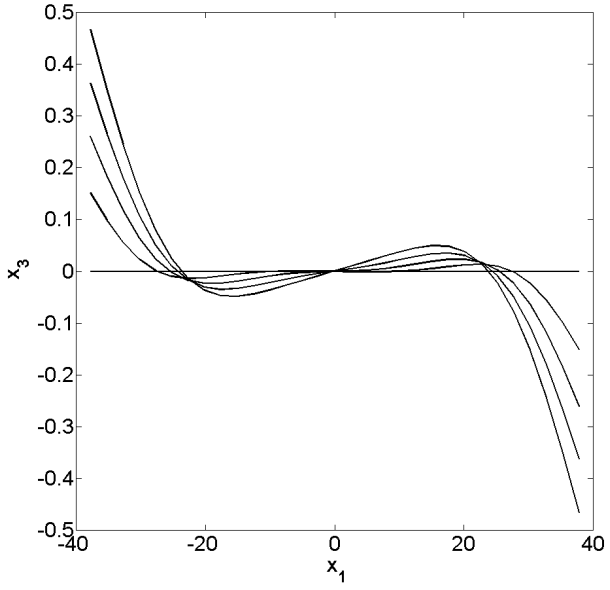

Figure 3.3: Deformation of a flexible fiber ($N = 1, N_r = 30, a_r = 30, E/\eta\dot{\gamma} = 2 \times 10^3, r_c = 4.75$), initial unit direction vector $\boldsymbol{p} = [1, 0, 0]^T$).

the distribution function $\psi(\boldsymbol{p}) = \frac{1}{4\pi}$. A random distribution of fiber orientations will result in an orientation tensor of the following form

$$\mathbf{a} = \begin{bmatrix} \frac{1}{3} & 0 & 0 \\ 0 & \frac{1}{3} & 0 \\ 0 & 0 & \frac{1}{3} \end{bmatrix}$$

whereas a unidirectional distribution of fiber orientations along the x_1 direction will result in the following form

$$\mathbf{a} = \begin{bmatrix} 1 & 0 & 0 \\ 0 & 0 & 0 \\ 0 & 0 & 0 \end{bmatrix}$$

The bulk orientation response is shown in Figure 3.5 for a pure shear flow with a fiber aspect ratio of 30. The flexible fiber equations of motion are solved for the same aspect ratio and flow parameters as the Jeffery model solution and for a suspension of 1000 discrete flexible fibers. The form of Equation (3.2) assumes a continuous function of orientation, but for a finite sample set, the orientation tensor can be approximated as

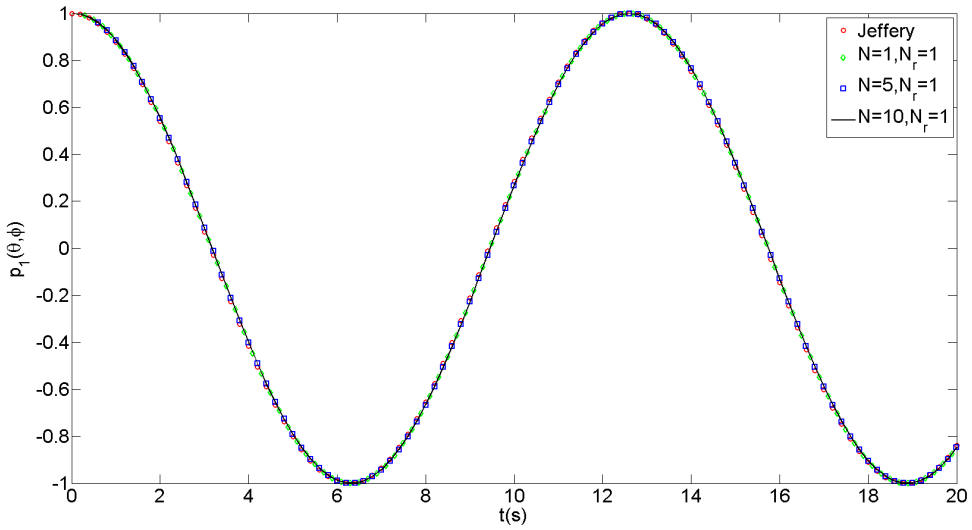

Figure 3.4: Number of beads N does not alter the motion period when rod number $N_r = 1$ ($E/\eta\dot{\gamma} = 2 \times 10^5, r_c = 21.13$).

$$a_{ij} = \frac{\sum_{n=1}^{N_f} p_i p_j}{N_f} \tag{3.3}$$

where N_f is the number of fibers in the sample. The evolution of the orientation tensor from Jeffery's model is shown in Figure 3.5 as well as that obtained from the rod chain model for the 1000 samples. As show in Figure 3.5, initially the fibers are randomly orientated with $a_{11} = a_{22} = a_{33} = \frac{1}{3}$, and the Jeffery model predicts a periodical change of the components of the orientation tensor, which corresponds to the evolution of the unit direction vector shown in Figure 3.2.

The result given by the rod chain model deviates from the one given by the Jeffery model in two aspects. The motion period for the flexible fibers are reduced and there is an orbit drifting phenomenon happening, as for the black curves in the plots of Figure 3.5, the a_{22} component decreases toward 0 and at the same time the a_{11}, a_{33} and a_{13} components change periodically. This discrepancy arises because of the flexibility of fibers. Notice the fibers have aspect ratios of 30, which is much large than the critical buckle aspect ratio. The ability of rod chain model to address

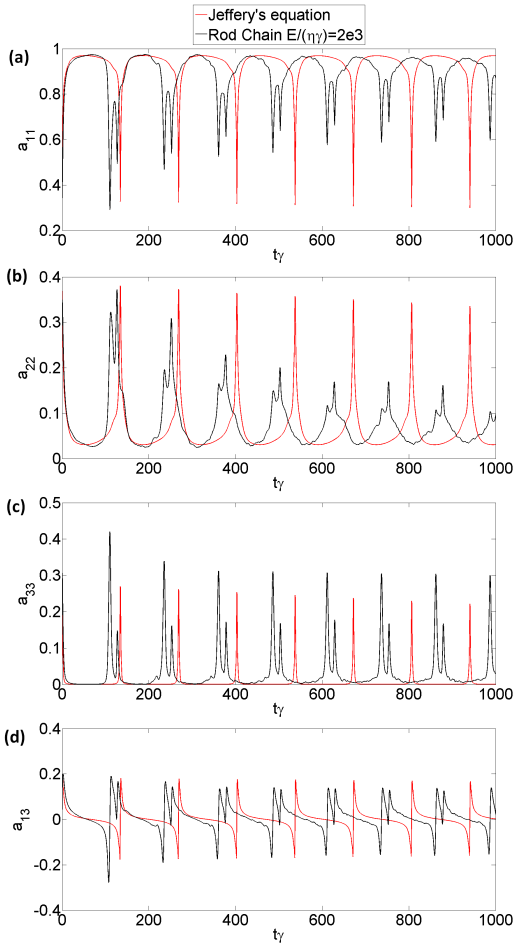

Figure 3.5: Comparison of the evolution of the components of the orientation tensor ($N = 1, N_r = 30, a_r = 30, r_c = 4.75, N_f = 1000$).

this flexibility of fibers result in the discrepancy described above. The influence of the fiber flexibility on the drifting behavior of the motion orbit will be discussed in Chapter Four.

Another difference for the plots of the evolution of the seconde order orientation tensor in Figure 3.5 is there is a "double-peaks" behavior for the results given by the rod chain model for flexible fibers. The "double-peaks" indicate there is a sudden bouncing back of the ends of the fibers when the fiber is significantly bent. For a flexible fiber, it has a small stiffness, but when the fiber is deformed significantly, the stiffness of the fiber will react strongly to straighten the fiber, which will cause a

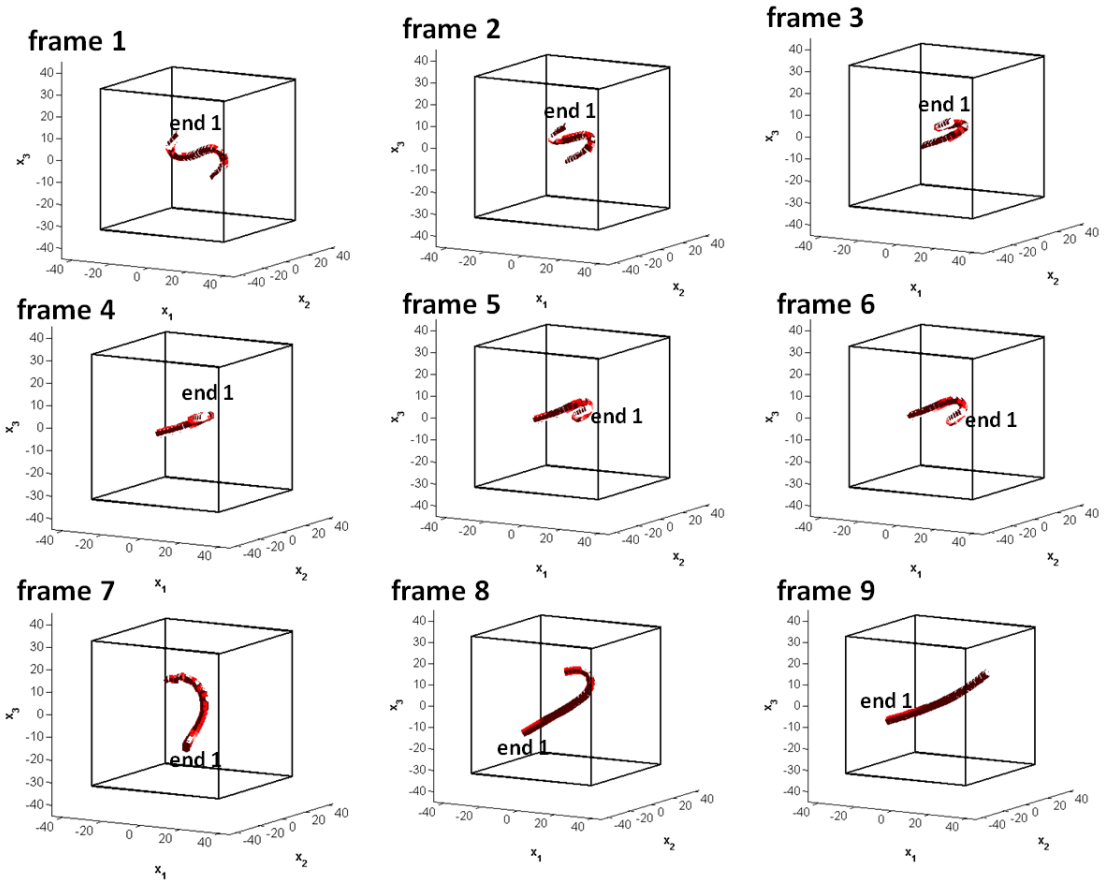

Figure 3.6: Deformation of a flexible fiber in a pure shear flow, $N = 1, N_r = 30, a_r = 30, E/\eta\dot{\gamma} = 1 \times 10^4$.

sudden bouncing back of the ends of the fiber. Figure 3.6 shows 9 consecutive frames for the motion of a flexible fiber. The marker "end 1" in the figure indicates one of the ends of the fiber, so that the same end can be recognized in all 9 frames. From the figure we can see that the fiber is very flexible and there is significant deformation on the fiber. Frame 6 $\sim$ 9 show the sudden bouncing back of the ends of the fiber.

When the fiber becomes significantly flexible, deformation of the fiber may cause it cutting cross itself, which makes the physics become more complicated. The fiber shown in Figure 3.6 is flexible enough to cut cross itself when it is deformed heavily. Frame 3 through 5 show that the fiber cuts cross and passes through itself. It is not physical that the fiber passes through itself, as it means that at some time

point during the deformation, two different parts of the fiber occupy the same position in the space, which is not possible. This shows the deficiency of the rod chain model, which means it can not be applied to a fiber that is so flexible that it cuts cross and passes through itself under heavy deformation.

CHAPTER FOUR

Material Properties Prediction of Flexible Fiber Reinforced Composites

This chapter covers the prediction of material properties, specifically the stiffness tensor, based on the orientation and waviness of flexible fibers caused by the flow kinetics during injection molding of polymeric composites. A grain decomposition approach is employed and the prediction of the value of the stiffness tensor is done in two steps, similar to that proposed in Jack and Smith's publication [5]. The first step is to decompose the whole part of the material under consideration into a set of smaller aggregates of uniaxially aligned fibers with the same concentration of fibers, and the stiffness tensor of each aggregate is predicted using micro-mechanical approaches. The second step is to predict the expectation value, which is the sample mean, for the stiffness tensor over each of the aggregates whose orientation is sampled from the orientation and flexure distribution functions. The resulting expectation is the stiffness tensor for the polymeric composite.

4.1 Flexible Fiber Orientation

For a rigid fiber, the orientation of the fiber is described by a single unit direction vector along the major axis of the fiber. The orientation of the fiber can then be fully described by the two angle parameters θ and ϕ, as shown in Figure 2.2 and defined in Equation (2.1) where a fiber can have any orientation from $\theta \in [0, \pi]$ and $\phi \in [0, 2\pi)$. Conversely, a flexible fiber will display a wavy configuration under the influence of the flow (as shown in Figure 3.1), and a normalized end-to-end vector will be used to describe the orientation of the fiber, as shown in Figure 3.3. This normalized unit direction vector, which is also associated with the same two angle parameters, can

capture the approximate orientation of a flexible fiber in the flow, and this is also a common way to describe the orientation of a curved or flexed body.

4.2 Flexible Fiber Waviness

One salient characteristic of long flexible fibers is that they will become wavy under the influence of the flow. The fibers display curved configuration in the flow and it is possible, depending on the viscous characteristics, curing kinetics and the stiffness of the fiber, that it will remain curved in the processed composites. The fiber wavy configuration is assumed to be a planar sinusoidal curve [4] and defined by

$$z' = A \sin \frac{2\pi x'}{L} \tag{4.1}$$

where A and L are the amplitude and the range of the sinusoidal curve, respectively. z' and x' are the two perpendicular axes of the coordinate system in the plane where the fiber is, as shown in Figure 4.1. x' is the axis along the end-to-end vector of the flexible fiber, and y' and z' form a right-handed coordinate system with x' and z' lying in the fiber plane and y' normal to the fiber plane.

The fiber waviness α is defined as

$$\alpha = 2\pi \frac{A}{L} \tag{4.2}$$

An in-house code is developed to calculate fiber waviness, and is provided in Appendix B. The idea is to fit a sinusoidal curve to the fiber configuration based on the local coordinates of each rod of the fiber (Figure 4.2). The local coordinates of each rod (x_i', z_i') are obtained by running the rod chain model for the fiber defined in Equations (2.69) $\sim$ (2.85) and using the MATLAB code provided in Appendix B. By minimizing

$$R \equiv (z_i' - A \sin \frac{2\pi x_i'}{L})^2 \tag{4.3}$$

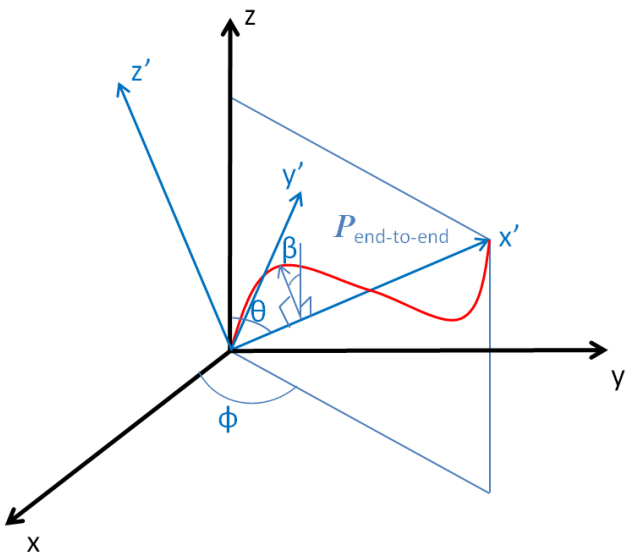

Figure 4.1: Flexible fiber orientation and configuration.

using a least square method, the amplitude A that minimizes equation (4.3) is

$$A = \frac{\sum z_i' \sin \frac{2\pi x_i'}{L}}{\sum (\sin \frac{2\pi x_i'}{L})^2} \tag{4.4}$$

4.3 Investigation of the Influence of Fiber Waviness on Fiber Orientations

This section discusses how fiber waviness influences fiber orientations. The motions of individual fibers with different waviness are compared in terms of the unit end-to-end vectors. The motions of groups of fibers are compared as well in terms of the second orientation tensor and the differences are shown as a result of different flexibility/waviness.

As defined in Chapter Three, the unit end-to-end vector $\boldsymbol{p}_{end-to-end}$ is used to describe the orientation of a flexible fiber. Figure 4.3 shows the evolution of the components of $\boldsymbol{p}_{end-to-end}$ for single flexible fibers with different flexibility and $\boldsymbol{p}$ for a single rigid fiber moving in a pure shear flow. The pure shear flow has velocities along the x_1 direction and velocity gradient along the x_3 direction given by

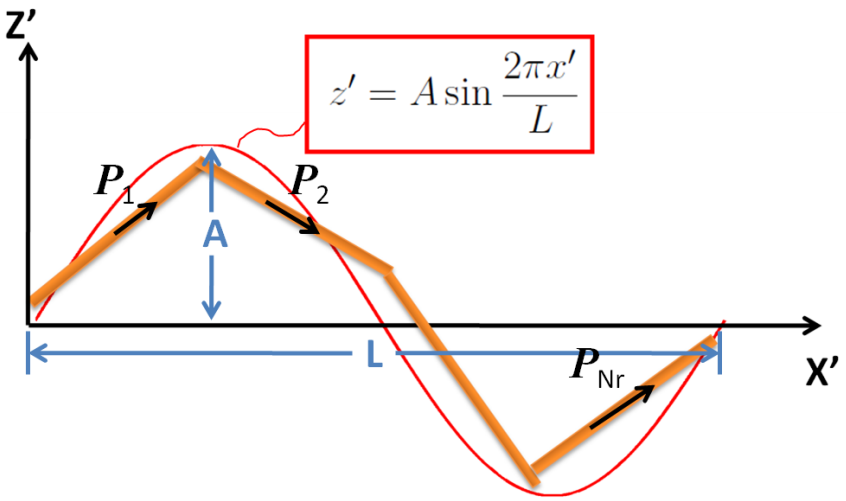

Figure 4.2: The scheme of calculating the fiber waviness.

$$\boldsymbol{\kappa} = \begin{bmatrix} 0 & 0 & 1 \\ 0 & 0 & 0 \\ 0 & 0 & 0 \end{bmatrix} \tag{4.5}$$

For the rigid fiber scenario, the fiber has an initial orientation with the two angle parameters $\theta = \frac{\pi}{4}$ and $\phi = \frac{\pi}{4}$, which make the unit direction vector along the $[\frac{1}{2}, \frac{1}{2}, \frac{1}{\sqrt{2}}]^T$ direction. For the three flexible fiber scenarios, each fiber is straight initially and along the $[\frac{1}{2}, \frac{1}{2}, \frac{1}{\sqrt{2}}]^T$ direction. The motion of the rigid fiber in terms of the unit direction vector $\boldsymbol{p}$ is given by the solution of Jeffery's equation, shown in Figure 4.3 as the red line, and it can be seen that the periodic motion previously alluded to in a shearing fluid is exhibited. The motions of flexible fibers, given by the solution of the rod chain model, in terms of $\boldsymbol{p}_{end-to-end}$ are shown with a range of fiber stiffness presented to demonstrate the effects of flexure on the orientation. For the rod chain model, when the fiber has a large elastic modulus relative to the strength of the flow field, the motion of the fiber is visually identical to that of a rigid fiber with the same aspect ratio solved using Jeffery's equation, shown as the green line in Figuire 4.3. The evolution of $\boldsymbol{p}_{end-to-end}$ for flexible fibers are not as perfectly periodical as that of the rigid fiber given by Jeffery's equations, which is due to the drifting the orbits.

But it is worthwhile to note that before the drifting starts, flexible fibers undergo periodical motions in the pure shear flow with a decreasing motion period as the strength of the fibers decreases.

Unlike the motion of a rigid straight fiber in a shear flow, which rotates in a stable orbit (see Figure 3.1) with fiber orbit constant (see Equation (2.9)) ranging from 0 to ∞, the ends of a flexible fiber does not follow a stable orbit and the orbit drifts toward $C = \infty$ or $C = 0$ depending on a big C ($C > 0.2$) or a small C ($C < 0.05$) [22]. $C = \infty$ indicates a rotating motion in the $x_1 - x_3$ plane, whereas $C = 0$ indicates a spinning motion with the fiber along the x_2 direction, which is the direction of the vorticity of the flow filed. However, it is found in this research that the motion orbit of a flexible fiber drifts also depending on the magnitude of the flexibility (waviness) of the fiber.

As shown in Figure 4.3, for the flexible fiber with $E/\eta\dot{\gamma} = 1 \times 10^4$, which corresponds to a less flexible fiber in this research, the p_3 component of the unit end-to-end vector is decreasing toward 0 whereas the p_1 and p_2 components change periodically, which means the motion orbit drifts to $C = 0$. It is not surprising that the p_1 component hasn't decreased in the time range of the plot (p_1 will eventually goes to 0, supposedly) and the p_2 component hasn't increased much (p_2 will eventually goes to 1, supposedly), as it has been reported [22] that the drifting of the orbit to $C = 0$ is slow. For the more flexible fiber in this research with $E/\eta\dot{\gamma} = 5 \times 10^3$, the p_2 component decreases rapidly toward 0 whereas the p_1 and p_3 components change periodically, which indicates that the orbit drifts to $C = \infty$. Notice that the two flexible fibers have the same aspect ratio and the same initial orientation, which should have given the same drifting behavior, but their orbits drift toward

two different directions. Thus it is believed that the different flexibility of the fibers causes the different drifting behaviors.

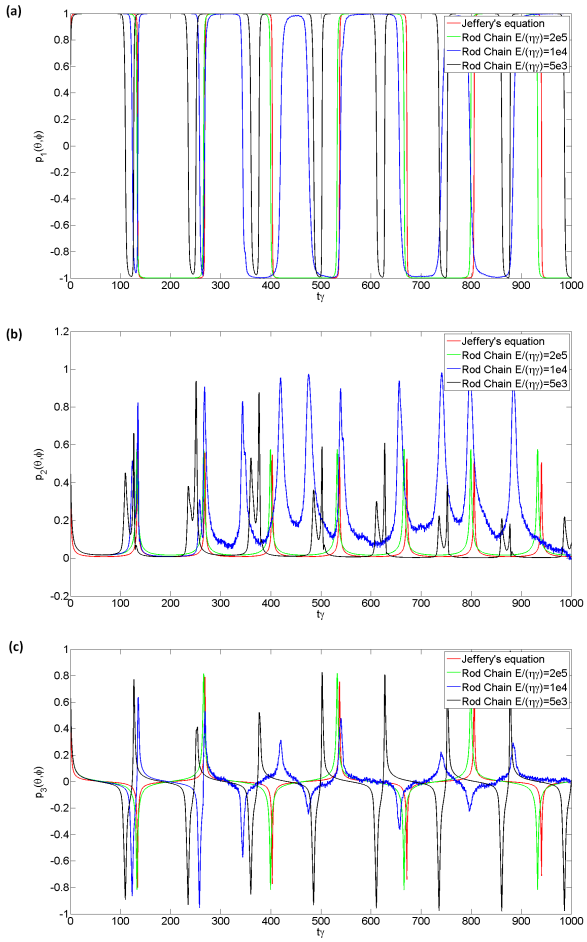

Figure 4.3: Evolution of the orientation of single isolated fibers, $\boldsymbol{p}_{initial} = [\frac{1}{2}, \frac{1}{2}, \frac{1}{\sqrt{2}}]^T$, $N = 1$, $N_r = 30$, $a_r = 30$, $Re = 0.1$, $\gamma = 1.0 sec^{-1}$: (a) the first component; (b) the second component; (c) the third component.

It also can be seen from the plots in Figure 4.3 that there is disturbance or noise on the curves of the less flexible fiber, which is marked by the blue line. One possible explanation for the occurrence of the noise is associated with the deformation or the wavy configuration of the flexible fibers. The unit end-to-end vector adopted to characterize the orientation of a flexible fiber is fundamentally not equivalent to the unit direction vector of a rigid straight fiber, which is always along its axis. The

direction change of the unit direction vector is only caused by the rotation of the rigid fiber, whereas the direction change of the unit end-to-end vector is caused by both the rotation of the flexible fiber as well as the deformation of the fiber, especially the bending deformation of the two ends of the fiber. It can be imagined that the direction change of the unit direction vector due to the bending deformation of the ends must be very sensitive compared to the rotating motion of the fiber simply because of the definition of the end-to-end vector, which is a vector drawn between the two ends of the fiber. Thus the evolution of the unit end-to-end vector is caused by the combination of two kinds of "motion", one of which is the rotation of the flexible fiber, the other the deformation of the flexible fiber, which is shown as the noise on the plots.

The flexibility of fibers comes into play when fibers have small elastic moduli compared to the strength of the flow field (see Equation (3.1) for a description of this critical buckle aspect ratio). Fibers under the influence of a given flow may experience a different flexibility/waviness response due to their individual material makeup. This is demonstrated in Figure 4.4 where the flexure response for fibers with differing stiffnesses' is plotted for a shearing flow. The vertical axis is the fiber waviness. When this ratio is zero a fiber is straight, and as the ratio increases the degree of flexure of a fiber increases. For the relatively rigid fiber (indicated by the green line in Figure 4.4), the waviness remains a zero, but as the stiffness is reduced, the maximum magnitude a given fiber is flexed increases. It is interesting to note that the semi-rigid fiber ($E/\eta\gamma = 1 \times 10^4$) actually spends more time in flexure as compared to the flexible fiber, but the maximum peak of the waviness ratio is the greatest for the soft fiber. This is due to the drifting of the orbit resulting in the change of the motion period.

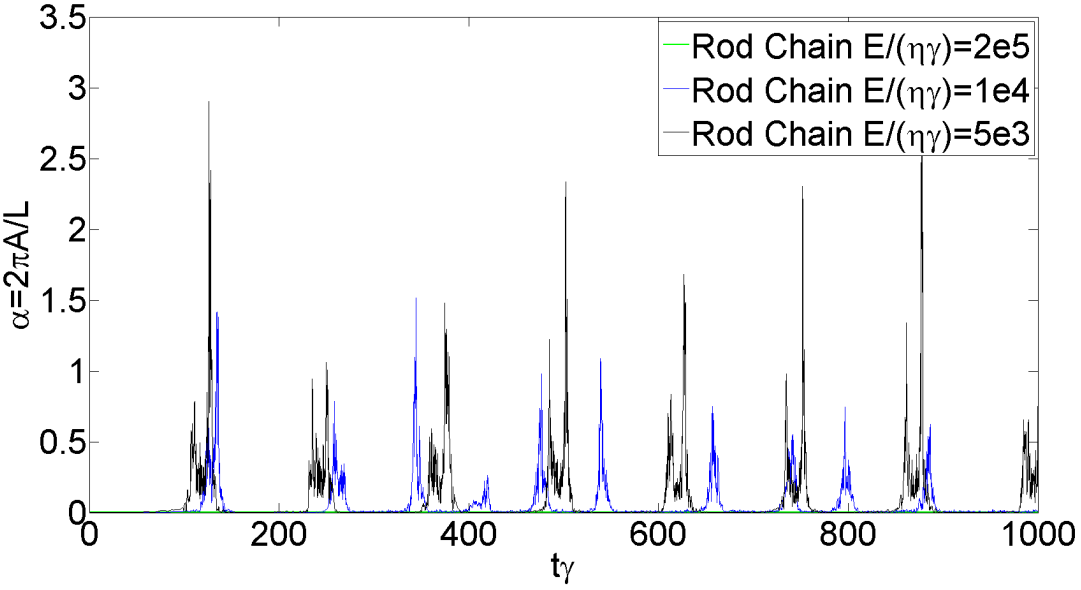

Figure 4.4: Evolution of the waviness of a single flexible fiber, N=1, Nr=30, ar=30, Re=0.1, $\gamma = 1.0sec^{-1}$.

For industrial composites, the motion of an individual fiber is somewhat irrelevant, but it is the bulk response that is important. Therefore we look at a set of fibers randomly sampled from an initially isotropic orientation distribution $\psi(\theta, \phi) = \frac{1}{4\pi}$ and plot the components of the orientation tensor from Equation (3.3). The change of motion period is also seen from the evolution of the components of the second order orientation tensor for rigid fibers as indicated by Figure 4.5. For each of the four situations depicted in Figure 4.5, there are initially 1000 fibers randomly orientated in the flow, which corresponds to a $\frac{1}{3}$ value for a_{11}, a_{22} and a_{33}. Note that due to the finite size of samples, results given by Jeffery's equation and the rod chain model for rigid fibers don't perfectly overlap with each other, but the changes of these two curves follow the same pattern. The drifting of the orbits can be seen from the plots as well. For the less flexible fibers with $E/\eta\dot{\gamma} = 1 \times 10^4$, the a_{33} and a_{13} components decrease toward 0 whereas the a_{11} component decreases slowly and a_{22} component increases slowly and both of them change periodically, which means the orbits of all

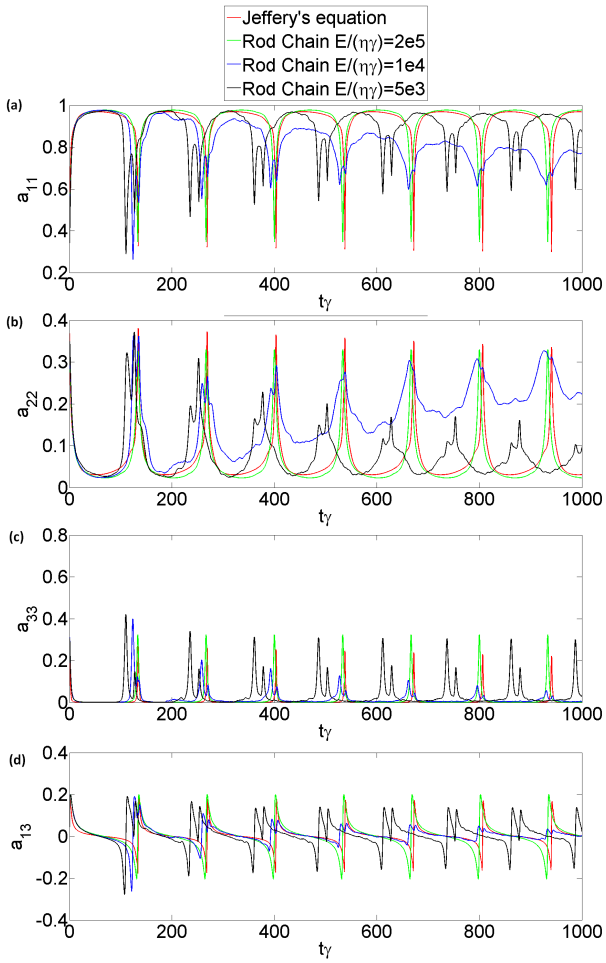

Figure 4.5: Evolution of the second order orientation tensor for 1000 initially randomly orientated fibers, $N = 1$, $N_r = 30$, $a_r = 30$, $Re = 0.1$, $\gamma = 1.0sec^{-1}$.

the fibers drift to $C = 0$. For the more flexible fiber with $E/\eta\dot{\gamma}$, the a_{22} component decreases toward 0 whereas the a_{11}, a_{33} and a_{13} components change periodically, which indicates that the orbits of all the fibers drift toward $C = \infty$.

The orbit drifting of all the fibers indicates its independence of the initial orientations. But from Equation (2.9), the initial fiber orbit constant depends on the orientation of the fiber, and the initial fiber orbit constant tells how the orbit drifts. One possible explanation is when fiber has a large aspect ratio, the drifting behavior largely depends on the flexibility of the fiber. This new observation invites investigation of the drifting behavior of long flexible fibers.

4.4 Material Properties Prediction

The material stiffness tensor is addressed through the grain decomposition approach discussed in Jack and Smith's paper [5]. A modification is made to adapt the method to flexible wavy fiber composites. The first step is to decompose the whole part into a set of smaller aggregates of unidirectionally aligned wavy fibers with the same concentration of fibers as the representative volume. The stiffness tensor of each of the aggregates is then predicted using a micro-mechanics approach, which in this study is the method from Hsiao and Daniel [4]. The second step is to obtain material stiffness values by computing the expectation value from the aggregates of unidirectional wavy fibers using the fiber orientation distribution function $\psi(\theta, \phi, \beta)$. Notice, unlike rigid fibers, there are three orientation parameters to capture the plane in which the fiber flexure is contained within. The three angle parameters are shown in Figure 4.1 where θ is the angle between the fiber end-to-end vector and the global z-axis. ϕ is the angle between the projection of the end-to-end vector on the xy-plane and the global x-axis, and β is the angle between the fiber plane and the plane formed by the global z-axis and the projection of the end-to-end vector on the xy-plane. For the present study we will assume that at the mold inlet all fibers in the flow are straight and are well represented by an isotropic three dimensional orientation distribution. The initial straight fiber assumption of the fibers is sufficiently described by the angle parameters θ and ϕ, and the associated fiber orientation distribution function initially is only a function of θ and ϕ, which is $\psi(\theta, \phi) = \frac{1}{4\pi}$. The expectation value of the material stiffness tensor after the composite is processed is formulated from the non-correlated aggregate of unidirectional fibers defined as the first moment of the fiber orientation probability distribution function $\psi(\theta, \phi, \beta)$ as [5]

$$\langle C_{ijkl} \rangle = \oint_{\mathbb{S}} Q_{pi}(\theta, \phi, \beta) Q_{qj}(\theta, \phi, \beta) Q_{rk}(\theta, \phi, \beta) Q_{sl}(\theta, \phi, \beta) \bar{C}_{pqrs} \psi(\theta, \phi, \beta) d\mathbb{S} \quad (4.6)$$

where $\langle C_{ijkl} \rangle$ is the expectation value of the stiffness tensor, $\bar{C}_{pqrs}$ is the unidirectional wavy fiber stiffness tensor of the aggregate with respect to the coordinate system along the aggregate's principal directions, and $Q_{pi}(\theta,\phi,\beta)Q_{qj}(\theta,\phi,\beta)Q_{rk}(\theta,\phi,\beta)Q_{sl}(\theta,\phi,\beta)\bar{C}_{pqrs}\psi(\theta,\phi,\beta)$ is the unidirectional wavy fiber stiffness tensor with respect to the global coordinate. The rotation matrix $Q(\theta,\phi,\beta)$ in Equation (4.6) is defined as

$$Q = \begin{bmatrix} \sin\theta\cos\phi & \sin\theta\sin\phi & \cos\theta \\ -\sin\phi\cos\beta - \cos\theta\cos\phi\sin\beta & \cos\phi\cos\beta - \cos\theta\sin\phi\sin\beta & \sin\theta\sin\beta \\ \sin\phi\sin\beta - \cos\theta\cos\phi\cos\beta & -\cos\phi\sin\beta - \cos\theta\sin\phi\cos\beta & \sin\theta\cos\beta \end{bmatrix} \quad (4.7)$$

The derivation of the rotation matrix is shown in Appendix C.

An in-house code has been developed in Matlab to solve the stiffness response of long fiber reinforced composites, as shown in Appendix B following the procedures shown below.

1. Run the rod chain model for each one of a group of initially randomly oriented flexible fibers, which is implemented by the scripts in Appendix A. The random initial orientations are generated by the scripts in Appendix B on page 119.
2. Obtain the compliance of the unidirectional lamina referred to the principal material axes by the Tandon-Weng theory, which is implemented by the scripts in Appendix B on page 120.
3. Calculate the waviness for each fiber based on the results given by the rod chain model and obtain the elastic properties of each of the aggregates of a unidirectional composite with uniform fiber waviness from the equations given by Hsiao and Daniel [4], which is implemented by the scripts in Appendix B on page 115.
4. Obtain the stiffness tensor for each of the aggregates of a unidirectional composite with uniform fiber waviness, which is implemented by the scripts in Appendix B on page 124.

5. Calculate the rotation matrix for each of the aggregates and rotate the respective stiffness tensor into the global coordinate and obtain the sample mean of the stiffness tensor by averaging the stiffness tensors over all the aggregates, which is implemented by the scripts in Appendix B on page 117.

The following sub-sections in this section discusses the implementation of the above method and give the simulation results. Section 4.4.1 describes the model by Hisao and Daniel for predicting the stiffness response of a unidirectional flexible fiber reinforced composite. Section 4.4.2 describes the orientation averaging method by Jack and Smith for the stiffness prediction with statistical sampling. Section 4.4.3 gives the simulation results.

4.4.1 Material Stiffness Prediction of Aggregates

The analytical model used to predict the elastic properties of a unidirectional composite with uniform fiber waviness is based on a model proposed by Hisao and Daniel [4] for the representative volume considered in Figure 4.6. The configuration of the fiber is assumed to be a planar sinusoidal curve. This assumption may not be valid when fiber is heavily deformed as the fiber configuration may form a spatial 3-D curve. Hsiao and Daniel divide the volume into infinitesimally thin slices of thickness dx', x' being the end-to-end vector direction and the load direction. They then obtain the compliance of each of the slice from the compliance transformation relations, and then integrate the strains in the x' direction over the range of the sine function, with the elastic properties of the composite determined from these average strains. Note that the configuration of the flexible fiber can be assumed to be a planar curve other than the sinusoidal curve only requiring a different definition for the fiber waviness. The whole derivation of the equations is in Hsiao and Daniel's paper [4] with the following equations for calculating the elastic properties of a unidirectional

composite with uniform fiber waviness in the global reference frame provided here for completeness

$$
\begin{aligned}
E_{x'} &= \frac{1}{S_{11}+(2S_{12}+S_{66})I_3+S_{22}I_5} \\
\nu_{x'y'} &= -\frac{S_{12}I_6+S_{23}I_8}{S_{11}+(2S_{12}+S_{66})I_3+S_{22}I_5} \\
\nu_{x'z'} &= -\frac{(S_{11}S_{22}-S_{66})I_3+S_{12}(I_1+I_5)}{S_{11}+(2S_{12}+S_{66})I_3+S_{22}I_5} \\
E_{y'} &= \frac{1}{S_{22}} \\
\nu_{y'x'} &= -\frac{S_{12}I_6+S_{23}I_8}{S_{22}} \\
\nu_{y'z'} &= -\frac{S_{23}I_6+S_{12}I_8}{S_{22}} \\
E_{z'} &= \frac{1}{S_{11}I_5+(2S_{12}+S_{66})I_3+S_{22}I_1} \\
\nu_{z'y'} &= -\frac{(S_{11}+S_{22}-S_{66})I_3+S_{12}(I_1+I_5)}{S_{11}I_5+(2S_{12}+S_{66})I_3+S_{22}I_1} \\
\nu_{z'y'} &= -\frac{S_{23}I_6+S_{12}I_8}{S_{11}I_5+(2S_{12}+S_{66})I_3+S_{22}I_1} \\
G_{x'y'} &= \frac{1}{2(S_{22}-S_{23})I_8+S_{66}I_6} \\
G_{y'z'} &= \frac{1}{2(S_{22}-S_{23})I_6+S_{66}I_8} \\
G_{x'z'} &= \frac{1}{4(S_{11}+S_{22}-2S_{12})I_3+S_{66}(I_1-2I_3+I_5)}
\end{aligned}
\tag{4.8}
$$

where E is the young's modulus, ν is the Poisson's ratio and G is the shear modulus. S_{ij}, for $i,j=1,2,3,4,5,6$, are the components of the compliance tensor of the unidirectional lamina of straight fibers given in the principal material axes, marked by 1, 2, 3 and as shown in Figure 4.6.

There are many methods to calculate the compliances of unidirectional straight fiber composites, as was discussed in the Chapter Two. In this study, the unidirectional straight fiber compliances are calculated based the Tandon-Weng theory [89] by an in-house code in the Appendix B, Section 2.3. I_i, for $i=1,3,5,6,8$, in Equation

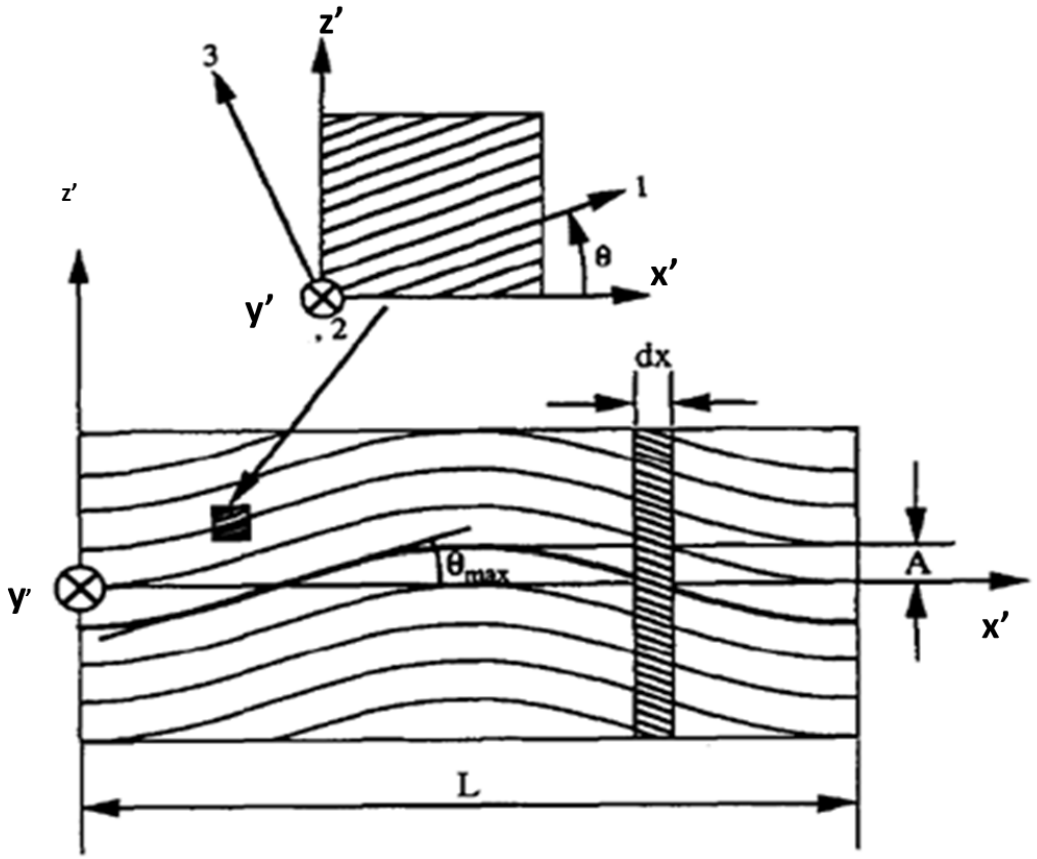

Figure 4.6: A representative volume and coordinates for a unidirectional composite with uniform waviness (image copied from [4]).

(4.8) are functions of the fiber waviness and are defined as

$$\begin{aligned} I_1 &= \frac{1+\alpha^2/2}{(1+\alpha^2)^{3/2}} \\ I_3 &= \frac{\alpha^2/2}{(1+\alpha^2)^{3/2}} \\ I_5 &= 1 - \frac{1+3\alpha^2/2}{(1+\alpha^2)^{3/2}} \\ I_6 &= \frac{1}{(1+\alpha^2)^{1/2}} \\ I_8 &= 1 - \frac{1}{(1+\alpha^2)^{1/2}} \end{aligned} \tag{4.9}$$

where α is the fiber waviness defined by Equation (4.2).

The stiffness tensor $\mathbf{C}$ of the unidirectional fiber composite with uniform waviness can be concisely expressed as the 6×6 matrix as

$$\bar{\mathbf{C}} = \begin{bmatrix} \frac{1}{E_{x'}} & \frac{-\nu_{y'x'}}{E_{y'}} & \frac{-\nu_{z'x'}}{E_{z'}} & 0 & 0 & 0 \\ \frac{-\nu_{x'y'}}{E_{x'}} & \frac{1}{E_{y'}} & \frac{-\nu_{z'y'}}{E_{z'}} & 0 & 0 & 0 \\ \frac{-\nu_{x'z'}}{E_{x'}} & \frac{-\nu_{y'z'}}{E_{y'}} & \frac{1}{E_{z'}} & 0 & 0 & 0 \\ 0 & 0 & 0 & \frac{1}{G_{y'z'}} & 0 & 0 \\ 0 & 0 & 0 & 0 & \frac{1}{G_{x'z'}} & 0 \\ 0 & 0 & 0 & 0 & 0 & \frac{1}{G_{x'y'}} \end{bmatrix}^{-1} \tag{4.10}$$

where the components are defined in Equation (4.8).

The Tandon-Weng model for unidirectional straight fiber reinforced composites predicts that the longitudinal modulus E_{11} increases as the fiber aspect ratio increases and then reaches a plateau when the aspect ratio is large enough, whereas the transverse modulus E_{22} and the Poisson's ratio ν_{12} hardly change with the aspect ratio. Figure 4.7 shows these relationships for a piece of fiber reinforced composite with the component material properties $E_f/E_m = 100$, as plotted according to the model. As for the model of Hsiao and Daniel for unidirectional wavy fiber reinforced composites, they show that the major modulus deteriorates with the increase of fiber waviness. Figure 4.8 shows E_{11} decreases rapidly with the increase of fiber waviness whereas E_{22} is hardly influenced by the waviness of the fiber. It is not surprising that E_{22} does not change with fiber waviness, as no fiber aligns in the x_2 direction. Note that the Poisson's ratio decreases initially with the increase of the fiber waviness and then increases. The influence of the fiber aspect ratio and waviness will come into play more when the ratio E_f/E_m becomes larger. The properties of long flexible fiber reinforced composites are undermined by the fiber waviness when one intends to use fibers with a larger aspect ratio. The balance between the aspect ratio of the fibers and the waviness determines the final properties of the material.

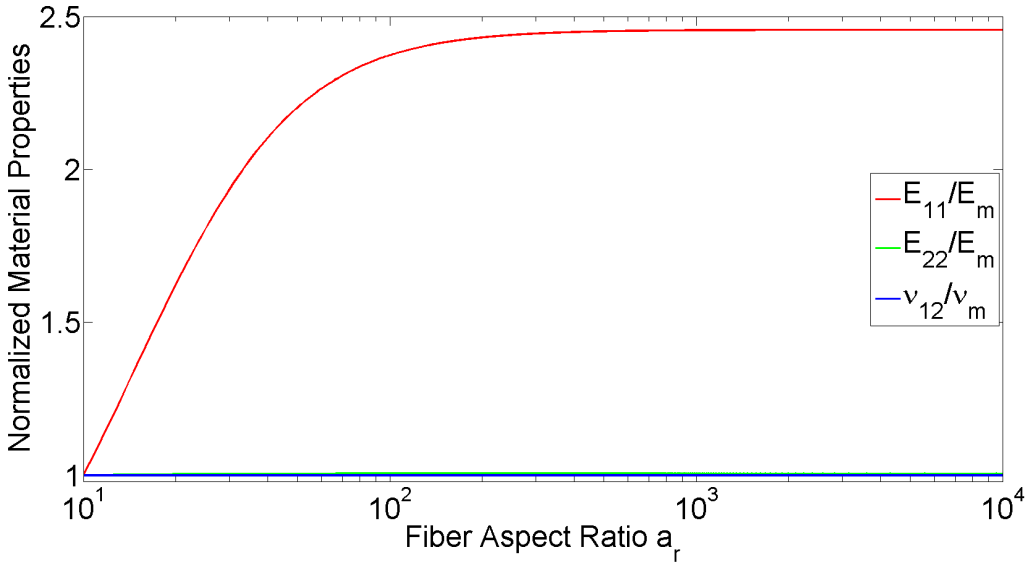

Figure 4.7: Normalized material properties change with fiber aspect ratio, $E_f/E_m = 100$.

4.4.2 Stiffness Prediction with Statistical Sampling

The sample mean of the stiffness tensor, Equation (4.12), is calculated as an average value over a number of aggregates of unidirectional wavy fiber reinforced composites, which is based on the orientation averaging model of Jack and Smith [5] and the wavy fiber model of Hisao and Daniel [4]. The orientation of each aggregate is represented by the orientation of a flexible fiber (Figure 4.9.) This work assumes when the processing of the composite is finished, the part is cured instantly and all the aggregates maintain their instantaneous orientations at the time when processing is finished. The rod chain model is utilized to simulate the motion of all the representing fibers/aggreagtes individually to gain information of the orientation and configuration of each aggregate at the time when processing is finished. This work considers the case where the initial fiber orientation distribution before processing is known and the method of Monte-Carlo is employed to generate statistical data for the initial orientations of the fibers. In the present context, the fibers are set to be initially straight with an isotropic/random orientation. The orientation along with the flexure

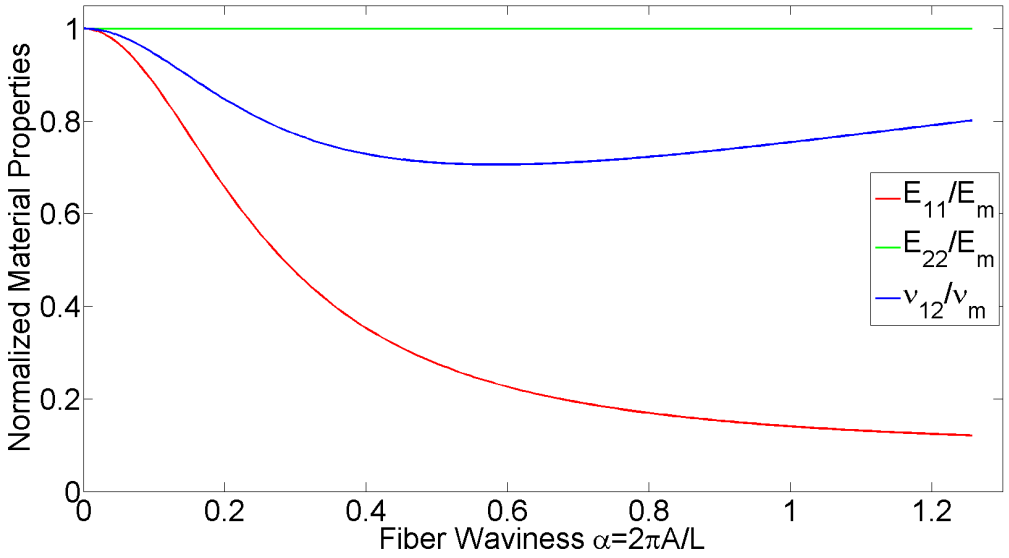

Figure 4.8: Normalized material properties change with fiber waviness, $E_f/E_m = 100$.

information gained from the rod chain model is then used to analyze the sample mean of the material stiffness tensor using Equation (4.6).

4.4.2.1 The Monte-Carlo Simulation Method. The Monte-Carlo method is also called the Random Simulation Method, the Random Sampling Method or the Statistical Testing Method [93]. This method uses the average value of randomly generated data from a distribution to approach the mean value of the distribution. In this research, the idea of the Monte-Carlo simulation is utilized as to randomly generating pairs of the two angle parameter variables (Θ, Φ) of the initial direction vectors of the fibers, representing the orientation of aggregates. And these randomly oriented fibers undergo the processing simulated by the rod chain model to give final orientations as the part is processed. Then the final orientation information is utilized to analyze the stiffness response.

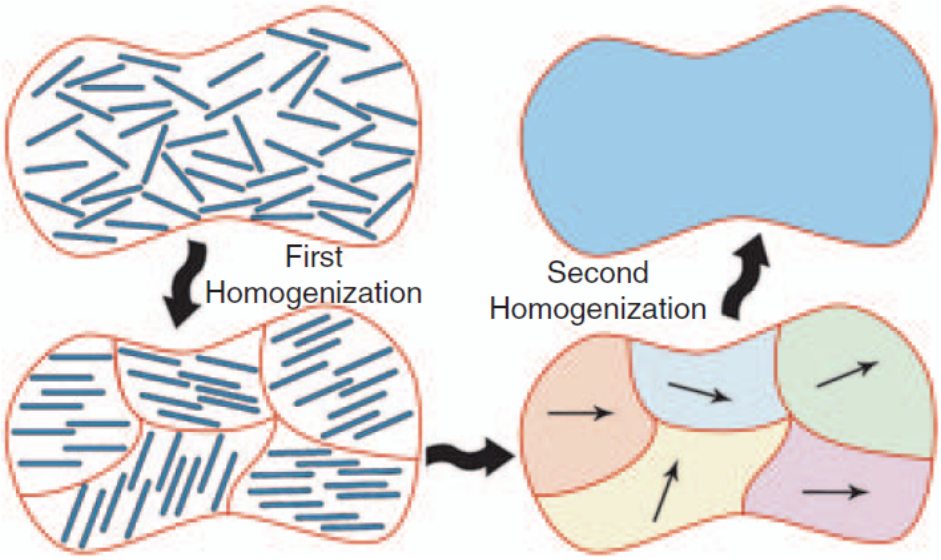

Figure 4.9: Orientation homogenization model [5].

4.4.2.2 Accept Reject Generation Algorithm. An appropriate set of angle pairs is selected in this research using the Accept-Reject Generation Algorithm (ARGA). This part of work is completely based on the Ph.D. thesis of Jack [34] under the help of Dr. David A. Jack. The ARGA numerically generates a sample set for any given probability distribution function, such as $\psi(\theta, \phi) \in \mathbb{S}^2$ using a uniform random number generator that provides a distribution on $(0, 1) \in \mathbb{R}$. The basic idea of the one dimension ARGA is to develop a continuous random variable X whose probability distribution function is $f(x)$ from the probability distribution function $g(x)$ where the random variable Y, an observation from $g(x)$, is sufficiently easy to generate.

If there exists some constant $K \in \mathbb{R}^+$, such that $\forall x \in (-\infty, +\infty)$ the probability distribution functions satisfy the relationship $f(x) \leq Kg(x)$, the ARGA can be performed by the following algorithm [34].

- Generate numerical samples from the random variables Y and U
- If $U \leq \frac{f(Y)}{Kg(Y)}$, then set the random variable X equal to Y
- Then the random variable X will have the probability distribution function f(x)

Jack [34] has found that in this study the most effective choice of constant K is to set $K = (\max_{x\in\mathbb{R}} f(x))(1+\epsilon)$ where ϵ is a small positive number. The random variable Y in this study follows a uniform distribution for ease of computation. To move from one dimension $\mathbb{R}$ to the surface of the sphere $\mathbb{S}$, AGRA is accomplished for the random variable pair Θ and Φ belonging to the probability distribution $\psi(\theta,\phi)\sin(\theta)$. For a group of initially randomly oriented fibers, the following procedures [34] are used to generate a sample set of Θ and Φ values on the sphere at discrete points $(\theta,\phi) = (\frac{i-1}{N_\theta-1}\pi, \frac{j-1}{N_\phi-1}2\pi)$ for $i \in \{1,2,...,N_\theta\}$ and $j \in \{1,2,...,N_\phi\}$, and N_θ and N_ϕ are the numbers of the steps in θ and ϕ, respectively (distribution function symmetry is assumed).

1. Pick $K = (\max_{(\theta,\phi)\in\mathbb{S}} \psi(\theta,\phi))(1+\epsilon)$ where $\epsilon \sim 10^{-2}$
2. Pick a value for (θ,ϕ) where the observation will be made
3. Generate a random observation U from the uniform distribution
4. If $KU < \psi(\theta,\phi)\sin\theta$, then set $\Theta = \theta$ and $\Phi = \phi$
5. Step 2 through 4 are repeated at each point on the sphere

4.4.2.3 Central Limit Theorem. The central limit theorem gives conditions under which the mean of a sufficiently large number of independent random variables, each with finite mean and variance, will approximately follow a normal distribution. The general form of the central limit theorem states: let $X_1, X_2, ..., X_n$ be n independent variables with their distinct and finite mean μ_i and variance σ_i respectively for $i \in \{1,2,...,n\}$. Then for the variable $X = X_1 + X_2 + ... + X_n$ with mean $\mu = \mu_1 + \mu_2 + ... + \mu_n$ and variance $\sigma = \sqrt{\sigma_1^2 + \sigma_2^2 + ... + \sigma_n^2}$, for sufficiently large n, X approximately follows a normal distribution with mean μ and variance σ. It is common that $X_1, X_2, ..., X_n$ are independent and follow the same distribution, then for sufficiently large n, X approximately follows a normal distribution with mean $n\mu$ and

variance $\sqrt{n\sigma^2}$, or given $\bar{X}_n = \frac{1}{n}\sum_{i=1}^{n} X_i$ as the mean of the set of random samples, the random variable

$$Y_n = \sqrt{n}\frac{\bar{X}_n - \mu}{\sigma} \tag{4.11}$$

will approximately follow a standard normal distribution for sufficiently large n.

4.4.3 Simulation Results of the Prediction of Material Stiffness

Given a set of N angle combinations $\{(\theta_n, \phi_n, \beta_n) : n = 1, 2, 3, ..., N\}$ corresponding to each of the N unidirectional waviness fiber aggregates, it is assumed that the mean strain is constant over each aggregate. Thus, the sample mean m_{ijkl} for the stiffness tensor from the corresponding stress field is

$$m_{ijkl} = \frac{1}{N}\sum_{n=1}^{N}(Q^n_{qi}Q^n_{rj}Q^n_{sk}Q^n_{tl}\bar{C}_{qrst}) \tag{4.12}$$

with

$$Q^n_{ij} \equiv Q_{ij}(\theta_n, \phi_n, \beta_n) \tag{4.13}$$

where $i, j, k, l, q, r, s, t \in 1, 2, 3$, $\bar{C}_{qrst}$ is the unidirectional stiffness tensor in Equation (4.14), and the repeated indices on q, r, s, t imply summation. The results are shown in terms of the elastic properties (i.e., elastic modulus) as the stiffness tensor components relate to the elastic properties of the material in the following way

$$\bar{\mathbf{C}} = \begin{bmatrix} \frac{1}{E_{11}} & \frac{-\nu_{21}}{E_{22}} & \frac{-\nu_{31}}{E_{33}} & 0 & 0 & 0 \\ \frac{-\nu_{12}}{E_{11}} & \frac{1}{E_{22}} & \frac{-\nu_{32}}{E_{33}} & 0 & 0 & 0 \\ \frac{-\nu_{13}}{E_{11}} & \frac{-\nu_{23}}{E_{22}} & \frac{1}{E_{33}} & 0 & 0 & 0 \\ 0 & 0 & 0 & \frac{1}{G_{23}} & 0 & 0 \\ 0 & 0 & 0 & 0 & \frac{1}{G_{13}} & 0 \\ 0 & 0 & 0 & 0 & 0 & \frac{1}{G_{12}} \end{bmatrix}^{-1} \tag{4.14}$$

Note that in each aggregate the material is orthotropic based on the assumption that each aggregate is a unidirectional composite. Thus the stiffness tensor, which is a

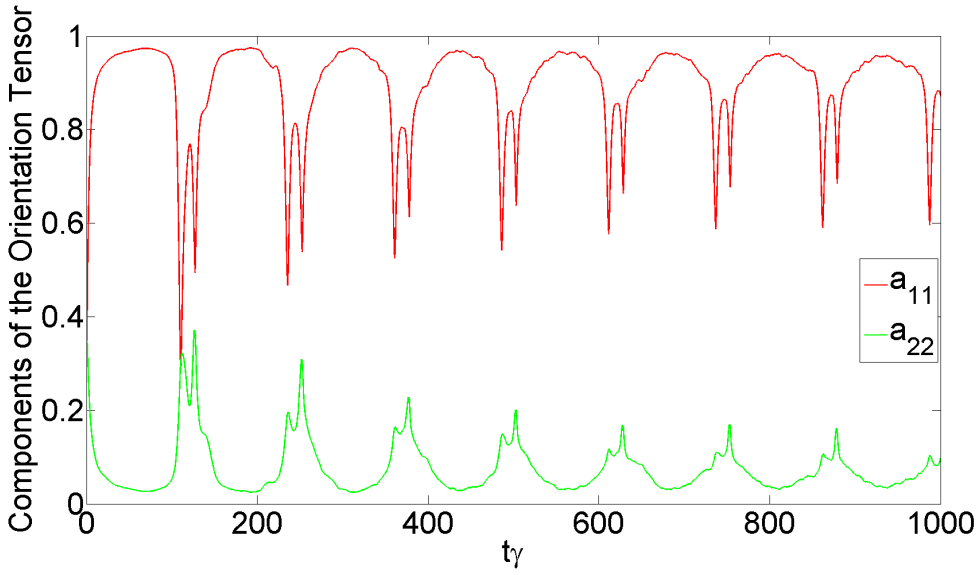

Figure 4.10: The first component of the second order orientation tensor.

fourth order tensor, of each aggregate can be expressed as a 6×6 matrix based on the following properties

$$C_{ijkl} = C_{klij} = C_{jikl} = C_{ijlk} = C_{jilk} \tag{4.15}$$

E_{11} represents the longitudinal modulus, which is along the x_1 direction, E_{22} the transverse modulus along the x_2 direction, E_{33} the transverse modulus along the x_3 direction, ν_{12} the Poisson's ratio between the x_2 direction and the x_1 direction, which is also called the major Poisson's ratio, ν_{21} the Poisson's ratio between the x_1 direction and the x_2 direction, ν_{13} the Poisson's ratio between the x_3 direction and the x_1 direction, ν_{31} the Poisson's ratio between the x_1 direction and the x_3 direction, ν_{23} the Poisson's ratio between the x_3 direction and the x_2 direction, ν_{32} the Poisson's ratio between the x_2 direction and the x_3 direction, G_{12} the shear modulus along the x_1 direction and in the $x_1 - x_3$ plane, G_{23} the shear modulus along the x_2 direction and in the $x_1 - x_2$ plane, and G_{13} the shear modulus along the x_1 direction and in the $x_1 - x_2$ plane. Figure 4.11 shows the predicted values

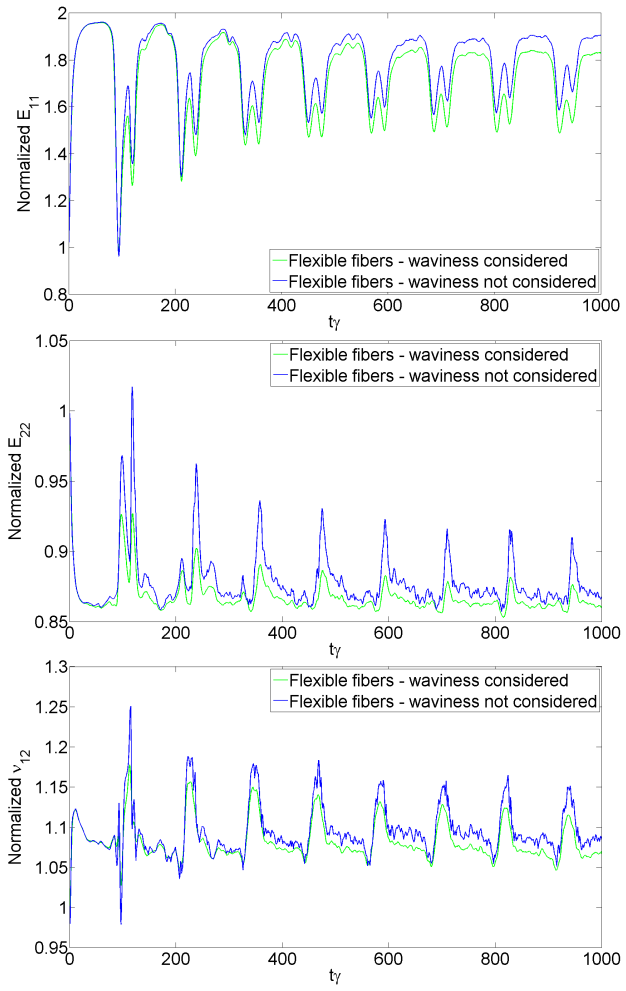

Figure 4.11: The predicted material properties of a processed part ($E_f/E_m = 100$, $v_f = 0.03$, $\nu_f = 0.30$, $\nu_m = 0.35$, $a_r = 30$, $N_f = 1000$): (a) longitudinal modulus E_{11}; (b) transverse modulus E_{22}; and (c) major Possion's ratio ν_{12}.

of the longitudinal modulus, transverse modulus and the major Poisson's ratio for a composite part with $E_f/E_m = 100$, $v_f = 0.03$, $\nu_f = 0.30$, $\nu_m = 0.35$, $a_r = 30$. In this research, 1000 fibers/aggregates are used for calculation. In the plot, the x-axis does not mean the material property changes with flow time. It means at each time when the processing is shut down and the part is cured based on the assumption that all the fibers/aagregates in the flow field will keep their instantaneous configurations at the specific time. The values of the longitudinal elastic modulus is extracted from the first component of the predicted stiffness tensor using the above discussed method.

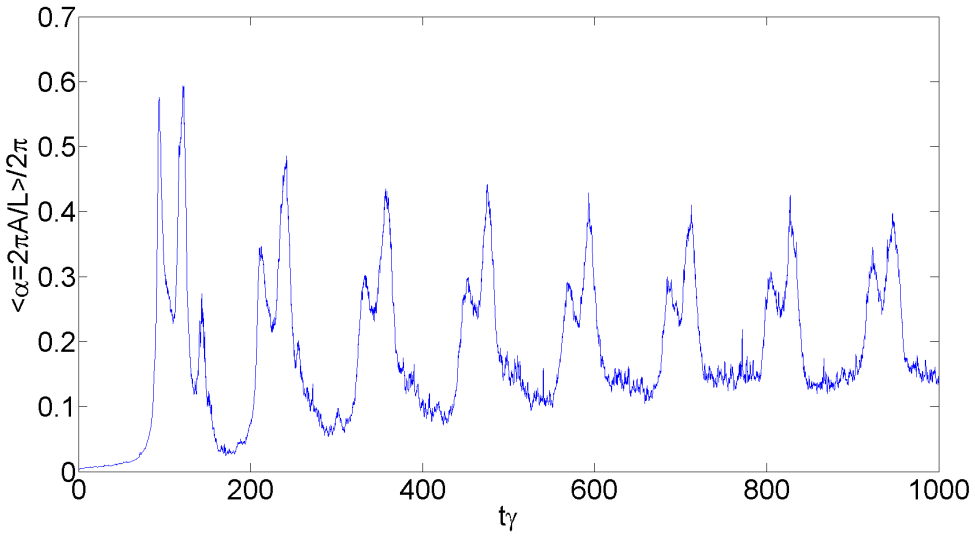

Figure 4.12: The averaged waviness of all the fibers.

In this discussion, 1000 fibers/aggregates are used in the simulation with a random distribution of initial fiber orientations in the flow (as shown in Figure 4.10, $a_{11} \approx \frac{1}{3}$ initially). Note Figure 4.11 (a) and the red curve in Figure 4.10 follow a similar pattern. When a_{11} has a value close to 1, which will occur when most of the fibers aligned along the x_1 direction, the elastic modulus in the x_1 direction will increase. The same phenomenon happens for Figure 4.11 (b) and the green curved in Figure 4.10.

There are two curves provided in each of the plots of Figure 4.11. The blue curve corresponds to the material properties computed using a straight fiber micro-mechanics model, which is the Tandon-Weng model in this research, and the green line corresponds to the material properties computed from the flexible fiber modle by Hsiao and Daniel. Figure 4.12 shows the corresponding averaged fiber waviness for the green lines in Figure 4.11. Notice the comparison between the two lines in Figure 4.11 (a), it clearly shows when there is a large averaged fiber waviness shown in Figure 4.12, the discrepancy between the respective predicted longitudinal moduli E_{11} under the two circumstances is large. To be more specific, without considering

the waviness of the fibers, an overly optimistic longitudinal modulus E_{11} will be predicted, especially when there is a large averaged fiber waviness. The same change happens for the transverse modulus, which is shown in Figure 4.11 (b). This seems contradictive from Figure 4.8, which shows the E_{22} is not influenced by fiber waviness. The contradiction does not exist as in Figure 4.8, all the fibers are unidirectional along the x_1 direction. In Figure 4.11 (b), fibers have a distribution of orientation whenever the process is finished and it is possible there is a large number of fibers orient along the x_2 direction, where fiber waviness will come into play to influence E_{22}. The major Poisson's ratio is slightly influenced by the averaged fiber waviness as shown in Figure 4.8 (c).

CHAPTER FIVE

Conclusions and Recommendations

Fiber orientation kinematics during the processing of discontinuous fiber reinforced composites determines the resulting material properties of the final product. In the literature there exists a considerable number of models to simulate the motion of rigid fibers based on the original work of Jeffery [13] with the most popular in industry being the Folgar-Tucker [14] model for dense suspensions of rigid fibers. However, these models are not suitable for simulating the motion of long flexible fibers as the fibers are treated as perfectly rigid bodies. With the desire to enhance the part stiffness, there is a desire to incorporate longer fibers, but they will have a greater tendency to flex during processing and to follow orientation paths that differ from those of straight fibers. This becomes an urgent problem as the interest in incorporating long fibers in the making of fiber reinforced composites continues to grow. Several models to simulate the motion and orientation evolution of long flexible fiber suspensions have been previously created and were described in the literature chapter. This thesis chose to use the rod chain model created by Wang and his coworkers [21] to study the motion of long flexible fiber suspensions in a simple shear flow because of the clarity of the physics, the simplicity of the model and the potential for conversion over to a probability distribution form.

In this research, the end goal in researching fiber motion kinematics is to predict the material properties of a fiber reinforced composite based on the fiber orientation and flexure distribution in the composite. Previous models neglect either the flexibility of long fibers or the orientational distribution of the fibers. This work adapts the work by Jack and Smith [5] for predicting the elastic properties of straight

fiber composites with a distribution of flexible fiber orientations in the matrix to model the material properties of long flexible fiber composites.

The significant scientific contributions of this work to assist in solving the preceding issues are briefly summarized in the following list.

- A methodology has been proposed in this research for the prediction of material properties of long fiber reinforced composites. This methodology adopts the rod chain model to obtain the information of the orientation and waviness of the fibers, which is then, combined with the orientation averaging method, used to predict the material properties.
- This work has given a thorough study of the rod chain model for simulating the motion of long flexible fibers in a simple shear flow. The deficiency of the model has been studied and shown. When the rod number $N_r = 1$, the bead number N does not alter the evolution of the unit direction vector $\boldsymbol{p}$ of the fiber, as discussed in Chapter Three. It is important to avoid using a rod number of 1.
- Unlike rigid fibers, which move in stable orbits in a pure shear flow, as predicted by Jeffery's equation, the orbits of flexible fibers drift as the fibers move. Researcher have shown that the drifting behavior depends on the initial orientation and aspect ratio of the fiber. This work has shown the dependence of the orbit drifting behavior on the flexibility of the fiber through the utilization of the rod chain model.
- This work has shown the influence of including the waviness of the fiber into the orientation of the fiber distribution, and just as importantly on the resulting material property prediction. This has been done by comparing the simulation results of the evolution of the fiber unit end-to-end vector from both Jeffery's

equation for rigid fibers and the rod chain model for flexible fibers, and by comparing the resulting material property prediction with and without fiber waviness taken into consideration. Governing equations developed in the future for flexible fiber motion should incorporate fiber waviness.

- This work has incorporated the fiber flexure into the material property prediction for fibers sampled from a known orientation distribution function. Combined with the approach used by Jack and Smith [5] for rigid fibers, the rod chain model has been used to gather the information of the distribution of fiber orientations to predict the stiffness response of long flexible fiber reinforced composites. The difference of the material properties predicted when fiber flexure is taken into account invites a new model in industry application for long flexible fiber reinforced composite.
- This work has proposed a way to define the orientation and the configuration of a flexed fiber with three angle parameters. A rotation matrix has been given based on those three angle parameters. This new description, although novel, may pose additional modeling difficulties in the future as existing model for dense, rigid suspensions are unable to readily incorporate this third angle parameter of fiber orientation.
- This work has demonstrated the sudden "bouncing-back" behavior of the ends of a flexible fiber under heavy deformation, which causes the "double-peaks" on the orientation tensor plot for a suspension of flexible fibers. This demonstrates that the trends of the distribution of flexible fibers are notably different from those of rigid fibers.

There is still much work to be undertaken in the area of the simulation of flexible fiber motion and material property prediction, and several thoughts for the direction of future research are presented below.

- Modification of the rod chain model can be done to address fiber-fiber interactions when this model is used to simulate the motion of semi-dilute/semi-concentrated or concentrated flexible fiber suspensions. New forces need to be created in the model to address these interactions. Some researchers [61, 65] have proposed using frictional and lubricant forces to simulate the interactions between fibers in their models. Similar forces can be adopted to be accommodated into the rod chain model. As shown in Figure 5.1, the strength of interaction force depends on the distance of the two parts (either two rods from a flexible fiber or two different flexible fibers) and the direction is along $n_{ij} = \frac{\boldsymbol{p}_i \times \boldsymbol{p}_j}{\|\boldsymbol{p}_i \times \boldsymbol{p}_j\|}$.
- The equations for calculating the forces and torques in the rod chain model need to be modified if a non-newtonian fluid is employed in the simulation. In the current rod chain model, forces and torques are calculated proportional to the relative translational velocity and rotational velocity, independent of the flow properties, such as viscosity, which is not necessarily true when the fiber is moving in a non-newtonian flow. Changes can be made by forming a non-linear relationship between the relative velocities and forces and torques. For example, the friction force can be expressed as

$$\mathbf{F}^h = c_0 + c_1 \Delta v + c_2 \Delta v^2 \tag{5.1}$$

  where Δv is the difference between the velocity of the fiber and the microscopic flow field. c_0, c_1 and c_2 are coefficients.
- The orientation probability distribution function approach introduced in section 2.2.1 may be applied to flexible fibers as well. The probability distribution function will be a function of a pair three angle parameters (θ, ϕ, β), as shown

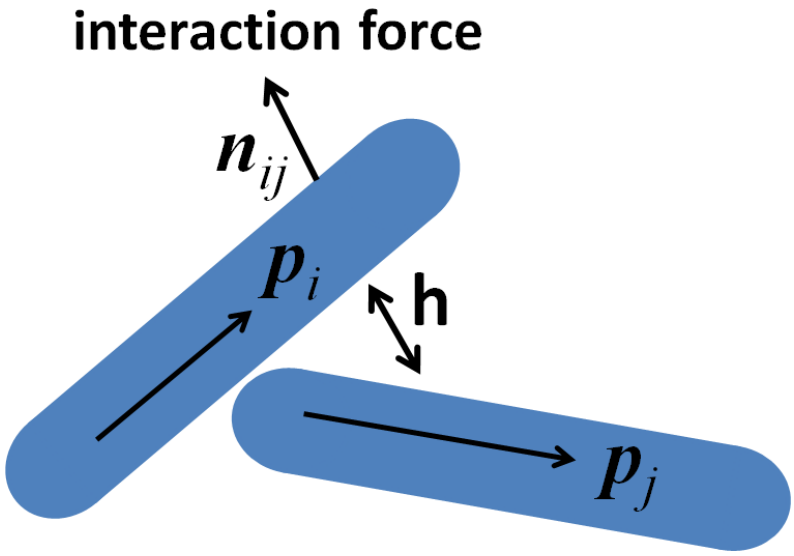

Figure 5.1: Interaction of fibers.

in Figure 4.1. An evolution equation of the probability function $\psi(\theta, \phi, \beta)$ may be developed.

- The prediction of material properties assumes all the fibers have the same aspect ratio, which in reality follows a distribution instead of being a single number. Some modification can be made to Jack and Smith's [5] approach to accommodate the distribution of the fiber aspect ratio as a factor. For each aggregate, they will have a different fiber aspect ratio used to calculate the stiffness of the aggregate and address the distribution of fiber aspect ratio. An analytical solution of the mean and variance of the predicted stiffness of a piece of composite with varying fiber aspect ratio is believed to exist as well and can be developed.
- A finite element analysis can be done to validate the method used to predict the material properties in this research. A representative element of a composite can be chosen to study and analyze.
- Current research adopts the rod chain model to gain information of the evolution of fiber orientation and then calculate the waviness of the fiber. It will simplify the calculation if concise forms of the evolution of flexible fiber orientation and

waviness can be developed, which will be eventually mapped into industrial forms for real application.

- Modification of the rod chain model needs to be made to address the "cutting cross and passing through" behavior of a flexible fiber if it will be applied to an extremely flexible fiber. Conditions may be set up so that when a fiber is heavily deformed and it cuts cross itself, the two bent parts can only contact each other but not occupy the same position.

APPENDICES

APPENDIX A

Scripts for the Rod Chain Model

1.1 Main Code

```
%%%%%%%%%%%%%%%%%%%%%%%%%%%%%%%%%%%%%%%%%%%%%%%%%%%%%%%%%%%%%%%%%%%%%%%%%%%%
%This code is used to simulate the motion of a single flexible fiber moving
%in a simple shear flow based on the rod chain model proposed by Wang and
%his coworkers
%Written by: Cong Zhang
%Last Modified: Apr. 13, 2010
%%%%%%%%%%%%%%%%%%%%%%%%%%%%%%%%%%%%%%%%%%%%%%%%%%%%%%%%%%%%%%%%%%%%%%%%%%%%

%%%%%%%%%%%%%%%%%%%%%%%%%%%%%%%%%%%%%%%%%%%%%%%%%%%%%%%%%%%%%%%%%%%%%%%%%%%%
%giving the parameters and properties of the flow filed
kappa = [0 0 1; 0 0 0; 0 0 0];  %velocity gradient
w = 1/2*(kappa - kappa');       %vorticity tensor
D = 1/2*(kappa + kappa');       %deformation rate tensor
gamma = sqrt(2*trace(D^2));     %shear rate
eta = 10;                       %viscosity of the flow
Re = 0.1;                       %Reynolds number of the flow
%%%%%%%%%%%%%%%%%%%%%%%%%%%%%%%%%%%%%%%%%%%%%%%%%%%%%%%%%%%%%%%%%%%%%%%%%%%%

%%%%%%%%%%%%%%%%%%%%%%%%%%%%%%%%%%%%%%%%%%%%%%%%%%%%%%%%%%%%%%%%%%%%%%%%%%%%
%giving the parameters and the properties of the fiber
N = 1;                          %number of beads in each rod
Nr = 30;                        %number of road in the fiber
rho = 0.2;                      %density of the fiber
a = sqrt(Re*eta/(pi*rho*gamma));%radius of the cross-section
E = 2*10^5*eta*gamma;           %modulus of the fiber
nu = 0.3;                       %poisson's ratio of the fiber
G = E/(2*(1+nu));               %shear modulus of the fiber
k_b = E*pi*a^4/4/(2*N*a);       %bending stiffness of the fiber
k_t = G*pi*a^4/2/(2*a);         %twisting stiffness of the fiber
t = 1000;                       %time of simulation
delt = 0.001;                   %time step
T = 0:delt:t;                   %time array
row = length(T);                %the row length of the matrices
delt_plot = 100;                %this dictates which data to be saved
size_plot = floor(1+row/delt_plot);%the size of variabls saved
T_plot = zeros(size_plot,1);    %the time variable for making plots
script = 1;                     %this counts the number of data points to
                                %be saved
%%%%%%%%%%%%%%%%%%%%%%%%%%%%%%%%%%%%%%%%%%%%%%%%%%%%%%%%%%%%%%%%%%%%%%%%%%%%
```

```
%%%%%%%%%%%%%%%%%%%%%%%%%%%%%%%%%%%%%%%%%%%%%%%%%%%%%%%%%%%%%%%%%%%%%%%%%%%%
%nondimenstionalizing the quantities
kappa = kappa/gamma;
k_b = k_b/(pi*eta*a^3*gamma);
k_t = k_t/(pi*eta*a^3*gamma);
%%%%%%%%%%%%%%%%%%%%%%%%%%%%%%%%%%%%%%%%%%%%%%%%%%%%%%%%%%%%%%%%%%%%%%%%%%%%

%%%%%%%%%%%%%%%%%%%%%%%%%%%%%%%%%%%%%%%%%%%%%%%%%%%%%%%%%%%%%%%%%%%%%%%%%%%%
%defining the variables
rm = [0 0 0];                    %fiber center of mass
p = zeros(row,3*Nr);             %the unit direction vectors, each row for
                                 %a time step, each three columns for a rod
r = zeros(row,3*Nr);             %the position vectors, each row for a time
                                 %step, each three columns for a rod
u = zeros(row,3*Nr);             %body-fixed vector
v = zeros(row,3*Nr);             %translational velocity of each rod
omega = zeros(row,3*Nr);         %angular velocity of each rod
omega_inf = 1/2*[kappa(3,2)-kappa(2,3);kappa(1,3)-kappa(3,1);...
            kappa(2,1)-kappa(1,2)];
                                 %bulk angular velocity
Fh = zeros(row,3*Nr);            %hydrodynamic friction force acted on each
                                 %rod
Th = zeros(row,3*Nr);            %angular friction torque acted on each rod
Tb = zeros(row,3*(Nr+1));        %bending torque acted between two
                                 %connected rods
                                 %0 at the head and the end
Tt = zeros(row,3*(Nr+1));        %twisting torque acted between two
                                 %connected rods
                                 %0 at the head and the end
X = zeros(row,3*(Nr+1));         %internal constraint force between two
                                 %connected rod,0 at the head and the end
%%%%%%%%%%%%%%%%%%%%%%%%%%%%%%%%%%%%%%%%%%%%%%%%%%%%%%%%%%%%%%%%%%%%%%%%%%%%

%%%%%%%%%%%%%%%%%%%%%%%%%%%%%%%%%%%%%%%%%%%%%%%%%%%%%%%%%%%%%%%%%%%%%%%%%%%%
%defining the varibales to save for post-processing
p_plot = zeros(size_plot,3*Nr);
r_plot = zeros(size_plot,3*Nr);
u_plot = zeros(size_plot,3*Nr);
%%%%%%%%%%%%%%%%%%%%%%%%%%%%%%%%%%%%%%%%%%%%%%%%%%%%%%%%%%%%%%%%%%%%%%%%%%%%

%%%%%%%%%%%%%%%%%%%%%%%%%%%%%%%%%%%%%%%%%%%%%%%%%%%%%%%%%%%%%%%%%%%%%%%%%%%%
%giving the initial configuration of the fiber and the flow field
initial_condition
%%%%%%%%%%%%%%%%%%%%%%%%%%%%%%%%%%%%%%%%%%%%%%%%%%%%%%%%%%%%%%%%%%%%%%%%%%%%

%%%%%%%%%%%%%%%%%%%%%%%%%%%%%%%%%%%%%%%%%%%%%%%%%%%%%%%%%%%%%%%%%%%%%%%%%%%%
```

```
%solving for the internal constraint force X
iplot = 1;                      %this indicates when to save the data
                                %points
for k=2:row


    %%%%%%%%%%%%%%%%%%%%%%%%%%%%%%%%%%%%%%%%%%%%%%%%%%%%%%%%%%%%%%%%%%%%%%%%%%%%
    %updating angular velocity omega
    for i=1:Nr
        iii = 3*i-2:3*i;
        jjj = 3*(i+1)-2:3*(i+1);
        domegadt = 3*pi/(Re*8*N^3)*(Th(k-1,iii)+...
                   Tb(k-1,iii)-Tb(k-1,jjj)...
                   +Tt(k-1,iii)-Tt(k-1,jjj)...
                   -N*my_cross(p(k-1,iii),(X(k-1,iii)+...
                   X(k-1,jjj))));
        omega(k,iii) = omega(k-1,iii)+ delt*domegadt;
    end
    %%%%%%%%%%%%%%%%%%%%%%%%%%%%%%%%%%%%%%%%%%%%%%%%%%%%%%%%%%%%%%%%%%%%%%%%%%%%



    %%%%%%%%%%%%%%%%%%%%%%%%%%%%%%%%%%%%%%%%%%%%%%%%%%%%%%%%%%%%%%%%%%%%%%%%%%%%
    %updating center of mass rm
    rm_temp = [0 0 0];
    for i=1:Nr
        rm_temp = rm_temp + v(k-1,3*i-2:3*i);
    end
    rm = rm + delt*rm_temp/Nr;
    %%%%%%%%%%%%%%%%%%%%%%%%%%%%%%%%%%%%%%%%%%%%%%%%%%%%%%%%%%%%%%%%%%%%%%%%%%%%



    %%%%%%%%%%%%%%%%%%%%%%%%%%%%%%%%%%%%%%%%%%%%%%%%%%%%%%%%%%%%%%%%%%%%%%%%%%%%
    %updating unit direction vector p
    for i=1:Nr
        iii = 3*i-2:3*i;
        p(k,iii) = p(k-1,iii)+ my_cross(omega(k,iii),...
                   p(k-1,iii))*delt;
        p(k,iii) = p(k,iii)/norm(p(k,iii));

        u(k,iii) = u(k-1,iii)+ my_cross(omega(k,iii),...
                   u(k-1,iii))*delt;
        u(k,iii) = u(k,iii)/norm(u(k,iii));
    end
    %%%%%%%%%%%%%%%%%%%%%%%%%%%%%%%%%%%%%%%%%%%%%%%%%%%%%%%%%%%%%%%%%%%%%%%%%%%%

    %%%%%%%%%%%%%%%%%%%%%%%%%%%%%%%%%%%%%%%%%%%%%%%%%%%%%%%%%%%%%%%%%%%%%%%%%%%%
```

```
%calling a created function get_r to update the the position vectors
r(k,:) = get_r(Nr,N,rm,p(k,:)); %position vectors of each rod
%%%%%%%%%%%%%%%%%%%%%%%%%%%%%%%%%%%%%%%%%%%%%%%%%%%%%%%%%%%%%%%%%%%%%%%



%%%%%%%%%%%%%%%%%%%%%%%%%%%%%%%%%%%%%%%%%%%%%%%%%%%%%%%%%%%%%%%%%%%%%%%
%updating the translational velocity
for i=1:Nr
    iii = 3*i-2:3*i;
    v(k,iii) = (r(k,iii) - r(k-1,iii))/delt;
end
%%%%%%%%%%%%%%%%%%%%%%%%%%%%%%%%%%%%%%%%%%%%%%%%%%%%%%%%%%%%%%%%%%%%%%%



%%%%%%%%%%%%%%%%%%%%%%%%%%%%%%%%%%%%%%%%%%%%%%%%%%%%%%%%%%%%%%%%%%%%%%%
%calculating hydrodynamic friction force and angular friction torque
for i=1:Nr
    iii = 3*i-2:3*i;
    Fh(k,iii) = 6*N*(kappa*(r(k,iii))'-v(k,iii)');
                               %hydrodynamic friction force on each
                               %rod
    Th(k,iii) = -2*N^3*(omega(k,iii)'-omega_inf);
                               %angular friction torque on each rod
end
%%%%%%%%%%%%%%%%%%%%%%%%%%%%%%%%%%%%%%%%%%%%%%%%%%%%%%%%%%%%%%%%%%%%%%%

%%%%%%%%%%%%%%%%%%%%%%%%%%%%%%%%%%%%%%%%%%%%%%%%%%%%%%%%%%%%%%%%%%%%%%%
%calculating bending torque and twisting torque
for i=2:Nr
    iii = 3*i-2:3*i;
    jjj = 3*(i-1)-2:3*(i-1);
    p1 = p(k,jjj);
    p2 = p(k,iii);
    temps1 = my_dot(p1,p2);
    if(abs(1-temps1)<10*eps)
        theta_b = 0;
        Tb(k,iii) = 0;
    else
        theta_b = acos(temps1);
        nb = my_cross(p1,p2);
        nb = nb/norm(nb);
        Tb(k,iii) = -k_b*theta_b*nb;
    end
end

for i=2:Nr
```

```
        iii = 3*i-2:3*i;
        jjj = 3*(i-1)-2:3*(i-1);
        temps2 = u(k,jjj)- my_dot(u(k,jjj),...
            p(k,iii))*p(k,iii);
        temps3 = my_dot(u(k,jjj),temps2)/norm(temps2);
        if(abs(1-temps3)<10*eps)
            theta_t = 0;            %twisting angle
            Tt(k,iii) = 0;
        else
            theta_t = acos(temps3); %twisting angle
            Tt(k,iii) = -k_t*theta_t*p(k,iii);
                                    %twisting torque
        end
    end
    %%%%%%%%%%%%%%%%%%%%%%%%%%%%%%%%%%%%%%%%%%%%%%%%%%%%%%%%%%%%%%%%%%%%%%%%%%%

    %%%%%%%%%%%%%%%%%%%%%%%%%%%%%%%%%%%%%%%%%%%%%%%%%%%%%%%%%%%%%%%%%%%%%%%%%%%
    %calling a created function get_x to solve for internal
    %constraint force X
    X(k,:) = get_X(Nr,N,Re,p(k,:),omega(k,:),Fh(k,:),Tb(k,:),Th(k,:),...
    Tt(k,:));
    %%%%%%%%%%%%%%%%%%%%%%%%%%%%%%%%%%%%%%%%%%%%%%%%%%%%%%%%%%%%%%%%%%%%%%%%%%%

    %%%%%%%%%%%%%%%%%%%%%%%%%%%%%%%%%%%%%%%%%%%%%%%%%%%%%%%%%%%%%%%%%%%%%%%%%%%
    %save the desired data points
    iplot = iplot+1;
    if iplot == delt_plot
        iplot = 0;
        script = script+1;
        T_plot(script) = T(k);
        p_plot(script,:) = p(k,:);
        u_plot(script,:) = u(k,:);
        r_plot(script,:) = r(k,:);
    else
    end
    %%%%%%%%%%%%%%%%%%%%%%%%%%%%%%%%%%%%%%%%%%%%%%%%%%%%%%%%%%%%%%%%%%%%%%%%%%%
end
%%%%%%%%%%%%%%%%%%%%%%%%%%%%%%%%%%%%%%%%%%%%%%%%%%%%%%%%%%%%%%%%%%%%%%%%%%%%

%%%%%%%%%%%%%%%%%%%%%%%%%%%%%%%%%%%%%%%%%%%%%%%%%%%%%%%%%%%%%%%%%%%%%%%%%%%%
%give the initial values of the variables to save
p_plot(1,:) = p(1,:);
u_plot(1,:) = u(1,:);
r_plot(1,:) = r(1,:);
%%%%%%%%%%%%%%%%%%%%%%%%%%%%%%%%%%%%%%%%%%%%%%%%%%%%%%%%%%%%%%%%%%%%%%%%%%%%

%%%%%%%%%%%%%%%%%%%%%%%%%%%%%%%%%%%%%%%%%%%%%%%%%%%%%%%%%%%%%%%%%%%%%%%%%%%%
```

```
%This part of code is to post-process the data obtained

%Dimensionlize the time variable
T = T/gamma;
T_plot = T_plot/gamma;
r = r*a;
r_plot = r_plot*a;

%calculating the end-to-end vector
p_end_to_end = zeros(size_plot,3);
p_magnitude = zeros(size_plot,1);
c_Nr = 3*Nr-2:3*Nr;
for i=1:size_plot
    p_end_to_end(i,:) = (r_plot(i,c_Nr)+ N*a*p_plot(i,c_Nr))...
        -(r_plot(i,1:3)- N*a*p_plot(i,1:3));
    p_magnitude(i) = norm(p_end_to_end(i,:));
    p_end_to_end(i,:) = p_end_to_end(i,:)/norm(p_end_to_end(i,:));
end
%%%%%%%%%%%%%%%%%%%%%%%%%%%%%%%%%%%%%%%%%%%%%%%%%%%%%%%%%%%%%%%%%%%%%%%%%%%%
```

1.2 Initial Configuration

```
%%%%%%%%%%%%%%%%%%%%%%%%%%%%%%%%%%%%%%%%%%%%%%%%%%%%%%%%%%%%%%%%%%%%%%%%%%%%
%This code gives the initial configuration of the fiber and calculating the
%initial forces and torques
%%%%%%%%%%%%%%%%%%%%%%%%%%%%%%%%%%%%%%%%%%%%%%%%%%%%%%%%%%%%%%%%%%%%%%%%%%%%

%%%%%%%%%%%%%%%%%%%%%%%%%%%%%%%%%%%%%%%%%%%%%%%%%%%%%%%%%%%%%%%%%%%%%%%%%%%%
%giving initial orientation of the rods in the fiber
theta = 0;
phi = pi/2;

p_ini = [sin(theta)*cos(phi) sin(theta)*sin(phi) cos(theta)];
                    %direction vector of the rods
u_ini = cross([1 1 1],p_ini);
                    %body fixed vector of the rods
p_ini = p_ini/norm(p_ini);
u_ini = u_ini/norm(u_ini);
                    %normalize the vectors
for i=1:Nr
    p(1,3*i-2:3*i) = p_ini;
                    %all rods pointing to the same direction initially
                    %which also means the fiber is straight initially
    u(1,3*i-2:3*i) = u_ini;
                    %all rods having the same body-fixed vector

end
```

```
    r(1,:) = get_r(Nr,N,rm,p(1,:));
                    %position vectors of each rod
%%%%%%%%%%%%%%%%%%%%%%%%%%%%%%%%%%%%%%%%%%%%%%%%%%%%%%%%%%%%%%%%%%%%%%%%%%%%%%%

%%%%%%%%%%%%%%%%%%%%%%%%%%%%%%%%%%%%%%%%%%%%%%%%%%%%%%%%%%%%%%%%%%%%%%%%%%%%%%%
%calculating hydrodynamic friction force and angular friction torque
for i=1:Nr
    Fh(1,3*i-2:3*i) = 6*N*(kappa*(r(1,3*i-2:3*i))'-v(1,3*i-2:3*i)');
                    %hydrodynamic friction force on each rod
    Th(1,3*i-2:3*i) = -2*N^3*(omega(1,3*i-2:3*i)'-omega_inf);
                    %angular friction torque on each rod
end
%%%%%%%%%%%%%%%%%%%%%%%%%%%%%%%%%%%%%%%%%%%%%%%%%%%%%%%%%%%%%%%%%%%%%%%%%%%%%%%

%%%%%%%%%%%%%%%%%%%%%%%%%%%%%%%%%%%%%%%%%%%%%%%%%%%%%%%%%%%%%%%%%%%%%%%%%%%%%%%
%calculating bending torque and twisting torque
for i=2:Nr
    p1 = p(1,3*(i-1)-2:3*(i-1));
    p2 = p(1,3*i-2:3*i);
    temps1 = dot(p1,p2);
    if(abs(1-temps1)<10*eps)
        theta_b = 0;
        Tb(1,3*i-2:3*i) = 0;
    else
        theta_b = acos(temps1);
        nb = cross(p1,p2);
        nb = nb/norm(nb);
        Tb(1,3*i-2:3*i) = -k_b*theta_b*nb;
    end
end

for i=2:Nr
    temps2 = u(1,3*(i-1)-2:3*(i-1))- dot(u(1,3*(i-1)-2:3*(i-1)),...
        p(1,3*i-2:3*i))*p(1,3*i-2:3*i);
    temps3 = dot(u(1,3*(i-1)-2:3*(i-1)),temps2)/norm(temps2);
    if(abs(1-temps3)<10*eps)
        theta_t = 0;
        Tt(1,3*i-2:3*i) = 0;
    else
        theta_t = acos(temps3);
        Tt(1,3*i-2:3*i) = -k_t*theta_t*p(1,3*i-2:3*i);
    end
end
%%%%%%%%%%%%%%%%%%%%%%%%%%%%%%%%%%%%%%%%%%%%%%%%%%%%%%%%%%%%%%%%%%%%%%%%%%%%%%%
```

1.3 Internal Constraint Forces

```
%%%%%%%%%%%%%%%%%%%%%%%%%%%%%%%%%%%%%%%%%%%%%%%%%%%%%%%%%%%%%%%%%%%%%%%%%%%%%%%
```

```
%calculating the internal constraint forces by calling a function
X(1,:) = get_X(Nr,N,Re,p(1,:),omega(1,:),Fh(1,:),Tb(1,:),Th(1,:),Tt(1,:));
%%%%%%%%%%%%%%%%%%%%%%%%%%%%%%%%%%%%%%%%%%%%%%%%%%%%%%%%%%%%%%%%%%%%%%%%%%%


%%%%%%%%%%%%%%%%%%%%%%%%%%%%%%%%%%%%%%%%%%%%%%%%%%%%%%%%%%%%%%%%%%%%%%%%%%%
%This function solves for the internal constraint force X
%%%%%%%%%%%%%%%%%%%%%%%%%%%%%%%%%%%%%%%%%%%%%%%%%%%%%%%%%%%%%%%%%%%%%%%%%%%

function X = get_X(Nr,N,Re,p,omega,Fh,Tb,Th,Tt)

A = zeros(3*(Nr-1),3*(Nr+1));
R = zeros(3*(Nr-1),1);

c1 = 0.75/N;
c2 = 2*Re*N^2/pi;

for i=1:(Nr-1)
  pi1 = p(1,3*i-2);
  pi2 = p(1,3*i-1);
  pi3 = p(1,3*i);
  piplus11 = p(1,3*(i+1)-2);
  piplus12 = p(1,3*(i+1)-1);
  piplus13 = p(1,3*(i+1));

  Ksm = zeros(3,9);
  Ksm(1,1)=1-0.75*pi2^2 - 0.75*pi3^2;
  Ksm(1,2)=0.75*pi1*pi2;
  Ksm(1,3)=0.75*pi1*pi3;
  Ksm(1,4)=-2-0.75*pi2^2-0.75*pi3^2-0.75*piplus12^2-0.75*piplus13^2;
  Ksm(1,5)=0.75*pi1*pi2+0.75*piplus11*piplus12;
  Ksm(1,6)=0.75*pi1*pi3+0.75*piplus11*piplus13;
  Ksm(1,7)=1-0.75*piplus12^2-0.75*piplus13^2;
  Ksm(1,8)=0.75*piplus11*piplus12;
  Ksm(1,9)=0.75*piplus11*piplus13;
  Ksm(2,1)=Ksm(1,2);
  Ksm(2,2)=1-0.75*pi1^2-0.75*pi3^2;
  Ksm(2,3)=0.75*pi2*pi3;
  Ksm(2,4)=Ksm(1,5);
  Ksm(2,5)=-2-0.75*pi1^2-0.75*pi3^2-0.75*piplus11^2-0.75*piplus13^2;
  Ksm(2,6)=0.75*pi2*pi3+0.75*piplus12*piplus13;
  Ksm(2,7)=Ksm(1,8);
  Ksm(2,8)=1-0.75*piplus11^2-0.75*piplus13^2 ;
  Ksm(2,9)=0.75*piplus12*piplus13;
  Ksm(3,1)=Ksm(1,3);
  Ksm(3,2)=Ksm(2,3);
  Ksm(3,3)=1-0.75*pi1^2-0.75*pi2^2 ;
```

```
  Ksm(3,4)=Ksm(1,6);
  Ksm(3,5)=Ksm(2,6);
  Ksm(3,6)=-2-0.75*pi1^2-0.75*pi2^2-0.75*piplus11^2-0.75*piplus12^2;
  Ksm(3,7)=Ksm(1,9);
  Ksm(3,8)=Ksm(2,9);
  Ksm(3,9)=1-0.75*piplus11^2-0.75*piplus12^2;
  A((3*i-2):(3*i),(3*i-2):(3*i+6)) = Ksm;
  ii = 3*i-2:3*i;
  jj = 3*(i+1)-2:3*(i+1);
  kk = 3*(i+2)-2:3*(i+2);
  atemp = Th(1,ii) + Tb(1,ii) - Tb(1,jj) + Tt(1,ii) - Tt(1,jj);
  btemp = Th(1,jj) + Tb(1,jj) - Tb(1,kk) + Tt(1,jj) - Tt(1,kk);

  R(ii,1 )=(Fh(1,jj) - Fh(1,ii)) ...
    -c1*(my_cross( atemp , [pi1 pi2 pi3]) + my_cross(btemp,[piplus11...
    piplus12 piplus13]))-c2*(my_double_cross_special(omega(1,ii)...
    ,[pi1 pi2 pi3]) + my_double_cross_special(omega(1,jj),...
    [piplus11 piplus12 piplus13]));
end

A = A(:,4:3*Nr);
X = A\R;
X = [0;0;0;X;0;0;0]';
%%%%%%%%%%%%%%%%%%%%%%%%%%%%%%%%%%%%%%%%%%%%%%%%%%%%%%%%%%%%%%%%%%%%%%%%%%%%
```

1.4 Position Vectors of Each Rod

```
%%%%%%%%%%%%%%%%%%%%%%%%%%%%%%%%%%%%%%%%%%%%%%%%%%%%%%%%%%%%%%%%%%%%%%%%%%%%
%This function solves for the position vectors r
%%%%%%%%%%%%%%%%%%%%%%%%%%%%%%%%%%%%%%%%%%%%%%%%%%%%%%%%%%%%%%%%%%%%%%%%%%%%

function r = get_r(Nr,N,rm,p)

r = zeros(1,3*Nr);

if(round(Nr/2)==(Nr/2))    %Even number of rods
    r(1,3*(Nr/2+1)-2:3*(Nr/2+1)) = rm + N*p(1,3*(Nr/2+1)-2:3*(Nr/2+1));
                           %Put one fiber to the right
    r(1,3*(Nr/2)-2:3*(Nr/2)) = rm - N*p(1,3*(Nr/2)-2:3*(Nr/2));
                           %Put one fiber to the left

    for i=(Nr/2+2):Nr      %Place the rods that are to the right of center
        p_sum = [0 0 0];
        for n=(Nr/2+2):i
            p_sum = p_sum + p(1,3*(n-1)-2:3*(n-1))+p(1,3*n-2:3*n);
        end
        r(1,3*i-2:3*i) = r(1,3*(Nr/2+1)-2:3*(Nr/2+1))+ N*p_sum;
```

```
    end

    for i=(Nr/2-1):-1:1    %Place the rods that are to the left of center
        p_sum = [0 0 0];
        for n = (Nr/2-1):-1:i
            p_sum = p_sum + p(1,3*n-2:3*n)+p(1,3*(n+1)-2:3*(n+1));
        end
        r(1,3*i-2:3*i) = r(1,3*(Nr/2)-2:3*(Nr/2))- N*p_sum;
    end
else                        %Odd number of rods
    r(1,3*(Nr+1)/2-2:3*(Nr+1)/2) = rm;   %The rod at the center
    for i=((Nr+1)/2+1):Nr  %The rods to the right
        p_sum = [0 0 0];
        for n=((Nr+1)/2+1):i
            p_sum = p_sum + p(1,3*(n-1)-2:3*(n-1))+p(1,3*n-2:3*n);
        end
        r(1,3*i-2:3*i) = rm + N*p_sum;
    end
    for i=(((Nr+1)/2)-1):-1:1%The rods to the left
        p_sum = [0 0 0];
        for n=(Nr+1)/2-1:-1:i
            p_sum = p_sum + p(1,3*n-2:3*n)+p(1,3*(n+1)-2:3*(n+1));
        end
        r(1,3*i-2:3*i) = rm - N*p_sum;
    end
end
%%%%%%%%%%%%%%%%%%%%%%%%%%%%%%%%%%%%%%%%%%%%%%%%%%%%%%%%%%%%%%%%%%%%%%%%%%%%
```

1.5 Subroutines

```
%%%%%%%%%%%%%%%%%%%%%%%%%%%%%%%%%%%%%%%%%%%%%%%%%%%%%%%%%%%%%%%%%%%%%%%%%%%%
%the following functions are created to save computational time for
%calculating the cross and dot products
%%%%%%%%%%%%%%%%%%%%%%%%%%%%%%%%%%%%%%%%%%%%%%%%%%%%%%%%%%%%%%%%%%%%%%%%%%%%

%%%%%%%%%%%%%%%%%%%%%%%%%%%%%%%%%%%%%%%%%%%%%%%%%%%%%%%%%%%%%%%%%%%%%%%%%%%%
function c = my_cross(a,b)

c = [-a(3)*b(2) + a(2)*b(3), a(3)*b(1)-a(1)*b(3),-a(2)*b(1) + a(1)*b(2)];
%%%%%%%%%%%%%%%%%%%%%%%%%%%%%%%%%%%%%%%%%%%%%%%%%%%%%%%%%%%%%%%%%%%%%%%%%%%%

%%%%%%%%%%%%%%%%%%%%%%%%%%%%%%%%%%%%%%%%%%%%%%%%%%%%%%%%%%%%%%%%%%%%%%%%%%%%
function c = my_cross_col_vec(a,b)

c = [-a(3)*b(2) + a(2)*b(3); a(3)*b(1)-a(1)*b(3);-a(2)*b(1) + a(1)*b(2)];
%%%%%%%%%%%%%%%%%%%%%%%%%%%%%%%%%%%%%%%%%%%%%%%%%%%%%%%%%%%%%%%%%%%%%%%%%%%%
```

```
%%%%%%%%%%%%%%%%%%%%%%%%%%%%%%%%%%%%%%%%%%%%%%%%%%%%%%%%%%%%%%%%%%%%%%%%%%%%
%this subroutine computes the triple cross product, but for the special
%case of c = a x (a x b)
function c = my_double_cross_special(a,b)

c = [-a(2)^2*b(1) - a(3)^2*b(1) + a(1)*a(2)*b(2) + a(1)*a(3)*b(3),...
     a(1)*a(2)*b(1) - a(1)^2*b(2) - a(3)^2*b(2) + a(2)*a(3)*b(3) ,...
     a(1)*a(3)*b(1) + a(2)*a(3)*b(2) - a(1)^2*b(3) - a(2)^2*b(3)];
%%%%%%%%%%%%%%%%%%%%%%%%%%%%%%%%%%%%%%%%%%%%%%%%%%%%%%%%%%%%%%%%%%%%%%%%%%%%

%%%%%%%%%%%%%%%%%%%%%%%%%%%%%%%%%%%%%%%%%%%%%%%%%%%%%%%%%%%%%%%%%%%%%%%%%%%%
function c = my_dot(a,b)

c = a(1)*b(1) + a(2)*b(2) + a(3)*b(3);
%%%%%%%%%%%%%%%%%%%%%%%%%%%%%%%%%%%%%%%%%%%%%%%%%%%%%%%%%%%%%%%%%%%%%%%%%%%%
```

APPENDIX B

Scripts for the Material Property Prediction

2.1 Main Code

```
%%%%%%%%%%%%%%%%%%%%%%%%%%%%%%%%%%%%%%%%%%%%%%%%%%%%%%%%%%%%%%%%%%%%%%%%%%%%
%This code is to calculate the sample mean stiffness tensor for a fiber
%reinforced composite material at a specific time during processing
%%%%%%%%%%%%%%%%%%%%%%%%%%%%%%%%%%%%%%%%%%%%%%%%%%%%%%%%%%%%%%%%%%%%%%%%%%%%

clear all
close all
clc

%%%%%%%%%%%%%%%%%%%%%%%%%%%%%%%%%%%%%%%%%%%%%%%%%%%%%%%%%%%%%%%%%%%%%%%%%%%%
%getting data for unit direction vectors and position vectors for a group
%of fibers

newSeed = sum(100*clock);
RandStream.setDefaultStream(RandStream('mt19937ar','seed',newSeed));
defaultStream = RandStream.getDefaultStream;
newState = defaultStream.State;

th_vec = [];
phi_vec = [];
Nth  = 2E3;%number of angle theta
Nphi = 2E3;%number of angle phi
           %these two combined decide the number of fiber
[th_rand,phi_rand] = ARGA_3D(Nth,Nphi);
           %call the function ARGA_3D to generate a group of randomly
           %oriented fibers
a = rand(length(th_rand),1);
[b,c] = sort(a);
N_fiber = 100;
th_rand  = th_rand(c(1:N_fiber));
phi_rand = phi_rand(c(1:N_fiber));
clear a b c

n_previous = 0;
           %this gives how many fibers' motion has been simulated
           %previously. Here it is set to be 0, since no simulation is done
           %before.
%%%%%%%%%%%%%%%%%%%%%%%%%%%%%%%%%%%%%%%%%%%%%%%%%%%%%%%%%%%%%%%%%%%%%%%%%%%%
%The following save the data obtained from the rod chain model and save
```

```
%them with ordered file name for the convinence of future use.

for n=1:N_fiber

    flexible_fiber_motion
           %run the rod chain model simulation for each of the fiber

    if n+n_previous<10
        save(['p_000',num2str(n+n_previous)],'-ascii','p_plot')
        save(['u_000',num2str(n+n_previous)],'-ascii','u_plot')
        save(['p_end_to_end_000',num2str(n+n_previous)],'-ascii',...
        'p_end_to_end')
        save(['r_000',num2str(n+n_previous)],'-ascii','r_plot')
        save(['p_magnitude_000',num2str(n+n_previous)],'-ascii',...
        'p_magnitude')
    elseif n+n_previous<100
        save(['p_00',num2str(n+n_previous)],'-ascii','p_plot')
        save(['u_00',num2str(n+n_previous)],'-ascii','u_plot')
        save(['p_end_to_end_00',num2str(n+n_previous)],'-ascii',...
        'p_end_to_end')
        save(['r_00',num2str(n+n_previous)],'-ascii','r_plot')
        save(['p_magnitude_00',num2str(n+n_previous)],'-ascii',...
        'p_magnitude')
    elseif n+n_previous<1000
        save(['p_0',num2str(n+n_previous)],'-ascii','p_plot')
        save(['u_0',num2str(n+n_previous)],'-ascii','u_plot')
        save(['p_end_to_end_0',num2str(n+n_previous)],'-ascii',...
        'p_end_to_end')
        save(['r_0',num2str(n+n_previous)],'-ascii','r_plot')
        save(['p_magnitude_0',num2str(n+n_previous)],'-ascii',...
        'p_magnitude')
    else
        save(['p_',num2str(n+n_previous)],'-ascii','p_plot')
        save(['u_',num2str(n+n_previous)],'-ascii','u_plot')
        save(['p_end_to_end_',num2str(n+n_previous)],'-ascii',...
        'p_end_to_end')
        save(['r_',num2str(n+n_previous)],'-ascii','r_plot')
        save(['p_magnitude_',num2str(n+n_previous)],'-ascii',...
        'p_magnitude')
    end

end
%%%%%%%%%%%%%%%%%%%%%%%%%%%%%%%%%%%%%%%%%%%%%%%%%%%%%%%%%%%%%%%%%%%%%%%%%%%%

%%%%%%%%%%%%%%%%%%%%%%%%%%%%%%%%%%%%%%%%%%%%%%%%%%%%%%%%%%%%%%%%%%%%%%%%%%%%
%saving some of the variables for future use
save('T','-ascii','T')
```

```
save('T_plot','-ascii','T_plot')
save('size_plot','-ascii','size_plot')
save('N_fiber','-ascii','N_fiber')
save('kappa','-ascii','kappa')
save('Nr','-ascii','Nr')
save('N','-ascii','N')
save('w','-ascii','w')
save('D','-ascii','D')
save('a','-ascii','a')
save('Ef','-ascii','E')
%%%%%%%%%%%%%%%%%%%%%%%%%%%%%%%%%%%%%%%%%%%%%%%%%%%%%%%%%%%%%%%%%%%%%%%%%%%%%%%

%%%%%%%%%%%%%%%%%%%%%%%%%%%%%%%%%%%%%%%%%%%%%%%%%%%%%%%%%%%%%%%%%%%%%%%%%%%%%%%
%calculating the sample mean stiffness tensor

%loading the data
load N_fiber

for n=1:N_fiber

    if n<10
        load(['p_000',num2str(n)],'-ascii');
        load(['u_000',num2str(n)],'-ascii');
        load(['p_end_to_end_000',num2str(n)],'-ascii');
        load(['p_magnitude_000',num2str(n)],'-ascii');
        load(['r_000',num2str(n)],'-ascii');
    elseif n<100
        load(['p_00',num2str(n)],'-ascii');
        load(['u_00',num2str(n)],'-ascii');
        load(['p_end_to_end_00',num2str(n)],'-ascii');
        load(['p_magnitude_00',num2str(n)],'-ascii');
        load(['r_00',num2str(n)],'-ascii');
    elseif n<1000
        load(['p_0',num2str(n)],'-ascii');
        load(['u_0',num2str(n)],'-ascii');
        load(['p_end_to_end_0',num2str(n)],'-ascii');
        load(['p_magnitude_0',num2str(n)],'-ascii');
        load(['r_0',num2str(n)],'-ascii');
    else
        load(['p_',num2str(n)],'-ascii');
        load(['u_',num2str(n)],'-ascii');
        load(['p_end_to_end_',num2str(n)],'-ascii');
        load(['p_magnitude_',num2str(n)],'-ascii');
        load(['r_',num2str(n)],'-ascii');
    end
end
%%%%%%%%%%%%%%%%%%%%%%%%%%%%%%%%%%%%%%%%%%%%%%%%%%%%%%%%%%%%%%%%%%%%%%%%%%%%%%%
```

```
%%%%%%%%%%%%%%%%%%%%%%%%%%%%%%%%%%%%%%%%%%%%%%%%%%%%%%%%%%%%%%%%%%%%%%%%%%%%
%load some saved variables
load Ef
load N
load Nr
load size_plot
load N_fiber
load a
%%%%%%%%%%%%%%%%%%%%%%%%%%%%%%%%%%%%%%%%%%%%%%%%%%%%%%%%%%%%%%%%%%%%%%%%%%%%

%%%%%%%%%%%%%%%%%%%%%%%%%%%%%%%%%%%%%%%%%%%%%%%%%%%%%%%%%%%%%%%%%%%%%%%%%%%%
%giving parameters of the composite material
Ef = Ef; %young's modulus of fiber in Gpa
vf = 0.30; %possion's ratio of fiber
Em = Ef/10; %young's modulus of matrix
vm = 0.35; %possion's ratio of matrix
Vfrac = 0.001; %volume fraction of fiber
ar = N*Nr; %aspect ratio of fiber
%%%%%%%%%%%%%%%%%%%%%%%%%%%%%%%%%%%%%%%%%%%%%%%%%%%%%%%%%%%%%%%%%%%%%%%%%%%%

%%%%%%%%%%%%%%%%%%%%%%%%%%%%%%%%%%%%%%%%%%%%%%%%%%%%%%%%%%%%%%%%%%%%%%%%%%%%
%define the quantities to be used
A_over_L = zeros(size_plot,N_fiber); %the values of A/L,this will be
                                     %calculated for all time steps
distance = zeros(size_plot,Nr-1); %distance from the head of rod 1~Nr-1 to
                                  %the vector p_end_to_end
extent = zeros(size_plot, Nr-1); %distance from the head of the fiber to
                                 %the projection of the head pf each rod
                                 %on the end to end vector
x_coordinate = zeros(size_plot,Nr+1); %the x coordinate of the all the
                                      %heads and ends of rods in the
                                      %primed coordinates
y_coordinate = zeros(size_plot,Nr+1); %the y coordinate of the all the
                                      %heads and ends of rods in the
                                      %primed coordinates
theta = zeros(size_plot,1);%angle theta for all time steps
phi = zeros(size_plot,1);%angle phi for all time steps
beta = zeros(size_plot,1);%angle beta for all time steps
S_unwavy = zeros(6,6); %compliance tensor of the unwavy fibers composites
S_wavy = zeros(6,6); %compliance tensor of the wavy fibers composites
C_wavy = zeros(6,6); %stiffness tensor of the wavy fibers composites
Q = zeros(3,3);%rotation matrix
m = zeros(3,3,3,3); %the sample mean for the stiffness tensor
m_contracted = zeros(6,6); %the sample mean for the stiffness tensor in
                           %contracted notation
%%%%%%%%%%%%%%%%%%%%%%%%%%%%%%%%%%%%%%%%%%%%%%%%%%%%%%%%%%%%%%%%%%%%%%%%%%%%
```

```
%%%%%%%%%%%%%%%%%%%%%%%%%%%%%%%%%%%%%%%%%%%%%%%%%%%%%%%%%%%%%%%%%%%%%%%%%%%%
%calculating the compliance tensor for unwavy fibers composites by calling
%the function compliance_uni
S_unwavy = compliance_uni(Ef,vf,Em,vm,Vfrac,ar);
%%%%%%%%%%%%%%%%%%%%%%%%%%%%%%%%%%%%%%%%%%%%%%%%%%%%%%%%%%%%%%%%%%%%%%%%%%%%

%%%%%%%%%%%%%%%%%%%%%%%%%%%%%%%%%%%%%%%%%%%%%%%%%%%%%%%%%%%%%%%%%%%%%%%%%%%%
%calculating the sample mean stiffness tensor
for i=1:size_plot

    for ii=1:3
        for jj=1:3
            for kk=1:3
                for ll=1:3



                    for n=1:N_fiber

                        m_temp = 0;

                        %calculating A/L and angle beta
                        if n<10
                            p = eval(['p_000',num2str(n)]);
                            u = eval(['u_000',num2str(n)]);
                            p_end_to_end = eval(['p_end_to_end_000',...
                            num2str(n)]);
                            p_magnitude = eval(['p_magnitude_000',...
                            num2str(n)]);
                            r = eval(['r_000',num2str(n)]);
                        elseif n<100
                            p = eval(['p_00',num2str(n)]);
                            u = eval(['u_00',num2str(n)]);
                            p_end_to_end = eval(['p_end_to_end_00',...
                            num2str(n)]);
                            p_magnitude = eval(['p_magnitude_00',...
                            num2str(n)]);
                            r = eval(['r_00',num2str(n)]);
                        elseif n<1000
                            p = eval(['p_0',num2str(n)]);
                            u = eval(['u_0',num2str(n)]);
                            p_end_to_end = eval(['p_end_to_end_0',...
                            num2str(n)]);
                            p_magnitude = eval(['p_magnitude_0',...
                            num2str(n)]);
                            r = eval(['r_0',num2str(n)]);
```

```
else
    p = eval(['p_',num2str(n)]);
    u = eval(['u_',num2str(n)]);
    p_end_to_end = eval(['p_end_to_end_',...
    num2str(n)]);
    p_magnitude = eval(['p_magnitude_',...
    num2str(n)]);
    r = eval(['r_',num2str(n)]);
end

head_point = r(i,3*Nr-2:3*Nr)+ ...
N*a*p(i,3*Nr-2:3*Nr);
%the position of the head point of the fiber
for j=1:Nr-1
    head_point_rod = r(i,3*j-2:3*j)+ ...
    N*a*p(i,3*j-2:3*j);
    %the position of the head point of rod 1~Nr-1
    temp = my_cross(p_end_to_end(i,:),...
    head_point-head_point_rod);

    distance(i,j) = norm(temp);
    extent(i,j) = abs(my_dot(p_end_to_end(i,:),...
    head_point-head_point_rod));

    projection = head_point-extent(i,j)*...
    p_end_to_end(i,:);
    %the coordinate of the projection of
    %the head point of rod on the end to
    %end vector
    distance_direction = head_point_rod-projection;
    %the direction pointing from the
    %projection to the head point of rod

    if my_dot(u(i,3*j-2:3*j),distance_direction)>0
        y_coordinate(i,j+1) = distance(i,j);
    else
        y_coordinate(i,j+1) = -distance(i,j);
    end

    p_fiber_mid = head_point - 1/2*...
    p_magnitude(i,:)*p_end_to_end(i,:);
    temp_xx = projection - p_fiber_mid;

    if my_dot(temp_xx,p_end_to_end(i,:))>0
        x_coordinate(i,j+1) = norm(temp_xx);
    else
        x_coordinate(i,j+1) = -norm(temp_xx);
```

```
    end
end



%the following codes use least square to fit
%a sine curve y=A*sin(2*pi*x/L), where L is
%p_magnitude, for the fiber using x_coordinate
%and y_coordinate

sum11 = 0;
sum22 = 0;
for mm=1:Nr+1
    sum11 = sum11 + sin(2*pi*...
    x_coordinate(i,mm)/p_magnitude(i,:))*...
    y_coordinate(i,mm);
    sum22 = sum22 + (sin(2*pi*...
    x_coordinate(i,mm)/p_magnitude(i,:)))^2;
end

A = sum11/sum22;

A_over_L(i,n) = A/p_magnitude(i,:);
A_over_L(i,n) = abs(A_over_L(i,n));

plane_direction = ...
my_cross(p_end_to_end(i,:),[0 0 1]);
%the normal vector of the plane formed
%by fiber direction vector and z-axis
temp_1 = my_dot(u(i,3*Nr-2:3*Nr),...
plane_direction);
temp_2 = ...
my_dot(my_cross(u(i,3*Nr-2:3*Nr),...
plane_direction),p_end_to_end(i,:));

%the following lines give the value
%of beta depends on the position of
%body-fixed vector dut to the range
%of beta is [0,2*pi]
if temp_1>=0 && temp_2>0
    beta(i) = ...
    pi/2-acos(temp_1/...
    norm(plane_direction));
elseif temp_1>=0 && temp_2<0
    beta(i) = ...
    pi/2+acos(temp_1/...
    norm(plane_direction));
elseif temp_1<=0 && temp_2>0
```

```
    beta(i) = ...
    2*pi-(acos(temp_1/...
    norm(plane_direction))-pi/2);
elseif temp_1<=0 && temp_2<0
    beta(i) = ...
    pi/2+acos(temp_1/...
    norm(plane_direction));
end

theta(i) = ...
acos(my_dot(p_end_to_end(i,:)...
,[0 0 1]));

temp_3 = ...
[p_end_to_end(i,1) ...
p_end_to_end(i,2) 0];

if temp_3(1)>=0 && temp_3(2)>=0
    phi(i) = ...
    acos(my_dot(temp_3,...
    [1 0 0])/norm(temp_3));
elseif temp_3(1)<=0 &&...
 temp_3(2)>=0
    phi(i) = ...
    acos(my_dot(temp_3,...
    [1 0 0])/norm(temp_3));
elseif temp_3(1)<=0 &&...
 temp_3(2)<=0
    phi(i) = ...
    2*pi-acos(my_dot(temp_3,...
    [1 0 0])/norm(temp_3));
elseif temp_3(1)>=0 && ...
temp_3(2)<=0
    phi(i) = ...
    2*pi-acos(my_dot(temp_3,...
    [1 0 0])/norm(temp_3));
end

%calculating the elastic properties for
%unidirectional wavy fibers composites by calling
%the function elastic_properties_uni_wavy
[E1,v12,v13,E2,v21,v23,E3,v31,v32,G12,G23,G13]=...
    elastic_properties_uni_wavy(S_unwavy,...
    A_over_L(i,n));

%calculating the stiffness tensor for
%unidirectional wavy fiber composites by calling
```

```
%the function stiffness_uni_wavy
[S_wavy,C_wavy] = stiffness_uni_wavy(E1,v12,...
v13,E2,v21,v23,E3,v31,v32,G12,G23,G13);



%calculating the rotation matrix Q
Q(1,1) = sin(theta(i))*cos(phi(i));
Q(1,2) = sin(theta(i))*sin(phi(i));
Q(1,3) = cos(theta(i));
Q(2,1) = -sin(phi(i))*cos(beta(i))-...
cos(theta(i))*cos(phi(i))*sin(beta(i));
Q(2,2) = cos(phi(i))*cos(beta(i))-...
cos(theta(i))*sin(phi(i))*sin(beta(i));
Q(2,3) = sin(theta(i))*sin(beta(i));
Q(3,1) = sin(phi(i))*sin(beta(i))-...
cos(theta(i))*cos(phi(i))*cos(beta(i));
Q(3,2) = -cos(phi(i))*sin(beta(i))-...
cos(theta(i))*sin(phi(i))*cos(beta(i));
Q(3,3) = sin(theta(i))*cos(beta(i));


%calculating the sample mean stiffness tensor
for q=1:3
    for rr=1:3
        for s=1:3
            for t=1:3
                if q==1 && rr==1
                    qr=1;
                elseif q==2 && rr==2
                    qr=2;
                elseif q==3 && rr==3
                    qr=3;
                elseif q+rr==5
                    qr=4;
                elseif q+rr==4
                    qr=5;
                elseif q+rr==3
                    qr=6;
                end
                if s==1 && t==1
                    st=1;
                elseif s==2 && t==2
                    st=2;
                elseif s==3 && t==3
                    st=3;
                elseif s+t==5
                    st=4;
```

```
                                        elseif s+t==4
                                            st=5;
                                        elseif s+t==3
                                            st=6;
                                        end
                                        m_temp = m_temp+Q(q,ii)*...
                                        Q(rr,jj)*Q(s,kk)*Q(t,ll)*...
                                        C_wavy(qr,st);
                                    end
                                end
                            end
                        end
                        m(ii,jj,kk,ll) = m(ii,jj,kk,ll)+m_temp;
                    end

                    m(ii,jj,kk,ll) = m(ii,jj,kk,ll)/N_fiber;
                end
            end
        end
    end

%getting the contracted stiffness tensor
for ii=1:3
    for jj=1:3
        for kk=1:3
            for ll=1:3
                if ii==1 && jj==1
                    ij=1;
                elseif ii==2 && jj==2
                    ij=2;
                elseif ii==3 && jj==3
                    ij=3;
                elseif ii+jj==5
                    ij=4;
                elseif ii+jj==4
                    ij=5;
                elseif ii+jj==3
                    ij=6;
                end
                if kk==1 && ll==1
                    kl=1;
                elseif kk==2 && ll==2
                    kl=2;
                elseif kk==3 && ll==3
                    kl=3;
                elseif kk+ll==5
                    kl=4;
```

```
                elseif kk+ll==4
                    kl=5;
                elseif kk+ll==3
                    kl=6;
                end
                m_contracted(ij,kl)=m(ii,jj,kk,ll);
            end
        end
    end
end

%saving the stiffness tensor for each time step
if i<10
    save(['stiffness_000',num2str(i)],'-ascii','m_contracted')
elseif i<100
    save(['stiffness_00',num2str(i)],'-ascii','m_contracted')
elseif i<1000
    save(['stiffness_0',num2str(i)],'-ascii','m_contracted')
else
    save(['stiffness_',num2str(i)],'-ascii','m_contracted')
end

end
%%%%%%%%%%%%%%%%%%%%%%%%%%%%%%%%%%%%%%%%%%%%%%%%%%%%%%%%%%%%%%%%%%%%%%%%%%%%

%%%%%%%%%%%%%%%%%%%%%%%%%%%%%%%%%%%%%%%%%%%%%%%%%%%%%%%%%%%%%%%%%%%%%%%%%%%%
%save the fiber waviness for future use
save A_over_L.dat A_over_L '-ascii'
%%%%%%%%%%%%%%%%%%%%%%%%%%%%%%%%%%%%%%%%%%%%%%%%%%%%%%%%%%%%%%%%%%%%%%%%%%%%
```

2.2 Generation of Randomly Oriented Fibers

```
%%%%%%%%%%%%%%%%%%%%%%%%%%%%%%%%%%%%%%%%%%%%%%%%%%%%%%%%%%%%%%%%%%%%%%%%%%%%
%This function is to generate a randomly distributed fiber orientations
function [th_rand,phi_rand] = ARGA_3D(Nth,Nphi)
%%%%%%%%%%%%%%%%%%%%%%%%%%%%%%%%%%%%%%%%%%%%%%%%%%%%%%%%%%%%%%%%%%%%%%%%%%%%

%%%%%%%%%%%%%%%%%%%%%%%%%%%%%%%%%%%%%%%%%%%%%%%%%%%%%%%%%%%%%%%%%%%%%%%%%%%%
%Create the values of the distribution function to be sampled from
dist = zeros(Nth,Nphi);
for ii = 1:Nth
  for jj = 1:Nphi
    dist(ii,jj) = 1/(4*pi);
  end
end
%%%%%%%%%%%%%%%%%%%%%%%%%%%%%%%%%%%%%%%%%%%%%%%%%%%%%%%%%%%%%%%%%%%%%%%%%%%%
```

```
%%%%%%%%%%%%%%%%%%%%%%%%%%%%%%%%%%%%%%%%%%%%%%%%%%%%%%%%%%%%%%%%%%%%%%%%%%%%
%Get the maximum of the distribution function.
maxd=max(max(dist));
%%%%%%%%%%%%%%%%%%%%%%%%%%%%%%%%%%%%%%%%%%%%%%%%%%%%%%%%%%%%%%%%%%%%%%%%%%%%

%%%%%%%%%%%%%%%%%%%%%%%%%%%%%%%%%%%%%%%%%%%%%%%%%%%%%%%%%%%%%%%%%%%%%%%%%%%%
%Generate a random array of size (len_th+1)x(len_phi+1)
%with values between 0 and 1.
randval = rand(Nth,Nphi);
mur = mean(mean(randval));
%%%%%%%%%%%%%%%%%%%%%%%%%%%%%%%%%%%%%%%%%%%%%%%%%%%%%%%%%%%%%%%%%%%%%%%%%%%%

%%%%%%%%%%%%%%%%%%%%%%%%%%%%%%%%%%%%%%%%%%%%%%%%%%%%%%%%%%%%%%%%%%%%%%%%%%%%
%Then to select the points from the distribution function that are greater
%than the randomly generated value that is normalized by the quantity
%maxd/mur.
k = 0;
th_rand = zeros(Nth*Nphi,1);
phi_rand = zeros(Nth*Nphi,1);
for ii=1:Nth
  for jj=1:Nphi
    if(randval(ii,jj)*maxd/mur <= dist(ii,jj)*sin((ii-1)/(Nth-1)*pi))
      k=k+1;
      th_rand(k)=(ii-1)/(Nth-1)*pi;
      phi_rand(k)=(jj-1)/(Nphi-1)*2*pi;
    end
  end
end
th_rand((k+1):length(th_rand)) = [];
phi_rand((k+1):length(phi_rand)) = [];
%%%%%%%%%%%%%%%%%%%%%%%%%%%%%%%%%%%%%%%%%%%%%%%%%%%%%%%%%%%%%%%%%%%%%%%%%%%%
```

2.3 Compliance of the Unidirectional Lamina

```
%%%%%%%%%%%%%%%%%%%%%%%%%%%%%%%%%%%%%%%%%%%%%%%%%%%%%%%%%%%%%%%%%%%%%%%%%%%%
%This function returns the compliance (S) and stiffness (C) tensors in
%contracted notation given the Young's moduli of the fiber (EF) and the
%matrix (Em), the Poisson's Ratio of the fiber (vf) and the matrix (vm)
%along with the volume fraction (Vfrac) and the effective aspect ratio
%(ar)of the fiber.  The material stiffness and compliance tensors are
%computed using the Tandon-Weng theory (Tandon, G.P. and G.J. Weng.
%"The Effect of Aspect Ratio of Inclusions on the Elastic Properties
%of Unidirectionally Aligned Composites." Polymer Composites,
%5(4):327-333, October 1984). The paramter for v12 is selected to be
%the one given in Tucker and Liang ("Stiffness Predictions for
%Unidirectional Short-Fiber Composites: Review and Evaluation"
%Composites Science and Technology, 59:655-671, 1999) and provides
```

```
%an alternative for the iterative formulation originally presented in
%Tandon and Weng's paper.

function [S]=compliance_uni(Ef,vf,Em,vm,Vfrac,ar)
%%%%%%%%%%%%%%%%%%%%%%%%%%%%%%%%%%%%%%%%%%%%%%%%%%%%%%%%%%%%%%%%%%%%%%%%%%%%

%%%%%%%%%%%%%%%%%%%%%%%%%%%%%%%%%%%%%%%%%%%%%%%%%%%%%%%%%%%%%%%%%%%%%%%%%%%%
%Calculate Lame's constants
lm  = Em*vm / ( (1+vm)*(1-2*vm) );
mum = Em / ( 2*(1+vm) );
lf  = Ef*vf / ( (1+vf)*(1-2*vf) );
muf = Ef / ( 2*(1+vf) );
Gm  = Em / ( 2*(1+vm) );    %Notice this is the same as mum
Gf  = Ef / ( 2*(1+vf) );    %Notice this is the same as muf
%%%%%%%%%%%%%%%%%%%%%%%%%%%%%%%%%%%%%%%%%%%%%%%%%%%%%%%%%%%%%%%%%%%%%%%%%%%%

%%%%%%%%%%%%%%%%%%%%%%%%%%%%%%%%%%%%%%%%%%%%%%%%%%%%%%%%%%%%%%%%%%%%%%%%%%%%
%Compute the parameter g
g = ar/(ar^2-1)^(3/2) * (ar*(ar^2-1)^(1/2)-acosh(ar));
%%%%%%%%%%%%%%%%%%%%%%%%%%%%%%%%%%%%%%%%%%%%%%%%%%%%%%%%%%%%%%%%%%%%%%%%%%%%


%%%%%%%%%%%%%%%%%%%%%%%%%%%%%%%%%%%%%%%%%%%%%%%%%%%%%%%%%%%%%%%%%%%%%%%%%%%%
%Compute the Eshelby tensor components S_{ijkl}
S1111 = 1/(2*(1-vm)) * ...
        (1 - 2*vm + (3*ar^2-1)/(ar^2-1) - (1 - 2*vm + 3*ar^2/(ar^2-1))*g);
S2222 = 3/(8*(1-vm)) * ar^2/(ar^2-1)...
       +1/(4*(1-vm)) * (1 - 2*vm -9/(4*(ar^2-1)))*g;
S3333 = S2222;
S2233 = 1/(4*(1-vm)) * (ar^2/(2*(ar^2-1)) - (1-2*vm + 3/(4*(ar^2-1)))*g );
S3322 = S2233;
S2211 = -1/(2*(1-vm)) * ar^2/(ar^2-1) ...
       - 1/(4*(1-vm)) *(1-2*vm-3*ar^2/(ar^2-1))*g;
S3311 = S2211;
S1122 = -1/(2*(1-vm)) * (1 - 2*vm + 1/(ar^2-1)) ...
        +1/(2*(1-vm)) * (1 - 2*vm + 3/(2*(ar^2-1)))*g;
S1133 = S1122;
S2323 = 1/(4*(1-vm)) * (ar^2/(2*(ar^2-1)) + (1-2*vm-3/(4*(ar^2-1)))*g);
S3232 = S2323;
S1212 = 1/(4*(1-vm)) * ...
        (1-2*vm-(ar^2+1)/(ar^2-1)-1/2*g*(1-2*vm-3*(ar^2+1)/(ar^2-1)));
%%%%%%%%%%%%%%%%%%%%%%%%%%%%%%%%%%%%%%%%%%%%%%%%%%%%%%%%%%%%%%%%%%%%%%%%%%%%

%%%%%%%%%%%%%%%%%%%%%%%%%%%%%%%%%%%%%%%%%%%%%%%%%%%%%%%%%%%%%%%%%%%%%%%%%%%%
%Calculate the Di constants
D1 = 1+2*(muf-mum)/(lf-lm);
D2 = (lm+2*mum)/(lf-lm);
```

```
D3 = lm/(lf-lm);
%%%%%%%%%%%%%%%%%%%%%%%%%%%%%%%%%%%%%%%%%%%%%%%%%%%%%%%%%%%%%%%%%%%%%%%%%%%%

%%%%%%%%%%%%%%%%%%%%%%%%%%%%%%%%%%%%%%%%%%%%%%%%%%%%%%%%%%%%%%%%%%%%%%%%%%%%
%Calculate the Bi constants
B1 = Vfrac*D1 + D2 + (1-Vfrac)*( D1*S1111 + 2*S2211 );
B2 = Vfrac + D3 + (1-Vfrac)*( D1*S1122 + S2222 + S2233 );
B3 = Vfrac + D3 + (1-Vfrac)*( S1111 + (1 + D1)*S2211 );
B4 = Vfrac*D1 + D2 + (1-Vfrac)*( S1122 + D1*S2222 + S2233 );
B5 = Vfrac + D3 + (1-Vfrac)*( S1122 + S2222 + D1*S2233 );
%%%%%%%%%%%%%%%%%%%%%%%%%%%%%%%%%%%%%%%%%%%%%%%%%%%%%%%%%%%%%%%%%%%%%%%%%%%%

%%%%%%%%%%%%%%%%%%%%%%%%%%%%%%%%%%%%%%%%%%%%%%%%%%%%%%%%%%%%%%%%%%%%%%%%%%%%
%Calculate the Ai constants
A1 = D1*(B4+B5)-2*B2;
A2 = (1+D1)*B2 - (B4+B5);
A3 = B1 - D1*B3;
A4 = (1+D1)*B1 - 2*B3;
A5 = (1-D1)/(B4-B5);
A  = 2*B2*B3 - B1*(B4+B5);
%%%%%%%%%%%%%%%%%%%%%%%%%%%%%%%%%%%%%%%%%%%%%%%%%%%%%%%%%%%%%%%%%%%%%%%%%%%%

%%%%%%%%%%%%%%%%%%%%%%%%%%%%%%%%%%%%%%%%%%%%%%%%%%%%%%%%%%%%%%%%%%%%%%%%%%%%
%Calculate the material coefficients
E11 = Em / ( 1+Vfrac*(A1+2*vm*A2)/A );
E22 = Em / ( 1+Vfrac*(-2*vm*A3+(1-vm)*A4+(1+vm)*A5*A)/(2*A) );
%%%%%%%%%%%%%%%%%%%%%%%%%%%%%%%%%%%%%%%%%%%%%%%%%%%%%%%%%%%%%%%%%%%%%%%%%%%%

%%%%%%%%%%%%%%%%%%%%%%%%%%%%%%%%%%%%%%%%%%%%%%%%%%%%%%%%%%%%%%%%%%%%%%%%%%%%
%The following terms for G12 and G23 come from the original Tandon Wang
%paper.
G12 = Gm*(1+Vfrac/(Gm/(Gf-Gm)+2*(1-Vfrac)*S1212));
G23 = Gm*(1+Vfrac/(Gm/(Gf-Gm)+2*(1-Vfrac)*S2323));
v12 = (vm*A-vf*(A3-vm*A4))/(A+vf*(A1+2*vm*A2));
v23 = -1+E22/(2*G23);
%%%%%%%%%%%%%%%%%%%%%%%%%%%%%%%%%%%%%%%%%%%%%%%%%%%%%%%%%%%%%%%%%%%%%%%%%%%%

%%%%%%%%%%%%%%%%%%%%%%%%%%%%%%%%%%%%%%%%%%%%%%%%%%%%%%%%%%%%%%%%%%%%%%%%%%%%
%The compliance matrix for a transversely isotropic material
S=[     1/E11,  -v12/E11,  -v12/E11,      0,      0,     0;...

     -v12/E11,     1/E22,  -v23/E22,      0,      0,     0;...

     -v12/E11,  -v23/E22,     1/E22,      0,      0,     0;...

            0,         0,         0,  1/G23,      0,     0;...
```

```
            0,          0,          0,       0,  1/G12,      0;...

            0,          0,          0,       0,       0, 1/G12];

C = inv(S);
%%%%%%%%%%%%%%%%%%%%%%%%%%%%%%%%%%%%%%%%%%%%%%%%%%%%%%%%%%%%%%%%%%%%%%%%%%%%%%%
```

2.4 Elastic Properties of Each Aggregate

```
%%%%%%%%%%%%%%%%%%%%%%%%%%%%%%%%%%%%%%%%%%%%%%%%%%%%%%%%%%%%%%%%%%%%%%%%%%%%%%%
%This code calculates the elastic properties of composites with
%unidirectionally distributed wavy fibers
function [E1,v12,v13,E2,v21,v23,E3,v31,v32,G12,G23,G13]=...
    elastic_properties_uni_wavy(S,A_over_L)
%%%%%%%%%%%%%%%%%%%%%%%%%%%%%%%%%%%%%%%%%%%%%%%%%%%%%%%%%%%%%%%%%%%%%%%%%%%%%%%

%%%%%%%%%%%%%%%%%%%%%%%%%%%%%%%%%%%%%%%%%%%%%%%%%%%%%%%%%%%%%%%%%%%%%%%%%%%%%%%
%fiber waviness
alpha = 2*pi*A_over_L; %this quantity defines how curved the fiber is
%%%%%%%%%%%%%%%%%%%%%%%%%%%%%%%%%%%%%%%%%%%%%%%%%%%%%%%%%%%%%%%%%%%%%%%%%%%%%%%

%%%%%%%%%%%%%%%%%%%%%%%%%%%%%%%%%%%%%%%%%%%%%%%%%%%%%%%%%%%%%%%%%%%%%%%%%%%%%%%
%calculate the quantites needed to calculate the elastic properties
I1 = (1+alpha^2/2)/(1+alpha^2)^(3/2);
I3 = (alpha^2/2)/(1+alpha^2)^(3/2);
I5 = 1-(1+3*alpha^2/2)/(1+alpha^2)^(3/2);
I6 = 1/(1+alpha^2)^(1/2);
I8 = 1-1/(1+alpha^2)^(1/2);
%%%%%%%%%%%%%%%%%%%%%%%%%%%%%%%%%%%%%%%%%%%%%%%%%%%%%%%%%%%%%%%%%%%%%%%%%%%%%%%

%%%%%%%%%%%%%%%%%%%%%%%%%%%%%%%%%%%%%%%%%%%%%%%%%%%%%%%%%%%%%%%%%%%%%%%%%%%%%%%
%calculate the elastic properties
E1 = 1/(S(1,1)*I1+(2*S(1,2)+S(6,6))*I3+S(2,2)*I5);
v12 = -(S(1,2)*I6+S(2,3)*I8)/(S(1,1)*I1+(2*S(1,2)+S(6,6))*I3+S(2,2)*I5);
v13 = -((S(1,1)+S(2,2)-S(6,6))*I3+S(1,2)*(I1+I5))/...
    (S(1,1)*I1+(2*S(1,2)+S(6,6))*I3+S(2,2)*I5);
E2 = 1/S(2,2);
v21 = -(S(1,2)*I6+S(2,3)*I8)/S(2,2);
v23 = -(S(2,3)*I6+S(1,2)*I8)/S(2,2);
E3 = 1/(S(1,1)*I5+(2*S(1,2)+S(6,6))*I3+S(2,2)*I1);
v31 = -((S(1,1)+S(2,2)-S(6,6))*I3+S(1,2)*(I1+I5))/...
    (S(1,1)*I5+(2*S(1,2)+S(6,6))*I3+S(2,2)*I1);
v32 = -(S(2,3)*I6+S(1,2)*I8)/(S(1,1)*I5+(2*S(1,2)+S(6,6))*I3+S(2,2)*I1);
G12 = 1/(2*(S(2,2)-S(2,3))*I8+S(6,6)*I6);
G23 = 1/(2*(S(2,2)-S(2,3))*I6+S(6,6)*I8);
G13 = 1/(4*(S(1,1)+S(2,2)-2*S(1,2))*I3+S(6,6)*(I1-2*I3+I5));
%%%%%%%%%%%%%%%%%%%%%%%%%%%%%%%%%%%%%%%%%%%%%%%%%%%%%%%%%%%%%%%%%%%%%%%%%%%%%%%
```

```
%%%%%%%%%%%%%%%%%%%%%%%%%%%%%%%%%%%%%%%%%%%%%%%%%%%%%%%%%%%%%%%%%%%%%%%%%%%%
%This code calculates the stiffness tensor of composites with
%unidirectionally distributed wavy fibers
function[S,C] = stiffness_uni_wavy(E1,v12,v13,E2,v21,v23,E3,v31,v32,G12,...
G23,G13)
%%%%%%%%%%%%%%%%%%%%%%%%%%%%%%%%%%%%%%%%%%%%%%%%%%%%%%%%%%%%%%%%%%%%%%%%%%%%
```

2.5 Stiffness Tensor of Each Aggregate

```
%%%%%%%%%%%%%%%%%%%%%%%%%%%%%%%%%%%%%%%%%%%%%%%%%%%%%%%%%%%%%%%%%%%%%%%%%%%%
S=[     1/E1,  -v21/E2,  -v31/E3,      0,      0,     0;...

     -v12/E1,     1/E2,  -v32/E3,      0,      0,     0;...

     -v13/E1,  -v23/E2,     1/E3,      0,      0,     0;...

           0,         0,       0,  1/G23,      0,     0;...

           0,         0,       0,      0,  1/G13,     0;...

           0,         0,       0,      0,      0,     1/G12];

C = inv(S);
%%%%%%%%%%%%%%%%%%%%%%%%%%%%%%%%%%%%%%%%%%%%%%%%%%%%%%%%%%%%%%%%%%%%%%%%%%%%
```

APPENDIX C

Derivation of the Rotation Matrix

From basic coordinate rotation theory, a fourth-order tensor in a coordinate xyz is rotated right-handedly into a coordinate $x'y'z'$ by

$$\mathbf{T}' = QQ\mathbf{T}Q^TQ^T \tag{3.1}$$

where Q is the rotation matrix from the coordinate xyz into the coordinate $x'y'z'$. Q^T is the transpose of Q and Q is orthogonal. Let $Q = R^T$, then Equation (3.1) becomes

$$\mathbf{T}' = R^TR^T\mathbf{T}RR \tag{3.2}$$

where R is actually the rotation matrix from the coordinate $x'y'z'$ into the coordinate xyz. By pre-multiplying RR and op-multiplying R^TR^T on both sides of Equation (3.3), we can obtain the equation for rotating a fourth tensor right-handedly from coordinate $x'y'z'$ into coordinate xyz as

$$\mathbf{T} = RR\mathbf{T}'R^TR^T = Q^TQ^T\mathbf{T}'QQ \tag{3.3}$$

In this research, it's more straightforward to directly derive R than derive Q. So the following derivation is for developing the rotation matrix R, from coordinate $x'y'z'$ into xyz. In $\mathbb{R}^3$, coordinate system rotations about the $x-$, $y-$, and $z-$ axes in a counterclockwise direction when looking towards the origin give the rotation matrices as

$$\mathbf{R_x}(\alpha) = \begin{bmatrix} 1 & 0 & 0 \\ 0 & \cos\alpha & \sin\alpha \\ 0 & -\sin\alpha & \cos\alpha \end{bmatrix} \tag{3.4}$$

$$\mathbf{R_y}(m) = \begin{bmatrix} \cos m & 0 & -\sin m \\ 0 & 1 & 0 \\ \sin m & 0 & \cos m \end{bmatrix} \tag{3.5}$$

$$\mathbf{R_z}(\gamma) = \begin{bmatrix} \cos\gamma & \sin\gamma & 0 \\ -\sin\gamma & \cos\gamma & 0 \\ 0 & 0 & 1 \end{bmatrix} \tag{3.6}$$

From Figure 4.1, in order to rotate the coordinate $x'y'z'$ into the coordinate xyz, first rotate about the $x'-$axis clockwise by β, and then rotate about the $y'-$axis counterclockwise by $\frac{\pi}{2} - \theta$, and at last rotate about the $z'-$axis clockwise by ϕ, which makes the rotation matrix R a matrix product of three rotation matrices as

$$\mathbf{R} = \mathbf{R_{z'}}(\gamma = -\phi)\mathbf{R_{y'}}(m = \frac{\pi}{2} - \theta)\mathbf{R_{x'}}(\alpha = -\beta) \tag{3.7}$$

Thus from $Q = R^T$, we obtain the rotation matrix Q in Equation (3.8) as

$$\mathbf{a} = \begin{bmatrix} \sin\theta\cos\phi & \sin\theta\sin\phi & \cos\theta \\ -\sin\phi\cos\beta - \cos\theta\cos\phi\sin\beta & \cos\phi\cos\beta - \cos\theta\sin\phi\sin\beta & \sin\theta\sin\beta \\ \sin\phi\sin\beta - \cos\theta\cos\phi\cos\beta & -\cos\phi\sin\beta - \cos\theta\sin\phi\cos\beta & \sin\theta\cos\beta \end{bmatrix} \tag{3.8}$$

APPENDIX D

Vita

Cong Zhang was born to Jinguo Zhang and Ling Wu on August 7, 1986 in Xi'an, China, which is one of the oldest cities in China and one of the four Great Ancient Capital Cities together with Athens, Rome and Cairo. He graduated from Wuhuan High school in June 2004 and in the same year he ranked first in the National Matriculation Exam for Colleges and University in China among all the high schools in Baqiao District in Xi'an. In September 2004 he started his undergraduate study in the department of Polymer Materials and Engineering at Zhejiang University, which is one of most prestigious universities in China. In June 2008, he graduated with an Outstanding Undergraduate Thesis honor. In the same year, he was accepted by the department of Industrial and Manufacturing Engineering at Florida State University to pursue his masters with full scholarship, where he met Dr. David A. Jack and developed his research interest in computational mechanics. In fall 2009, Cong transferred to the department of Mechanical Engineering at Baylor University with Dr. Jack, who then became his mentor and advisor. Cong has received a fellowship from the graduate school of The Ohio State University (The OSU) and will start to pursue a Ph.D. in the department of Mechanical and Aerospace Engineering at The OSU in fall 2011.

BIBLIOGRAPHY

[1] S. Yamamota and T. Matsuoka. A Method for Dynamic Simulation of Rigid and Flexible Fibers in a Flow Field. *Journal of Chemical Physics*, **98**(1):644–650, 1993.

[2] S. Yamamota and T. Matsuoka. Viscosity of dilute suspensions of rodlike particles: A numerical simulation method. *Journal of Chemical Physics*, **100**:3317–3324, 1994.

[3] R.F. Ross and D.J. Klingenberg. Dynamic Simulation of Flexible Fibers Composed of Linked Rigib Bodies. *Jn. of Chemical Physics*, **106**:2949–2960, February 1997.

[4] H.M. Hsiao and I.M. Daniel. Elastic Properties of Composites with Fiber Waviness. *Composites, Part A*, **27**(10):931–941, 1996.

[5] D.A. Jack and D.E. Smith. Elastic Properties of Short-Fiber Polymer Composites, Derivation and Demonstration of Analytical Forms for Expectation and Variance from Orientation Tensors. *Journal of Composite Materials*, **42**(3):277–308, 2008.

[6] S.G. Advani and C.L. Tucker. The Use of Tensors to Describe and Predict Fiber Orientation in Short Fiber Composites. *Jn. of Rheology*, **31**(8):751–784, 1987.

[7] C.-S. Yeh. *A Study of Nanostructure and Properties of Mixed Nanotube Buckypaper Materials: Fabrication, Process Modeling Characterization and Property Modeling*. PhD thesis, Florida State University, December 2007.

[8] C.W. Camacho, C.L. Tucker, S. Yalvac, and R.L. McGee. Stiffness and Thermal Expansion Predictions for Hybird Short Fiber Composites. *Polymer Composites*, **11**(4):229–239, August 1990.

[9] C.G. Joung, N. Phan-Thien, and X.J. Fan. Viscosity of Curved Fibers in Suspension. *Journal of Non-Newtonian Fluid Mechanics*, **102**:1–17, 2002.

[10] S. Yamamota and T. Matsuoka. Dynamic Simulation of Microstructure and Rheology of Fiber Suspensions. *Polymer Engineering Science*, **36**(19):2396–2403, October 1996.

[11] B.E. VerWeyst and Tucker C.L. III. Fiber Suspensions in Complex Geometries: Flow-Orientation Coupling. *The Canadian Journal of Chemical Engineering*, **80**:1093–1106, December 2002.

[12] B.E. VerWeyst, C.L. Tucker, P.H. Foss, and J.F. O'Gara. Fiber Orientation in 3-D Injection Molded Features: Prediction and Experiment. *International Polymer Processing*, **14**:409–420, 1999.

[13] G.B. Jeffery. The Motion of Ellipsoidal Particles Immersed in a Viscous Fluid. *Proceedings of the Royal Society of London A*, **102**:161–179, March 1923.

[14] F.P. Folgar and C.L. Tucker. Orientation Behavior of Fibers in Concentrated Suspensions. *Jn. of Reinforced Plastics and Composites*, **3**:98–119, April 1984.

[15] J.H. Phelps and C.L. Tucker. An Anisotropic Rotary Diffusion Model for Fiber Orienation in Short- and LongFiber Thermoplastics. *Journal of Non-Newtonian Fluid Mechanics*, **156**:165–176, 2009.

[16] Montgomery-Smith, S.J., D.A. Jack, and D.E. Smith. A Systematic Approach to Obtaining Numerical Solutions of Jefferys Type Equations using Spherical Harmonics. *Composites, Part A*, **41**:827–835, 2010.

[17] N. Nguyen, S.K. Bapanapalli, J.D. Holbery, M.T. Smith, V. Kunc, B. Frame, J.H. Phelps, and C.L. Tucker. Fiber Length and orientation in Long-Fiber Injection-Molded Thermoplastics - Part I: Modeling of Microstructure and Elastic Properties. *Jn. of Composite Materials*, **42**(10):1003–1029, 2008.

[18] L.H. III Switzer. *Simulating Systems of Flexible Fibers*. PhD thesis, University of Wisconsin-Madison, December 2002.

[19] S.M. Dinh and R.C. Armstrong. A Rheological Equation of State for Semiconcentrated Fiber Suspensions. *Jn. of Rheology*, **28**(3):207–227, 1984.

[20] S. Yamamota and T. Matsuoka. Dynamic simulation of fiber suspensions in shear flow. *Journal of Chemical Physics*, **102**(5):2254, 1995.

[21] G. Wang, W. Yu, and C. Zhou. Optimization of the Rod Chain Model to Simulate the Motions of a Long Flexible Fiber in Simple Shear Flows. *European Journal of Mechanics*, **25**:337–347, 2006.

[22] P. Skjetne, R.F. Ross, and D.J. Klingenberg. Simulation of single fiber dynamics. *Journal of Chemical Physics*, **107**(6):2108–2121, 1997.

[23] C. F Schmid, L. H Switzer, and D. J Klingenberg. Simulations of fiber flocculation: Effects of fiber properties and interfiber friction. *Journal of Rheology*, **44**:781, 2000.

[24] Leonard H. Switzer III and Daniel J. Klingenberg. Rheology of sheared flexible fiber suspensions via fiber-level simulations. *Journal of Rheology*, **47**(3):759–778, May 2003.

[25] C. G. Joung, N. Phan-Thien, and X. J. Fan. Direct simulation of flexible fibers. *Journal of Non-Newtonian Fluid Mechanics*, **99**(1):1–36, April 2001.

[26] Musa R. Kamal. *Injection Molding: Technology and Fundamentals*. Hanser Verlag, 2009.

[27] Gerd Ptsch and Walter Michaeli. *Injection molding: an introduction*. Hanser Verlag, 2008.

[28] F. Truckenmller and H. -G Fritz. Injection molding of long fiber-reinforced thermoplastics: A comparison of extruded and pultruded materials with direct addition of roving strands. *Polymer Engineering & Science*, **31**(18):1316–1329, September 1991.

[29] Edward M Silverman. Effect of glass fiber length on the creep and impact resistance of reinforced thermoplastics. *Polymer Composites*, **8**(1):8–15, February 1987.

[30] C. L. Tucker and S. G. Advani. Processing of Short-Fiber Systems. In S.G. Advani, editor, *Flow and Rheology in Polymer Composites Manufacturing*, pages 147–202. Elsevier Science, Amsterdam, The Netherlands, 1994.

[31] S.G. Advani. *Prediction of Fiber Orientation During Processing of Short Fiber Composites*. PhD thesis, University of Illinois at Urbana-Champaign, August 1987.

[32] D.A. Jack and D.E. Smith. The Effect of Fiber Orientation Closure Approximations on Mechanical Property Predictions. *Composites, Part A*, **38**:975–982, 2007.

[33] C.L. Tucker and R.B. Dessenberger. Governing Equations for Flow and Heat Transfer in Stationary Fiber Beds. In S.G. Advani, editor, *Flow and Rheology in Polymer Composites Manufacturing*, pages 257–323. Elsevier Science, Amsterdam, The Netherlands, 1994.

[34] David Jack. *Advanced Analysis of Short-Fiber Polymer Composite Material Behavior With Higher-order Orientation Tensor Closure Methods*. PhD thesis, University of Missouri - Columbia, 2006.

[35] F.T. Fisher, R.D. Bradshaw, and L.C. Brinson. Effects of nanotube waviness on the modulus of nanotube-rinforced polymers. *Applied Physics Letters*, **80**(24):4467–4649, 2002.

[36] V. Anumandla and R.F. Gibson Gibson. A comprehensive closed form micromechanics model for estimating the elastic modulus of nanotube-reinforced composites. *Composites, Part A*, **37**:2178–2185, 2006.

[37] F. T. Fisher, R. D. Bradshaw, and L. C. Brinson. Fiber waviness in nanotube-reinforced polymer composites—I: modulus predictions using effective nanotube properties. *Composites Science and Technology*, **63**(11):1689–1703, 2003.

[38] R. D. Bradshaw, F. T. Fisher, and L. C. Brinson. Fiber waviness in nanotube-reinforced polymer composites—II: modeling via numerical approximation of the dilute strain concentration tensor. *Composites Science and Technology*, **63**(11):1705–1722, 2003.

[39] R. G. Cox. The motion of long slender bodies in a viscous fluid. part 2. shear flow. *Journal of Fluid Mechanics*, **45**(04):625–657, 1971.

[40] D. Zhang, D.A. Jack, D.E. Smith, and S. Montgomery-Smith. Investigation of the Effectiveness and Efficiency of the Exact Closures: Comparison with Industrial Closures and Spherical Harmonic Solutions. *Proceedings of ASME IMECE'10, Vancouver, British Columbia, Canada*, November 2010.

[41] D. Zhang, D.A. Jack, D.E. Smith, and S. Montgomery-Smith. Journal of Manufacturing Science and Engineering. *Journal of Composite Materials*, 2011.

[42] R.S. Bay. *Fiber Orientation in Injection Molded Composites: A Comparison of Theory and Experiment*. PhD thesis, University of Illinois at Urbana-Champaign, August 1991.

[43] R. B. Bird, R. C. Armstrong, and O. Hassager. *Dynamics of Polymeric Liquids*, volume 1: Fluid Mechanics. John Wiley & Sons, Inc., New York, NY, 2nd edition, 1987.

[44] R. B. Bird, C.F. Curtiss, R. C. Armstrong, and O. Hassager. *Dynamics of Polymeric Liquids*, volume 2: Kinetic Theory. John Wiley & Sons, Inc., New York, NY, 2nd edition, 1987.

[45] M. Doi. Molecular dynamics and rheological properties of concentrated solutions of rodlike polymers in isotropic and liquid crystalline phases. *Journal of Polymer Science Part B Polymer Physics*, 19:229–243, 1981.

[46] G.L. Hand. A Theory of Anisotropic Fluids. *Jn. of Fluid Mechanics*, **13**(1):33–46, May 1962.

[47] S.G. Advani and C.L. Tucker. Closure Approximations for Three-Dimensional Structure Tensors. *Jn. of Rheology*, **34**(3):367–386, 1990.

[48] J. S. Cintra and C.L. Tucker. Orthotropic Closure Approximations for Flow-Induced Fiber Orientation. *Jn. of Rheology*, **39**(6):1095–1122, 1995.

[49] C.V. Chaubal and L.G. Leal. A Closure Approximation for Liquid-Crystalline Polymer Models Based on Parametric Density Estimation. *Journal of Rheology*, **42**(1):177–201, January/February 1998.

[50] D.H. Chung and T.H. Kwon. Improved Model of Orthotropic Closure Approximation for Flow Induced Fiber Orientation. *Polymer Composites*, **22**(5):636–649, October 2001.

[51] K.-H. Han and Y.-T. Im. Numerical Simulation of Three-Dimensional Fiber Orientation in Short-Fiber-Reinforced Injection-Molded Parts. *Jn. of Materials Processing Technology*, **124**:366–371, 2002.

[52] B.K. Schache. *A Neural Network Based Closure for Modeling Short-Fiber Suspensions*. Undergraduate Honors Thesis, University of Missouri - Columbia, May 2006.

[53] D.E. Smith, B.K. Schache, and D.A. Jack. A Neural Network Based Closure for Modeling Short-Fiber Suspensions. *NSF Design, Service and Manufacturing Grantees and Research Conference*, July 2006.

[54] D.A. Jack, B.K. Schache, and D.E. Smith. Neural Network Based Closure for Modeling Short-Fiber Suspensions. *Polymer Composites*, **31**(7):1125–1141, 2009.

[55] S. Montgomery-Smith, D.A. Jack, and D.E. Smith. Fast Solutions for the Fiber Orientation of Concentrated Suspensions of Short-Fiber Composites Using the Exact Closure Methods. *Proceedings of ASME IMECE'10, Vancouver, British Columbia, Canada*, November 2010.

[56] Montgomery-Smith, S.J., D.A. Jack, and D.E. Smith. The Fast Exact Closure for Jeffery's Equation with Diffusion. *Journal of Non-Newtonian Fluid Mechanics*, 2010.

[57] D.A. Jack. Investigating the Use of Tensors in Numerical Predictions for Short-Fiber Reinforced Polymer Composites. Master's thesis, University of Missouri - Columbia, August 2003.

[58] D.A. Jack. *Advanced Analysis of Short-fiber Polymer Composite Material Behavior*. PhD thesis, University of Missouri - Columbia, December 2006.

[59] D.A. Jack and D.E. Smith. Assessing the Use of Tensor Closure Methods With Orientation Distribution Reconstruction Functions. *Jn. of Composite Materials*, **38**(21):1851–1872, 2004.

[60] O.L. Forgacs and S.G. Mason. Particle motions in sheared suspensions: IX. Spin and deformation of threadlike particles. *Journal of colloid science*, **14**(5):457–472, 1959.

[61] Y. Yamane, Y. Kaneda, and M. Dio. Numerical Simulation of Semi-Dilute Suspensions of Rodlike Particles in Shear Flow. *Jn. of Non-Newtonian Fluid Mechanics*, **54**:405–421, 1994.

[62] X. Fan, N. Phan-Thien, and R. Zheng. A Direct Simulation of Fibre Suspensions. *Jn. of Non-Newtonian Fluid Mechanics*, **74**:113–135, 1998.

[63] D. Qi. Direct simulations of flexible cylindrical fiber suspensions in finite reynolds number flows. *The Journal of chemical physics*, **125**:114901, 2006.

[64] Stefan B. Lindstrom and Tetsu Uesaka. Simulation of the motion of flexible fibers in viscous fluid flow. *Physics of Fluids*, **19**(11):113307–16, November 2007.

[65] Stefan B. Lindstrom and Tetsu Uesaka. Simulation of semidilute suspensions of non-Brownian fibers in shear flow. *The Journal of Chemical Physics*, **128**(2):024901–14, January 2008.

[66] C.L. Tucker and E. Liang. Stiffness Predictions for Unidirectional Short-Fiber Composites: Review and Evaluation. *Composites Science and Technology*, **59**:655–671, 1999.

[67] R Hill. The elastic behaviour of a crystalline aggregate. *Proceedings of the Physical Society. Section A*, **65**(5):349–354, May 1952.

[68] Z Hashin and S Shtrikman. On some variational principles in anisotropic and nonhomogeneous elasticity. *Journal of the Mechanics and Physics of Solids*, **10**(4):335–342, October 1962.

[69] Z. Hashin and S. Shtrikman. A variational approach to the theory of the elastic behaviour of multiphase materials. *Journal of the Mechanics and Physics of Solids*, **11**(2):127–140, March 1963.

[70] L.J. Walpole. On bounds for the overall elastic moduli of inhomogeneous systems–I. *Journal of the Mechanics and Physics of Solids*, **14**(3):151–162, May 1966.

[71] L.J. Walpole. On bounds for the overall elastic moduli of inhomogeneous systems–II. *Journal of the Mechanics and Physics of Solids*, **14**(5):289–301, September 1966.

[72] J. R. Willis. Bounds and self-consistent estimates for the overall properties of anisotropic composites. *Journal of the Mechanics and Physics of Solids*, **25**(3):185–202, June 1977.

[73] G.J. Weng. Explicit evaluation of willis' bounds with ellipsoidal inclusions. *International Journal of Engineering Science*, **30**(1):83–92, January 1992.

[74] R.F. Eduljee, R.L. McCullough, and J.W. Gillespie. The Influence of Inclusion Geometry on the Elastic Properties of Discontinuous Fiber Composites. *Polymer Engineering and Science*, **34**(4):352–360, February 1994.

[75] R.F. Eduljee, R.L. McCullough, and J.W. Gillespie. The Influence of Aggregated and Dispersed Textures on the Elastic Properties of Discontinuous-Fiber Composites. *Composites Science and Technology*, **50**:381–391, 1994.

[76] J.D. Eshelby. The Determination of the Elastic Field of an Ellipsoidal Inclusion, and Related Problems. *Proceedings of the Royal Society of London. Series A, Mathematical and Physical Sciences*, **241**(1226):376–396, August 1957.

[77] G. Lielens, P. Pirotte, A. Couniot, F. Dupret, and R. Keunings. Prediction of Thermo-Mechanical Properties for Compression Moulded Composites. *Composites Part A*, 29A:63–70, 1998.

[78] R. Hill. A self-consistent mechanics of composite materials. *Journal of the Mechanics and Physics of Solids*, **13**:213–222, August 1965.

[79] B. Budiansky. On the elastic moduli of some heterogeneous materials. *Journal of the Mechanics and Physics of Solids*, **13**:223–227, August 1965.

[80] N. Laws and R. McLaughlin. The effect of fibre length on the overall moduli of composite materials. *Journal of the Mechanics and Physics of Solids*, **27**:1–13, February 1979.

[81] Tsu-Wei Chou, Seiichi Nomura, and Minoru Taya. A Self-Consistent approach to the elastic stiffness of Short-Fiber composites. *Journal of Composite Materials*, **14**:178 –188, January 1980.

[82] J. C. Halpin and J. L. Kardos. The Halpin-Tsai Equations: A Review. *Polymer Engineering and Science*, **16**(5):344–352, 1976.

[83] R.L. Hewitt and M.C. De Malherbe. An approximation for the longitudinal shear modulus of continuous fibre composites. *Journal of Composite Materials*, **4**(2):280 –282, January 1970.

[84] T. B Lewis and L. E Nielsen. Dynamic mechanical properties of particulate-filled composites. *Journal of Applied Polymer Science*, **14**(6):1449–1471, June 1970.

[85] Lawrence E. Nielsen. Generalized equation for the elastic moduli of composite materials. *Journal of Applied Physics*, **41**(11):4626, 1970.

[86] T. Mori and K. Tanaka. Average Stress in Matrix and Average Elastic Energy of Materials with Misfitting Inclusions. *Acta Metallurgica*, **21**:571–574, May 1973.

[87] M. Taya and T. Mura. On stiffness and strength of an aligned Short-Fiber reinforced composite containing Fiber-End cracks under uniaxial applied stress. *Journal of Applied Mechanics*, **48**(2):361–367, June 1981.

[88] Minoru Taya and Tsu-Wei Chou. On two kinds of ellipsoidal inhomogeneities in an infinite elastic body: An application to a hybrid composite. *International Journal of Solids and Structures*, **17**:553–563, 1981.

[89] G.P. Tandon and G.J. Weng. The Effect of Aspect Ratio of Inclusions on the Elastic Properties of Unidirectionally Aligned Composites. *Polymer Composites*, **5**(4):327–333, 1984.

[90] B.O. Agboola. Investigation of Dense Suspension Rotary Diffusion Models for Fiber Orientation Predictions During Injection Molding of Short-Fiber Refinforced Polymeric Composites. Master's thesis, Baylor University, 2011.

[91] A. Gusev, M. Heggli, H.R. Lusti, and P.J. Hine. Orientation Averaging for Stiffness and Thermal Expansion of Short Fiber Composites. *Advanced Engineering Materials*, **4**(12):931–933, 2002.

[92] O. L. Forgacs and S. G. Mason. Particle motions in sheared suspensions : X. orbits of flexible threadlike particles. *Journal of Colloid Science*, **14**:473–491, October 1959.

[93] Reuven Y. Rubinstein and Dirk P. Kroese. *Simulation and the Monte Carlo method*. Wiley-Interscience, 2008.